Analysis of the diurnal behavior of Evaporative Fraction

by

Pierre Gentine
Dipl. Ing. in Aerospace Engineering Sup'Aero, Toulouse, FRANCE

Submitted to the Department of Civil and Environmental Engineering
in partial fulfillment of the requirements for the degree of

Master of Science in Civil and Environmental Engineering

at the

MASSACHUSETTS INSTITUTE OF TECHNOLOGY

June 2006

Author .....
Department of Civil and Environmental Engineering
April 16, 2006

Certified by .....
Dara Entekhabi
Professor of Civil and Environmental Engineering
Thesis Supervisor

Accepted by .....
Andrew Whittle
Chairman, Departmental Committee for Graduate Students

Analysis of the diurnal behavior of Evaporative Fraction

by

Pierre Gentine

Dipl. Ing. in Aerospace Engineering Sup'Aero, Toulouse, FRANCE

Submitted to the Department of Civil and Environmental Engineering
on April 16, 2006, in partial fulfillment of the
requirements for the degree of
Master of Science in Civil and Environmental Engineering

Abstract

In this thesis, the diurnal behavior of Evaporative Fraction (EF) was examined. EF was shown to exhibit a typical concave-up shape, with a minimum usually reached in the middle of the day. The influence of the vegetation cover and the soil moisture conditions on EF diurnal shape was also investigated. We also checked the repercussion of a change in environmental conditions on EF. This study will finally allow a better understanding of EF and suggests some new methods to obtain a good estimate of EF and of evapotranspiration.

Thesis Supervisor: Dara Entekhabi
Title: Professor of Civil and Environmental Engineering

Acknowledgments

First, I would like to convey my appreciation to the whole SUDMED project team. They provided the data set necessary to make this thesis possible, and I had a invaluable experience working with them in Marrakech, Morocco.

Then, I would like to sincerely thank my thesis advisor, Professor Dara Entekhabi, for his amazing advice and ideas. I also would like to thank him for being so nice with any student, and respecting their ideas and point of view. I really enjoyed working with him.

Finally, I would like to warmly thank Marie, my family and Onur. They gave me the energy to overcome any moments.

Contents

List of Figures

List of Tables

Introduction

The purpose of this thesis is to understand the diurnal cycle of Evaporative Fraction (EF), which is defined as the ratio between the latent heat flux and the available energy at the land surface:

$$EF = \frac{\lambda E}{A}$$

λE is the latent heat flux (evaporation plus transpiration of the plants) and A is the available energy at the land surface. The energy budget at the land surface can be written as:

$$A = R_n - G = H + \lambda E$$

Where R_n is the net radiation at the surface, G is the soil heat flux and H is the sensible heat flux. So the available energy can be expressed in different ways, that can make the interpretation easier depending on the case.

The first part of the thesis describes the Sudmed project, which took place in Morocco in 2003. During this project a wheat field and an olive tree garden were fully instrumented with continuous measurements of soil moisture, radiative fluxes, turbulent heat fluxes and soil heat flux.

The second part of the thesis describes the frequency analysis of EF using flux measurements over a wheat parcel during an agricultural season nearby Marrakech.

The third part of the thesis is composed of the article submitted to Agricultural and Forest Meteorology in 2006. Additional discussions and results that are not included in the article are presented here in the thesis. The results provide better understanding of EF, its diurnal cycle and its dependency on environmental factors and soil/vegetation conditions.

Finally different EF models are presented and the performances of the resulting evapotranspiration (ET) estimation are compared.

Chapter 1

SUDMED project and main sites

1.1 Sites description

Our experiment is located in the region of Marrakech, Morocco (see Figure B-1) , which is a typical Mediterranean semi-arid region. In those regions the environmental conditions are extremely diverse. The air temperature, for instance, ranges from $-2°C$ at night in the winter, to $50°C$ in the hottest days of the summer. Moreover, those regions experience a wet period in the winter with flash rains and a very dry period in the summer. The study of semi-arid regions is suitable for understanding the main processes of the transfer of water into the atmosphere because over one year diverse environmental and soil moisture conditions are possible. This permits a better understanding of the main parameters regulating the evapotranspiration over the land surface. Moreover, vegetation is generally sparse in these regions, therefore the soil evaporation and the transpiration of the plants are typically of the same order. Hence, while studying the evapotranspiration in semi-arid regions, we can have an understanding of the factors influencing both evaporation and transpiration. These parameters may be different in certain cases.

The field studies were part of the SUDMED and IRRIMED projects. The SUDMED project is an applied study that deals with the characterization, modeling and forecasting of hydro-ecological resources of semi-arid Mediterranean regions, applied to the Tensift watershed around Marrakech. It aims were to develop sustainable man-

agement tools integrating field information, models and satellite measurements. The associate partners participating in this project are CESBIO (French Center for Biosphere Studies), IRD (French Research Institute for Development), Caddy Ayyad University in Marrakech, ORMVAH (Office de Mise en Valeur Agricole du Haous: Moroccan Agricultural Enhancer Agency), DREF (Direction Regionale des Eaux et Forets: Moroccan Water and Forest Regional Agency) and the Agence de Bassin du Tensift (Tensift Basin Agency). The follow-up of this project was called IRRIMED. The general scientific objective of this latter project is the assessment of temporal and spatial variability of water consumption of irrigated agriculture under limited water resources condition. Ground and satellite measurements are combined into models to determine evapotranspiration (ET) over large areas. This will ultimately allow an efficient and sustainable water management for irrigation. New participants were added to the previous project as this project had an international vocation: Wageningen University (Netherland), UoJ, NCARTT and MWI (Jordan), ACSAD (Syria) and INRGREF (Tunisia).

During the SUDMED project, two wheat parcels and one olive tree orchard were instrumented. Biomass, vegetation height, meteorological conditions and energy fluxes were measured in 2002 and 2003. Our two parcels of interest are named R3-B123 and R3-B130. Our sites are composed of typical sparse vegetation in which latent and sensible heat fluxes are of the same size and result in comparable amounts both from the bare soil and canopy heat surface processes. These parcels are located near Marrakech. The first site called R3 is located in an irrigated area in the Haouz plain surrounding Marrakech, where wheat is mainly cultivated. Each parcel was assigned a number based on the counting of all parcels in this zone. Our two parcels of interest are named R3-B123, and R3-B130. The second site, called Agdal, is located in the king Mohammed VI's gardens of Marrakech, which are also irrigated and contain different parcels of olive and orange trees. These two sites are composed of typical Mediterranean cultures, which are completely different in terms of root distribution: small shallow rooted specie for wheat and tall deep rooted specie for olive tree. Moreover, those two kinds of species are really different in terms of soil

occupation, yearly evolution and also age.

1.1.1 Agdal site

The site, a 275-ha olive trees orchard, is located in the royal gardens of the south-eastern part of the ancient fortified city of Marrakech. This site is characterized by a typical Mediterranean semi-arid climate. Precipitation falls mainly in the winter and spring: 192mm of the 253mm yearly precipitations falls from the beginning of November until the end of April. The climate in this region is very dry. The Agdal olive trees are very old generally exceeding 200 years. But a few old trees died and were replaced by younger and smaller trees. Therefore the olive trees size and age is variable over our entire site. Each olive tree is periodically irrigated using a network of small dams. The water reaches a closed area surrounding each olive tree ($\sim 45m^2$), which retains the water in each tree perimeter and creates a small pond around the trees. This method reduces important water loss. The average coverage of all olive trees reaches approximately 40% of the global orchard surface (for a mean olive tree LAI of 2.5), but this value can vary during a yearly period. Indeed the average olive tree LAI value can range from 2 after pruning compared to 3.5 before. The LAI may also greatly vary over the site because of the tree age heterogeneity. Our study takes place in the dry and warm season on two sub-sites: Southern Agdal and Northern Agdal, between June 13 and September 1 (DOY144-244). There are two irrigations applied in this period on June 17 (DOY168) and August 1 (DOY 213). Each irrigation event almost reaches 100 mm per olive tree. The Northern site is less dense than the Southern one, and the trees are younger too, therefore the average LAI on the Northern site is smaller than the one on the Southern one.

1.1.2 R3 site

The entire site called R3 is a 2800 ha wheat irrigated area of 593 agricultural parcels, located at around 45 km East of Marrakech. In this perimeter, two fields were fully equipped, namely the 123rd (R3-B123) and 130th (R3-B130) parcels. Those parcels

are wheat cultivated; the sowing dates are January 13 for parcel 123 and January 11 for parcel 130. The climate is identical to Agdal, and is also characterized by a dry and warm period with very little precipitation in the Summer and Fall, and almost 200 mm in the Winter and Spring. The observation period in which energy fluxes were continuously measured started on DOY 37 for B130 parcel, and DOY 35 for B123 parcel and lasted for the entire wheat season until DOY 141 for both parcels. This covered all cycles of a wheat season: sowing, vegetation installation, vegetative growth, fully grown vegetation and the senescence. Vegetation appears on February 7: DOY 38 for B123 and February 6: DOY 37 for B130, with a growth peak on April 20: DOY 110 (B123) and April 18: DOY 108 (B130), followed by the senescence period until the end of May. Both sites are periodically irrigated by flooding the entire parcel with a network of water channels. B123 is irrigated on February 4 (DOY 35), March 20 (DOY 79), April 13 (DOY 103) and April 21 (DOY 111) with a mean 25 mm supply. The B130 parcel, had been irrigated six times: on February 2nd (DOY32), February 20 (DOY 52), March 13 (DOY 73), April 7 (DOY 97) and April 24 (DOY 114) with a 25-mm irrigation and on March 20 (DOY 80) with half of this amount.

1.2 Experimental data set

All the fluxes and meteorological data was continuously measured and recorded every 30 minutes.Flux values derived from measurements which were either too high or too low were replaced by time interpolated values, and when data was missing or erroneous for more than one consecutive day, the fluxes for this period were rejected. The missing meteorological data could easily be interpolated using surrounding meteorological stations measurements. Finally, a continuous meteorological data set was obtained.

1.2.1 Agdal site

During the entire period, continuous measurements of both sensible and latent heat fluxes were recorded on two sub-sites: Northern Agdal and Southern Agdal, using

3D sonic anemometers (CSAT3, Campbell Scientific, Logan, UT) located on 8.8 high towers at approximately 2 m above the top of the olive trees canopy. Three heat flux plates monitored the 1cm-deep ground heat flux on each sub-site. Air temperature and humidity were measured at 8.8 m high with Vaisala HMP45C probes, and the shortwave incoming radiation was recorded at 9.2 m high using a BF2 Delta T radiometer. The net radiation was measured at a 8 m height, with a Kipp and Zonen CNR1 net radiometer. The soil temperatures had been monitored using 108B thermistances located at different depths. Two of them were located at 5 cm below the surface, 1 at 10 cm, 1 at 20cm and 1 at 40 cm. The soil moisture was measured using TDR sensors located at 5, 10, 20, 30 and 40 cm deep.

1.2.2 R3 site

Near-continuous measurements were recorded during the entire season on both sites. On parcel B123, sensible heat flux was measured with a 3D sonic anemometer (CSAT3, Campbell Scientific, Logan, UT) at 3 m high. A KH20 krypton hygrometer also measured the latent heat flux at this height. The soil heat flux is monitored by three heat flux plates at 1 cm below the surface, 2 plates at 10 cm and 1 plate located at 30 cm. The net radiation was monitored by a CNR1 located at 2 m below the surface. Moisture is monitored by TDR located at 5, 10, 20, 30, 40, 50 cm below the surface and soil temperatures are measured by thermistances located at the same depth. On parcel B130, sensible heat flux was measured by a Leader 81000 ultrasonic anemometer. There was no direct measurement of the latent heat flux, it was calculated as the result of the surface energy budget. Net radiation was monitored by a Q7 budgetmeter and a Skey located at 2 m above the ground. Soil moisture, temperatures, and ground heat flux sensors were identical to B123's. The climatic parameters were measured once for both parcels as the two parcels were close from each other. The air temperature was monitored at 6 m high by Vaisala HMP45C probes, and the shortwave incoming radiation was recorded by a 3 m high CM5 pyranometer.

The solar incoming radiation measured from DOY 35 to DOY 145 is shown on Figure B-2. Only few cloudy days are present during the whole period of measurements.

Cloudy conditions lead to a drop in solar incoming radiation and are therefore easy to determine compared to sunny days. The daily maximum value of solar incoming radiation is generally high, even in the mid-Winter maximum values of 700 $W.m^{-2}$ are common. In the late April, the solar incoming radiation can generally reach 900 to 1000 $W.m^{-2}$ at solar noon. Air temperature was recorded for the same period. As seen on Figure B-3, the range of air temperature is pretty large, with minimum temperature of about 2 $°C$ at night in January, and maximum temperatures of about 40 $°C$ in late April. Air specific humidity is generally low, as seen on Figure B-4. Indeed the relative humidity in the air is relatively small in this semi-arid region. Even when air temperature rises to 40 $°C$ in late April, the specific humidity rarely exceeds 10 g_{H2O}/kg_{air}. Wind speed was measured at 2m height. The wind speed cycle is shown on Figure B-3. Wind speed fluctuates faster than the other environmental variables and was generally below 5 $m.s^{-1}$. Net radiation was recorded at 2m above the ground, and usually reached a maximum of 400 $W.m^{-2}$ in February to almost 750 $W.m^{-2}$ in late April just before harvest. Some sensible and latent heat flux data was missing due to the sensor sensitivity to bad weather conditions, in particular after a strong rainfall event. Sensible heat flux was small at the beginning of the measurement period with a maximum value of about 100 $W.m^{-2}$, and became really high during the senescence period leading to daily maxima of the order of 250 $W.m^{-2}$. Latent heat flux was also pretty low at first, when the vegetation was growing and installing, but it became very large just before the senescence period, reaching high values of the order of 400 $W.m^{-2}$. The ground heat flux was calculated as the mean value of the 3 measuring plates. This mean value is seen on Figure B-9. The maximum possible values reached 150 $W.m^{-2}$ just after sowing, when there was almost no vegetation shade. The smallest amplitude of the flux was obtained before senescence, when the vegetation cover and the greenness were high.

1.3 Calibration and validation of the SVAT model

1.3.1 Calibration

The Soil-Vegetation-Atmospher-Transfer (SVAT) model is named ICARE SVAT and it is described in the article submitted to Agricultural and Forest Meteorology. This model describes the evolution of the soil water content and temperature profiles using the energy budget over the soil and canopy. Because the SVAT model requires a significant number of parameters, we first performed a sensitivity analysis in order to identify the importance of each parameter for calibration. We first used a priori values taken from both literature review and field measurements. The parameters calculated using field measurements or empirical models related to the soil composition are: the soil hydraulic conductivity at saturation k_{sat}, the shape parameter of Brooks and Corey retention curve B, the soil water content at field capacity θ_{fc}, the soil water content at wilting point θ_{wilt}, and the water content at saturation θ_{sat}. The parameters derived from literature review are the soil resistance parameters A_{rss}, B_{rss}, and the stress parameters of the stomatal resistance D_p, D_T and the minimum stomatal resistance $r_{sc,min}$. The calibration of the model was based on an iterative procedure, which compared the time series of estimated variables (Yest) and observed variables (Yobs) and minimized their difference by adjusting the chosen parameters. The optimization was obtained by minimizing the Root-Mean-Square Error (RMSE) between the two time series.

$$RMSE = \left[\frac{1}{N-1} \sum_{n=1}^{N} |Y_{obs}(i) - Y_{est}(i)|^2 \right]^{1/2}$$

with N: number of observations. The initial values of the parameters are the a priori values. The minimization treated the parameters following their importance, found after the sensitivity test. The optimization iteratively used the simplex search method on Matlab (The Mathworks Inc.).

1.3.2 R3 site

Samples of the soil were analyzed to determine the fractions of clay and sand. On R3-B123, 47.5 % of the soil was clay and 15.8 % was sand. On R3-B130, 36 % of the soil was clay and 16 % was sand. Then using gravimetry tests, Brooks and Corey 1964 retention curves were fitted to the data. On R3-B123, we obtained for the potential at saturation $\psi_{sat} = -0.3\ m$ and the shape parameter of the curve $B = 5.25$. Then the following values were found: soil water content at saturation $w_{sat} = 0.47\ m^3.m^{-3}$, soil water content at field capacity $w_{fc} = 0.37\ m^3.m^{-3}$ and soil water content at wilting point $w_{wilt} = 0.14\ m^3.m^{-3}$. On R3-B130, the following values were found: $\psi_{sat} = -0.135\ m$, $B = 4.5$, $w_{sat} = 0.46\ m^3.m^{-3}$, $w_{fc} = 0.30\ m^3.m^{-3}$ and $w_{wilt} = 0.09\ m^3.m^{-3}$. The soil hydraulic and thermal properties were also measured in situ. The following values were found on R3-B123: the soil dry density was 1.55 $kg.m^{-3}$, the soil specific heat was 900 $J.(kg.K)^{-1}$ and the dry thermal conductivity: $\lambda_{dry} = 0.03\ W/(K.m)$ and the hydraulic conductivity at saturation $k_{sat} = 1.25 * 10^{-6}\ m/s$.

Then the SVAT parameters that could not be directly measured were calibrated to fit the measured fluxes and observed radiative temperatures at 0° and at 55°. In particular, the parameters of the soil resistance to evaporation, were calibrated at the beginning of the measurements when the wheat was very short. The following coefficients were found $A_{rss} = 11.$ and $B_{rss} = 11.$. The roughness length of the substrate was found to be $z_{0,s} = 0.03\ m$.

After installation of the canopy, the calibration of the vegetation parameters was done. The minimum stomatal resistance was found to be: $r_{sc,min} = 90\ m.s^{-1}$, the water vapor deficit stress factor parameter of the Jarvis formulation: $D_P = 1.5e-4\ Pa^{-1}$, and the temperature stress factor parameter $D_T = 0.004\ K^{-2}$. All those parameters were calibrated on R3-B123 in 2003 and validated on R3-B130 during the same period. The best set of parameters matching both the calibration and validation were chosen.

1.3.3 Agdal site

The approach to calibration and validation of the parameters over Agdal is different than for the R3 site. At Agdal we had flux measurements for more than six months. Therefore, the parameters were calibrated on the first three months of measurements and validated on the second half. The soil thermal and hydraulic properties were found to be: soil composed of 20 % of clay and 56 % of sand, the potential at saturation $\psi_{sat} = -0.703\ m$, the shape parameter of the Brooks and Corey retention curve $B = 6.$, soil water content at saturation $\theta_{sat} = 0.38\ m^3.m^{-3}$, soil water content at field capacity $\theta_{fc} = 0.23\ m^3.m^{-3}$ and soil water content at wilting point $\theta_{wilt} = 0.08\ m^3.m^{-3}$, the soil dry density was 1.44 $kg.m^{-3}$, the soil specific heat was 840 $J.(kg.K)^{-1}$ and the dry thermal conductivity: $\lambda_{dry} = 0.03\ W.(K.m)^{-1}$ and the hydraulic conductivity at saturation $k_{sat} = 2.7 * 10^{-6}\ m.s^{-1}$.

The following evaporation and transpiration parameters were found: $A_{rss} = 11.75$ and $B_{rss} = 12.27$, $z_{0,s} = 8{*}10^{-3}\ m$, $r_{sc,min} = 150\ m.s^{-1}$, $D_P = 2.5e{-}4\ Pa^{-1}$ and $D_T = 0.0016\ K^{-2}$.

Chapter 2

Frequency analysis of EF

2.1 Frequency analysis of EF

2.1.1 Fast Fourier Transform (FFT)

To understand the diurnal behavior of EF, EF was first computed using the measured turbulent fluxes: the sensible heat flux H and the latent heat flux λE as:

$$EF = \frac{\lambda E}{H + \lambda E}$$

However as we can see on figures B-7 and B-8, some of the flux data was missing, therefore a FFT could not be computed as it requires continuous data, separated by the same interval of time.

2.1.2 Fast Fourier Transform (FFT) on moving window

To solve this problem, the first idea was to use a FFT on each window of non-missing data and then the resulting FFTs, weighted according to the energy of the window, to conserve energy. However, this method could not lead to satisfying results. Generally, the windows of non-missing data do not have the same length, leading to different Fourier base frequency. The resolution of the flux data set remains the same $T = 30minutes$, however when we have a window of non-missing data of length N,

the minimum Fourier frequency is: $\omega_F = \frac{2\pi}{N.T}$. All other frequencies are proportional to this frequency, so our set of Fourier frequencies is $\omega_n = n.\omega_F = \frac{2\pi n}{N.T}$. Therefore, the set of Fourier frequency is changing for each different window. This leads to a strong biases in the spectrum of EF. The spectrum cannot permit a satisfactory interpretation of EF diurnal behavior.

2.1.3 Lomb periodogram

The third approach was to use the Lomb periodogram approach as described in Van Dongen 1999 [55], Laguna 1998 [52] and Lomb 1976 [53]. This method allows a frequency analysis of unevenly spaced data. It was first developed for the frequency analysis of astrophysical data, that were available at different times, not necessary evenly spaced in time. This method is based on Discrete Fourier Transform (DFT) for unevenly sampled signal, $x(t_n), n = 1, 2, .., N$:

$$DFT(\omega) = \sum_{n=1}^{N} x(t_n) e^{-i\omega t_n}$$

with $\omega = 2\pi\nu$: angular frequency. This can be used to define the Lomb periodogram, which is not dependent on the initial time considered, like the commonly used periodogram.

$$P(\omega) = \frac{1}{2\sigma^2} \left(\frac{\left[\sum_{n=1}^{N} x(t_n) cos\left[\omega(t_n - \tau(\omega))\right]\right]^2}{\sum_{n=1}^{N} cos^2\left[\omega(t_n - \tau(\omega))\right]} + \frac{\left[\sum_{n=1}^{N} x(t_n) sin\left[\omega(t_n - \tau(\omega))\right]\right]^2}{\sum_{n=1}^{N} sin^2\left[\omega(t_n - \tau(\omega))\right]} \right)$$

Where σ^2 is the variance of $x(t_n)$ and:

$$\tau(\omega) = \frac{1}{2\omega} Arctan \left(\frac{\sum_{n=1}^{N} sin(2\omega t_n)}{\sum_{n=1}^{N} cos(2\omega t_n)} \right)$$

is an offset to achieve time translation invariance of the periodogram. The main idea of the Lomb periodogram is to fit a sinusoidal function of frequency ω to the data. This approach did not give satisfying results to estimate the main frequency

components of EF, using the measured turbulent heat fluxes. For instance, when trying to reconstruct the initial turbulent fluxes, using this method we obtained a very noisy resulting signal as seen on figures B-10 and B-11. This proves that the periodogram was not able to correctly determine the frequencies of interest in the fluxes. Indeed, the fluxes are very different from one day to another because of the varying environmental factors such as the solar incoming radiation, air temperature or wind speed. It is also clear that the frequency behavior of the environmental parameters is very complex because of the inherent variability of the environmental conditions.

Chapter 3

Analysis of EF diurnal behavior

3.1 Article submitted to Agricultural and Forest Meteorology

The following article was submitted to Agricultural and Forest Meteorology. This article describes the mean diurnal cycle of EF, depending on the different environmental and soil moisture conditions. Added discussions and plots, which could not fit into the paper required length are presented here after the article.

Analysis of Evaporative Fraction Diurnal Behavior

Pierre Gentine and *Dara Entekhabi (Correspondent author)*

gentine@mit.edu *and* darae@mit.edu

Department of Civil & Environmental Engineering

Massachusetts Institute of Technology (MIT)

Cambridge, Massachusetts

USA 02139

Abdelghani Chehbouni, Gilles Boulet and *Benoît Duchemin*

ghani@cesbio.cnes.fr, Gilles.Boulet@cesbio.cnes.fr and benoit.duchemin@cesbio.cnes.fr

Centre d'Etudes Spatiales de la Biosphère (CESBIO)

18 Avenue Edouard Belin

BPI 2801

31401 Toulouse CEDEX 9

France

Submitted to *Agricultural and Forest Meteorology*

April 7, 2006

Abstract

Experimental studies indicate that Evaporative Fraction (EF), the ratio between the latent heat flux and the available energy at the land surface, is a normalized diagnostic that is nearly constant during daytime under fair weather conditions (so-called daytime self-preservation). This study examines this indication and investigates contributions to the variability of EF due to both the environmental factors (air temperature, solar incoming radiation, wind velocity, soil water content or Leaf Area Index) and due to the natural phase shift between the surface energy balance components at the land surface. It is shown that the phase difference between soil heat flux and net radiation needs to be characterized fully for application of EF daytime self-preservation. The correlation of EF with the different environmental factors is then discussed. Finally the conditions under which the diurnally-constant EF assumption can be invoked are discussed. In the last part of the study, the effect of non-precipitating partial cloud cover on EF and evapotranspiration are analyzed. This latter test is important to extension of the EF measure to non-fair weather conditions.

Keywords: Evaporation, Evapotranspiration, Soil heat flux, Diurnal, Soil moisture.

1. Introduction and Motivation

Evapotranspiration (ET) is a flux linking water, energy and carbon cycles. Flux measurement networks (as FluxNet, EuroFlux, AmeriFlux) are only available in few tens of point locations around the Globe. They are costly both to install and maintain. Moreover there is a strong heterogeneity of the fluxes over the land surface because of the inherent physical diversity of the land and vegetation properties with wide range of length scale. Therefore the locally-measured fluxes cannot be representative of a whole region of interest.

The only currently available way to obtain ET mapping is to rely on remote sensing data that now have both nearly-continuous spatial coverage and adequate temporal sampling using constellation of satellites or geostationary platforms. It is not possible to directly measure fluxes using satellite information. In fact the remotely sensed measurements such as land surface temperature are only indirectly related to the state of the land surface and the corresponding heat fluxes.

Different methods have been developed to estimate ET using either empirical or physically based methods (see Capparrini et al. (2004) for review). In summary there are four main approaches:

1. The first approach is to use remote sensing data such as Normalized Difference Vegetation Index (NDVI) and Land Surface Temperature (LST) and to empirically link those variables to surface evapotranspiration, as in Gillies et al. (1997) and Moran et al. (1994). This approach is limited to locations where calibration and validation data are available. Extensions beyond the calibration region and the studied climate have unknown errors.
2. The second approach is based on using the LST and NDVI images to constrain the energy budget at the land surface. In this approach, the ground heat flux G is usually related to another flux such as the surface net radiation Rn, which can be more easily estimated from remote sensing. Several empirical relationships have been used, such as: $G/R_n = const.$ and $G/R_n = f(NDVI)$, as in ALEXI model; see Anderson et al. (1997), Mecikalski et al. (1999) or $G/R_n = f(NDVI, LST)$, as in SEBAL model; see Bastiaanssen et al. (1997, 1998 and 2005). However, the

soil heat flux cannot be simply related to the net radiation and depends on different factors that cannot be directly measured, in particular the soil moisture profile. Furthermore, the effect of solar angle (e.g Ma et al. 2002) and the time lag between G and R_n have to be accounted. In fact there are large phase differences between the two that can lead to serious errors in turbulent flux estimation based on the land surface energy budget.

3. The third approach uses the assimilation of remote sensing data into Soil Vegetation Atmosphere Transfer (SVAT) models, as described in Dunne and Entekhabi (2006), Pellenq and Boulet (2004) and Reichle et al. (2002). The ET at the land surface is physically constrained by the SVAT model whose state and intrinsic parameters are calibrated to fit the remotely sensed observations such as LST. Where micrometeorological measurements are continuously available, the water and temperature state of the model may be solved using the coupled hydraulic and energy budgets at the land-surface. Hence, ET time-series may hence be calculated at the time-step of the model.
4. The fourth approach has been introduced by Castelli et al. (1999) and Boni et al. (2000 and 2001) and extended by Capparrini et al. (2003 and 2004). It is based on a variational assimilation of LST into a surface energy balance model. In this approach there is no direct use of the water budget, but only of the energy budget at the land surface. The most interesting part of this approach is that it does not require any empirical relation linking ET to the remotely sensed data, and it also does not require any empirical relationship assumption between soil heat flux and net radiation. The main idea of this approach is to estimate the most sensitive parameters of flux estimation using sequences of satellite-based LST imagery. The first group of parameters is related to the influence of land surface characteristics on near-surface air turbulent conductivity, namely the roughness length scale for turbulent heat flux. The time changes in this parameter depending mainly on the phenological state of the vegetation (assumed to be monthly constant). The second group of parameters is related to the partitioning of the turbulent heat fluxes between sensible and latent heat flux. This partitioning is characterized by the daytime-EF that is linked to the soil moisture conditions.

The second and fourth approaches often rely on the daytime self-preservation of evaporative fraction EF, which is defined as the ratio between the latent heat flux and the available energy at the land surface $EF = \frac{\lambda E}{R_n - G}$, or a similar diagnostic of the surface energy balance. The robustness of this assumption and the range of its applicability under different environmental conditions is the rationale for this study.

The observation that EF is often constant during the daytime is based on Shuttleworth et al. (1989), Nichols and Cuenca (1993), Crago (1996a) and Crago and Brutsaert (1996). They use in situ measurements of surface energy balance components to show that EF is almost constant during the daytime hours under clear skies. EF supposedly removes available energy diurnal cycle and isolates surface control (soil and plant resistance to moisture loss) on turbulent heat flux partitioning. These controls vary on approximately daily time-scales.

In an important study Lhomme (1999) has shown that EF is not really constant during day-time especially in non-fair weather conditions. This leads to ET estimation errors, in particular in the morning and late afternoon due to the typical parabolical shape of EF. Lhomme (1999) is the foundation for this study and the analysis here is intended to provide additional detail. Lhomme (1999) and this study together should provide the basis to understand the daytime self-preservation of EF and assess the limitations of its application.

In order to better understand the diurnal behavior of EF and its environmental dependencies it is important to have long term field experiment data. In this paper we use a SVAT model in conjunction with field experimental data in order to assess the EF temporal behavior under diverse environmental conditions. The dual-source (soil and vegetation) SVAT model also allows the test of the influences of vegetation cover and soil moisture on EF daytime self-preservation. This model is also used to understand the possible phase shift between the different surface fluxes, which can lead to dramatic EF under/overestimation.

The field experiment data used in this study is first presented. The SVAT model outlined in Figure 1 is described in the Appendix. Then, the diurnal course of EF is physically explained through SVAT modeling and its consistency with Lhomme's (1999)

result is discussed. The partial soil moisture and vegetation cover influences on the EF diurnal shape is further analysed. Finally, the temporal correlations between EF and the main environmental factors are discussed and a strategy for the refinement of ET estimation using both land surface temperature and EF daytime self-preservation is forwarded.

2. Field Experiment Data Set

The SVAT model (see Appendix A) is calibrated and tested on two wheat parcels and one olive tree orchard during the 2002 and 2003 SUDMED project in the region of Marrakech, Morocco, described in further detail in Duchemin et al. (2006). The experiment area is a typical Mediterranean semi-arid region. This region is heterogeneous in terms of vegetation cover and climate both spatially and temporally. These conditions are particularly appropriate to test and apply SVAT models because of the sparse vegetation with strong phonological cycle permits variations in the contribution of soil and vegetation to the surface energy balance. The air temperature ranges from as low as 0°C in the Winter to 50°C in the Summer; LAI from 0 (sowing) to more than 5 before harvest.

The study site is composed of sparse vegetation (varies with season) in which latent and sensible heat fluxes are of comparable magnitude. There are both bare soil and canopy contributions to turbulent fluxes. The specific study site, named R3, is located in an irrigated area in the Haouz plain surrounding Marrakech, where wheat is the main cultivated plant.

The R3 site is a 2800 ha area where irrigated wheat is cultivated, located 45 km East of Marrakech. Two fields were equipped with instrumentation, namely the 123rd (R3-B123 used in this study) and 130th (R3-B130) parcels. The parcels are cultivated with wheat. The sowing date is January 13 (Day Of Year 13). The climate is characterised by a dry and warm period with very few precipitations events in Summer and Fall. Almost all of the annual precipitation occurs in Winter and Spring (see Fig. 2). The rainy period lasts 6 months from November to April and the cumulative precipitation is generally of the order of 250 mm per year. The site is periodically irrigated by flooding

the entire field. The parcel of interest in this study is r#-B123. Irrigation events occurred on February 4th (DOY 35), March 20th (DOY 79), April 13th (DOY 103) and April 21th (DOY 111) with a mean 25 mm supply each time (see 2).

Energy fluxes were continuously monitored starting February 4th (DOY 35) and lasted the entire wheat season until May 21st (DOY 141). It covered the whole wheat cycle: sowing, vegetative growth, full, canopy, and the senescence. Vegetation appears around February 7 (DOY 38), with a growth peak on April 20 (DOY 110), followed by the senescence period until the end of May (see Fig. 3).

Near-continuous measurements have been recorded during the entire wheat season. Sensible heat flux was measured with a 3D sonic anemometer (CSAT3, Campbell Scientific, Logan, UT) at 3m height. A KH20 krypton hygrometer also measured the latent heat flux at this height. The soil heat flux is monitored by three heat flux plates at 1 cm below the surface, 2 plates at 10 cm and 1 plate located at 30 cm. The net radiation is monitored by a CNR1 located at 2 m above the ground. Moisture is monitored by several Time Domain Reflectometry (TDRs) located at 5, 10, 20, 30, 40, 50 cm below the surface and soil temperatures are measured by some thermistances located at the same distance from the soil surface. Flux values derived from measurements that were obviously either too high or too low have been replaced by time-interpolated values, and when several errors occurred during one entire day, the flux data for that day was rejected.

The air temperature was monitored at 6 m height using Vaisala HMP45C probes, and the shortwave incoming radiation was recorded by a 3 m height with a CM5 pyranometer.

The meteorological conditions are highly variable. Solar incoming radiation varies between a diurnal maximum of 200 W.m^{-2} for a February cloudy day to a diurnal maximum between 900 and 1000 W.m^{-2} at the end of May (see Fig. 4). There is also a wide range of air temperatures with a minimum of 0°C in February and a maximum of 38°C by the end of May.

The average energy balance closure between the measured turbulent heat fluxes $H + \lambda E$ and the measured available energy $R_n - G$ is 79% and they have 89% explained variance correspondence.

Past experimental EF studies were only able to study the EF behaviour during a few days because continuous experimental flux data are both complicated and costly to maintain. The R3-B123 meteorological and flux dataset offer measurements for more than 100 days. Fig. 5 shows the daily course of EF using the measured latent and sensible heat fluxes averaged over the DAY 35 to DAY 141. EF exhibits a typical concave-up shape with a minimum around 12PM (all times are referenced to local solar conditions so 12PM is local solar noon). The EF values are nearly constant during mid-day period. Near sunrise or sunset EF and its standard deviation increase sharply. Available energy that appears in the denominator of EF is small near these times. Therefore the inclusion of early morning and late afternoon EF values in the estimation of daily EF can lead to non-negligible evapotranspiration estimation errors. The EF behaviour in those periods will clearly depend on environmental factors, soil water content, and phenological stage as well. Some of these influences were investigated in Lhomme (1999) through SVAT modelling. This study builds on the same approach but extends it in important ways. Specifically the contributions of soil and vegetation and the phase shifts between the energy balance components are the subject of analyses. Application with the extended-duration field observation data allows for realistic experimental conditions.

3. Lhomme (1999) Study

Lhomme (1999) analysed the daytime pattern of EF using the Penman-Monteith single-source model coupled to a convective boundary layer model. The influence of both the micrometeorological factors and soil water availability on the EF daily course was investigated in this article. Lhomme (1999) found that EF exhibits a typical concave-up shape, with a minimum around noon. Moreover EF appeared to be relatively constant around mid-day yet always lower than the mean daily value. The soil moisture availability was found to have a great importance on EF, and that EF was a strongly increasing function of soil water content, for high incoming radiation and wind speed values. When available energy is not limiting the EF amplitude is directly related to soil water availability. EF was also found to decrease when solar energy is increased for medium soil water conditions and high wind speed. Lhomme (1999) also found that the

air vapor saturation deficit only had a slight impact on EF amplitude and that wind velocity had almost no effect on EF.

However in his approach Lhomme (1999) assumed that the soil heat flux was a fraction of the net radiation energy. Hence the soil heat flux (G) and net radiation (R_n) were forced to be in phase. This can lead to large biases in the available energy (R_n-G) diurnal behaviour. Moreover G is generally negative in the mid-afternoon, leading to a much smaller EF.

4. Phase Difference Between G and Rn

Many previous studies have shown that the phase difference between soil heat flux and net radiation is an important characteristic of surface energy balance (Fuchs and Hadas 1972; Idso et al. 1975; Santanello and Friedl 2003). The difference between these two fluxes appears in the denominator of EF. In fact it is the normalization of latent heat flux diurnal cycle by the diurnal cycle of this difference that is key to the apparent daytime self-preservation of EF.

Usually EF exhibits a typical concave-up shape with a minimum in the early afternoon (See Fig 5). Few studies have tried to theoretically explain the EF shape. Among those studies Crago (1996b) and Lhomme (1999) explained the diurnal shape using a single-source Penman-Monteith formulation for ET since they focused on closed-canopy vegetation. In those studies, the soil heat flux was considered either negligible or a constant small fraction of the net radiation. However, some studies (Clothier et al. (1986), Kustas et al. (1990)) have shown that the soil heat flux can be an important part of the energy budget and expressing it as a fraction of the incoming radiation does not represent the physics of conduction. Indeed, soil heat flux is dependent on many factors such as vegetation cover, soil type and moisture or time of day. In particular, Fuchs and Hadas (1972), Idso et al. (1975) and Santanello and Friedl (2003) found important phase difference between G and R_n around solar noon.

When G is expressed as a fraction of the net radiation it is usually underestimating the real soil heat flux in the morning, and overestimation in the afternoon, leading to a corresponding underestimation of EF in the morning and overestimation in the afternoon.

Hence G is an important component of the surface energy budget and is also of drastic importance to understand and explain the EF diurnal shape.

In Fig. 6 and 7 the long duration SUDMED field experiment data and the SVAT model are used to estimate the fidelity of the in-phase G and R_n assumption. The SVAT model was run for different soil moisture, LAI and environmental conditions allowing the calculation of the constant fraction relating G and R_n with:

$$f = \frac{\int_{sunrise}^{sunset} G(t)dt}{\int_{sunrise}^{sunset} R_n(t)dt} \qquad (1)$$

The LAI and soil moisture were fixed but varied over a range in order to assess the role of surface water limitation and fractional vegetation-versus-soil energy balance contributions. Three LAI values (0.5, 2.5 and 4.5) were used to find the average value of f over the entire period with many soil moisture conditions. Soil moisture is specified for the top 5 cm and the profile is allowed to reach hydrostatic equilibrium. The mean values found were f=0.14 for LAI=0.5, f=0.11 for LAI=2.5. f=0.09 for LAI=4.5 using (1).

Figure 6 shows the difference between the SVAT modelled soil heat flux and the soil heat flux calculated as a fraction of the net radiation. The difference is negative during most of the day except in the morning, usually from 8AM to 12.30PM. When G is expressed as a fixed fraction of the incoming radiation (hence in phase), it is underestimating the soil heat flux in the morning and overestimating during the rest of the day in particular in the afternoon where the absolute difference can become large. Moreover, the difference is strongly depending on LAI: it is clearly increasing in sparse canopy cases, as the amplitude of both soil heat fluxes is increasing due to the increasing fraction of radiation reaching the ground. The difference is lightly dependent on soil moisture; with high soil moisture the surface thermal gradient is smaller because of the larger thermal inertia of the water within the porous medium. Even if the wet thermal conductivity is higher, the wet surface thermal gradient is so small that the surface soil heat flux is smaller in a wet case than a dry case in the morning. In the late afternoon, when the soil heat flux is becoming negative, the amplitude is still larger in the dry case because of the same surface thermal inertia effect. Fig. 6 shows that the two fluxes are

always out of phase. This can be seen more succinctly in Fig. 7 where the difference between the two are shown.

In Fig. 7 the soil heat flux error is generally maximum in the mid morning, for all LAI and soil moisture conditions. It becomes negative in the mid afternoon essentially cancelling the net radiation at that time. This strong asymmetry in the errors of the in-phase assumption will have an effect on the diurnal shape of EF. In particular, the EF shape is less parabolic than the one found by Lhomme (1999). Indeed the larger soil heat flux at the early daytime hours will sharpen the EF shape at the beginning of the day. Then as G is smaller and even negative in the afternoon, EF does not increase as rapidly as in the in-phase case. The increase will be present as long as the soil water content is not high because the presence of liquid water decreases the amplitude of the soil heat flux.

5. EF Diurnal Pattern Dependencies

The instantaneous Evaporative Fraction is defined for total, soil, and canopy as (respectively):

$$EF(t) = \frac{\lambda E(t)}{Rn(t) - G(t)} \tag{2}$$

$$EF_s(t) = \frac{\lambda E_s(t)}{Rn_s(t) - G(t)} \tag{3}$$

$$EF_c(t) = \frac{\lambda E_c(t)}{Rn_c(t)} \tag{4}$$

The degree of their convexity during the day (hence the violation of daytime self-preservation) is sensitive to the soil water control on evaporation as well as the sparsity of the canopy. The degree of dependence can be shown through SVAT modelling calibrated and forced with SUDMED observations and micrometeorological forcing. The two critical factors, soil moisture and LAI, are varied in order to quantitatively assess the effects. Figure 8 shows the diurnal behaviour of total EF under the different soil moisture and canopy cover conditions. The instantaneous EF values are averaged over the whole measurement period using (2). In every case EF exhibits a convex diurnal shape as found

using the in situ measured EF (Fig. 5). Soil moisture availability has a strong influence on EF because soil moisture is the main limiting factor for latent heat flux. This is evident in the rise in EF, especially at mid-day, with increasing soil moisture. This is a reminder of the value of the EF diagnostic as a measure of surface control (soil moisture availability) on turbulent flux partitioning.

There are two main features in Fig. 8 that are noteworthy. First the sharp rise in the EF during late afternoon is sensitive to LAI and the vegetation cover. When vegetation cover is full the rise is more pronounced and the daytime self-preservation is less evident. Second the instantaneous value of EF exceeds unity during late afternoon especially for well-watered and fuller canopies. These two features can be further broken down and analysed using the SVAT model data.

Figure 9 shows the bare soil component EF_s based on application of (3) and averaging over the entire experiment period. EF_s is generally increasing (rapidly rising to its mid-day value) until noon and then slowly decreasing in the afternoon until sunset. Contrary to the total EF, the soil evaporative fraction EF_s is a strongly increasing function of LAI. The late afternoon rapid rise observed for EF in Fig. 8 is not apparent for the bare soil fraction. In this respect the bare soil fraction daytime self-preservation of EF may be a better assumption. One noticeable feature is that, when LAI increases, the soil evaporative fraction EF_s exceeds unity when soil moisture is not limiting. Under full vegetation cover conditions the canopy temperature increases as it receives more energy, and the soil temperature is reduced due to the increasing shadow. For high LAI cases, a temperature inversion can occur leading to a negative soil sensible heat flux H_s and therefore a soil evaporative fraction EF_s greater than unity. This effect is particularly strong for high LAIs and high soil moisture conditions that clearly increase the possibility of soil-canopy temperatures inversion. This effect is confirmed when the average diurnal course of the sensible heat fluxes (total H, soil H_s, and canopy H_c) are plotted as a function of daytime hour for LAI=2.5, the mid-range value (Fig. 10). Whereas the total sensible heat flux to the atmosphere is generally positive (Fig. 10a), the soil and canopy components (Figs. 10b and 10c) show that thermal inversions are prevalent especially in the late afternoon and for bare soils. The result is a general downward sensible heat flux H during late afternoon and decrease in the denominator of instantaneous EF. The

impact is a sharp rise in EF during late afternoon (Figs. 5 and 8). The value of daytime EF diagnostic is lost if averaging includes these hours of the day.

The results can be viewed from another angle with similar understanding. Figure 11 shows the canopy EF_c averaged over the experiment period. The canopy evaporative fraction diurnal course is generally constant in the morning and increases sharply in the afternoon. Thereby a constant canopy evaporative fraction assumption can lead to large errors in evapotranspiration estimate if this sharp deviation in the afternoon due to thermal inversion in canopy-covered landscapes is included.

6. EF Covariation With Micrometeorological Factors

More insight about the factors that affect the degree to which daytime EF self-preservation is possible is obtained through the understanding of the link between EF and micrometeorological parameters such as air temperature, solar incoming radiation, wind speed or temperature gradient near the surface T_{ro} - T_a, where T_{ro} is the LST. All these factors affect the surface turbulent fluxes. Ideally EF should isolate only the surface control on latent heat flux (mostly soil moisture) and remain independent of fluctuations in micrometeorological parameters. The temporal covariations can be estimated from the SVAT data. The results are stratified for varying vegetation cover (LAI) and soil moisture conditions.

Here daytime EF is defined as

$$< EF >_{daily} = \frac{\int_{sunrise}^{sunset} \lambda E(t)dt}{\int_{sunrise}^{sunset} [H(t) + \lambda E(t)]dt} = \frac{\int_{sunrise}^{sunset} \lambda E(t)dt}{\int_{sunrise}^{sunset} [R_n(t) - G(t)]dt} \qquad (5)$$

No attempt is made to exclude the late afternoon values at this point. The reason is to be able to assess the dependencies of EF as EF is commonly used. Later in this paper the ideal daytime hours for a refined definition of EF will be addressed.

The principal source of available energy at the surface is solar radiation. Figure 12a shows the temporal correlation between EF and incoming solar radiation. The correlation is generally weak which is an advantage. There is however an interesting

shift in the correlation at about a soil moisture value greater than 0.2 [$m^3.m^{-3}$]. Above this threshold value EF is positively correlated to solar incoming radiation. At lower values of soil moisture the correlation is negative and the temporal fluctuations of the two variables are inversely (in sign) related, here ET is both water and atmosphere controlled. When the elements of EF are broken down into soil and canopy components, the causes of the shift in behaviour become evident. The numerator of EF is the latent heat flux and the denominator is the available energy given as R_n-G or λE+H. The cross-correlation between the latent heat flux and the solar incoming radiation is large as shown in Fig. 12b. For low LAI values and low soil moisture, evaporation is still possible even if lower compared to a high soil moisture case. Hence bare soil evaporation and solar incoming radiation will be positively and fairly well correlated. For higher LAI values (LAI>1), transpiration will be the main water transport process. However transpiration is limited when the soil water content is close to the wilting point, leading to decorrelation between solar incoming radiation and LE. At the same time, the available energy received at the surface is clearly directly dominated by the incoming solar radiation (Fig. 12c). Despite the two highly correlated numerator and denominator, the EF itself is only weakly correlated with incoming solar radiation. This is indicative of the effectiveness of EF to remove the most obvious and dominant factor with strong diurnal cycle from its dynamics. The exception is when soil moisture is apparently limiting evapotranspiration, below a value of 0.2 [$m^3.m^{-3}$] in this case (fine clay soil). This soil moisture-dependent transition from water-limited evaporation regime to energy-limited evaporation regime is highly model-dependent and, even in the field, dependent on factors such as rooting depth, plant species, and soil texture. Figure 13 shows the general shape of this function for the experiment here. The average ratio of evapotranspiration to potential evaporation shows a strong dependence on soil moisture and only weak dependence on LAI.

Another important forcing factor of turbulent exchange at the surface, beside the dominant role of incoming solar radiation in available energy, is wind-speed. Ideally the EF diagnostic should be independent of this factor in its dynamics.

The correlation between EF and the wind speed is generally small as shown in Fig. 14. This result agrees with Lhomme (1999) who also found that there was almost no influence of the wind speed on EF. Again here the EF definition is broken down in order

to understand the contributing reasons and their dependence on LAI and soil moisture. The EF-wind speed correlation also exhibits a change in sign around the transition point between water-limited and energy-limited evaporation regimes. The correlations amplitudes nevertheless remain small. The overall decorrelated effect is due to a compensation between the latent heat flux and available energy correlations. When the soil water content is limiting the latent heat flux remains small and the wind speed has almost no influence on its fluctuations (Fig. 14b). Available energy is only slightly correlated with wind speed through the decrease in surface temperature when wind speed increases, and consequently, the increase in net radiation. Therefore, the EF correlation with the wind speed remains small for low soil water contents. While the soil water becomes more available wind speed becomes one of the main limiting factors of latent heat flux amplitude, as the water availability is not anymore a limiting factor to evapotranspiration. Under these conditions latent heat flux is strongly correlated with the wind speed value (Fig. 14b) leading to a stronger correlation between EF and wind speed. Yet the stronger correlation of the latent heat flux is compensated by the non-negligible correlation between the available energy and the wind speed (Fig 14c).

Of practical consequence in remote sensing approaches to EF determination is the dependence of EF on observable states of the system such as physical temperatures. The correlation between EF and the air temperature is strong and positive for high soil water content and low LAI (Fig. 15). Under water-limited evaporation regime conditions evapotranspiration is forcibly reduced and generally decoupled from micrometeoroloical conditions. This is evident in both Figs. 15a and 15b for correlations when the soil moisture is low. The degree of decorrelation is strongly dependent on LAI as well. The bare soil surface can still evaporate even at very low soil moisture content, leading to a stronger correlation between evaporation and air temperature for low soil moisture. The plant however experiences stress and shuts down transpiration leading to the decoupling. Available energy is positively but weakly correlated to the air temperature regardless of the dominant soil moisture or vegetation canopy conditions (Fig. 15c). Unlike incoming solar radiation and wind speed, the compensating effect of the EF numerator and EF denominator are absent in the case of air temperature. However the sign and magnitude of the EF-air temperature correlation are highly dependent on the soil moisture and

vegetation canopy conditions. In this respect when soil moisture is limiting it is advantageous for the definition of EF that it does not depend on air temperature. However when the surface evaporation regime is energy-limited, then air temperature is a good indicator of EF. However the results are not totally reliable since the transition is not well-defined (in both models and field).

A more physically derived temperature diagnostic for turbulent flux estimation and for the determination of partitioning among sensible and latent heat fluxes needs to be used. This temperature measure is based on the difference between surface radiative and air temperature prognostics, namely $T_{r0} - T_a$. Sensible heat flux is clearly strongly correlated with $T_{r0} - T_a$ (of the order of 0.95) as shown in Fig. 16a because $T_{r0} - T_a$ is a direct driver of sensible heat flux. As shown in Fig. 6b the link between the latent heat flux and $T_{r0} - T_a$ is much more complex. When soil moisture is low (water-limited evaporation regime) and LAI≥1.5, a strong negative correlation exists between latent heat flux and $T_{r0} - T_a$ (Fig. 16b). The measure $T_{r0} - T_a$ is also an indicator of the plant stress, therefore $T_{r0} - T_a$ has a direct limiting effect on the latent heat flux. This is not true for low LAI (LAI<0.5), as the transpiration is really small compared to the direct soil evaporation (Fig. 16b). Evaporation can still occur at low soil moisture hence the difference $T_{r0} - T_a$ is limited in this case. When the soil moisture increases for high vegetation cover, the plant stress decreases hence allowing ET to increase, consequently increasing the correlation between ET and $T_{r0} - T_a$. When the soil moisture value is larger than the threshold (generally separating water-limited and energy-limited evaporations regimes in this case) and it is located far enough above the wilting point (w_{wilt}=0.14[$m^3.m^{-3}$] in our case), then root zone soil moisture is no longer a limiting factor for transpiration. Under these conditions transpiration plays the role of regulator on the surface temperature by preventing the canopy temperature to deviate far from air temperature. Hence a negative correlation between ET and $T_{r0} - T_a$ emerges and the correlation will once again decrease (Fig. 16b).

The available energy correlation with $T_{r0} - T_a$ can be seen as the correlation of the sum of the sensible heat flux and latent heat flux with $T_{r0} - T_a$. For low soil moisture H

dominant over λE and hence the sum is highly and positively correlated with $T_{r0} - T_a$. Therefore the available energy is also highly and positively correlated with $T_{r0} - T_a$. As soil moisture increases and it is no longer a limiting factor, latent heat flux dominates sensible heat flux and becomes a compensating effect due to its negative correlation with $T_{r0} - T_a$. This will lead to an almost decorrelation between available energy and $T_{r0} - T_a$ under energy-limited evaporation regimes.

Because of these effects (most clearly evident in Figs. 16b and 16c for λE and λE+H correlation with $T_{r0} - T_a$), EF itself is very strongly, consistently and negatively correlated with $T_{r0} - T_a$ as shown in Fig. 16d. This constitutes a promising result as this temperature measure could become the building block for estimating EF based on observations and for model design. Radiative temperature can be obtained through remote sensing imagery and the air temperature can be estimated based on micrometeorological station data or atmosphere analyses. The latter is generally more spatially correlated due to atmospheric advection and mixing. This may be a fruitful path ahead for remote sensing estimation of EF and eventually evapotranspiration.

7. EF Shifts Due to Non-Precipitation Clouds

It is important to understand the effect of intermittency in radiation on EF daytime self-preservation. Specifically the question is how the passage of a non-precipitating cloud can influence the EF behaviour. Generally EF is defined for fair-weather conditions. This test will allow understanding the limitations of partially cloudy conditions on EF daytime self-preservation.

A cloud passing over the region for a short time can be roughly represented by a drop of incoming solar radiation. A simulation of a cloud passing over the site is reproduced by simply decreasing the value of the solar incoming radiation from 11AM to 3PM (Fig. 17a). All other conditions are kept the same in order to understand the first-order partial effect.

This cloud passage has a noticeable influence on EF, producing a jump of 0.05 (Fig. 17b). The partially-cloudy sky value of EF is always stronger than the fair day case,

as it has been shown that EF is a decreasing function of the solar incoming radiation. Moreover, the passage effect on EF remains even after the cloud left the scene, even if the difference remains small. Using the fair-weather EF instead of the cloudy one leads to a latent heat flux estimation error that can reach 20 [$W.m^{-2}$] (Fig. 17b). This represents 15% percent of the maximum energy difference of $S_{\downarrow}$ between the fair and partially cloudy weather conditions. Therefore it is important to derive a reliable estimate of instantaneous EF in order to avoid overall ET estimation errors, during cloudy days.

8. Time-of-Day Representativeness of EF

As shown in Figs. 5 and 8 the convex shape of the EF during daytime hours, especially the sharp rise in the late afternoon creates possibly severe biases in the estimation of evapotranspiration based on daytime EF given by (5). For the period of the experiment, the error can reach up to 30% of cumulative evapotranspiration (Fig. 18). As discussed in the analyses sections of this study, the error is strongly dependent on soil moisture (evaporation regime) and vegetation canopy sparsity. In particular, for semi-humid soil water conditions the relative error is at least 10% for lowest LAI values and soil moisture values around 0.2 [$m^3.m^{-3}$].

Lhomme (1999) also reported that using the mean daily value of EF to calculate ET will underestimate the latter in most cases. Results in Fig. 18 provide insight on how well ET can be estimated depending on LAI and soil water content conditions.

A relevant question is if there is a time of day when EF is most representative of the effective-daily value that is useful for evapotranspiration estimation. This has relevance for remote sensing-based estimation of EF based on sun-synchronous observations. Figure 19 shows that the hour of EF estimation is important to evapotranspiration estimation. Due to the inherent convex shape of EF during daytime with a minimum around noon, there will always be an underestimation of the daily ET using mid-day EF. Moreover, when using a measure of EF between 11AM and 3PM, the estimation error of the cumulative ET ranges between 20 to 40%. Therefore, using a constant EF assumption and a LST image around noon can lead to large ET estimation errors. This is due to a compensating effect: if EF is taken as a constant, it is more

efficient to have a value in the mid-afternoon that does not underestimate EF. However, it seems difficult to give a global best hour of measurements valid for any site, because the compensation will for sure depend on the surface and meteorological conditions of the study site. However there does seem to be, for a given LAI condition, a local hour (here 4 PM) such that the soil moisture dependencies are minimum. This result has to be confirmed further with different models and field experiment locations.

9. Conclusions

This study is aimed at diagnosing and providing insights into the diurnal behaviour of EF and its link with the soil moisture, vegetation canopy and major atmospheric conditions. In particular EF is found to be almost independent of the major forcing factors, namely incoming solar radiation and wind speed, due to compensating effects that are traced to the elements of EF itself. However these compensating effects can have strong dependence on soil moisture availability and canopy cover. Furthermore the temperature difference $T_{r0} - T_a$ is demonstrated to be well-correlated with the values of EF. This constitutes a promising indicator and tool for remote sensing applications, as this strong correlation for any kind of conditions will permit to reach a better estimate of the instantaneous EF. The daytime self-preservation of EF is an assumption that can be revised in order to obtain a better estimate of evapotranspiration. The convex shape of EF is ubiquitous and largely due to thermal inversions under the vegetation canopy. Again the degree to which the EF daytime self-preservation is relevant or breaks down is dependent on the evaporation regime (water-limited versus energy-limited) and on the fraction vegetation cover. This study also showed that the soil component of EF, namely EFs, can safely be assumed as constant contrary to the canopy component EFc. This constitutes an important result for assimilation of LST for dual-source surface energy balance models, as self-preserved daily parameters can be estimated more easily.

Acknowledgments

This work was carried out with support from the grant titled "Direct Assimilation of Remotely Sensed Land Surface Temperature for the Estimation of Surface Fluxes" from the National Aeronautics and Space Administration to Massachusetts Institute of Technology. The authors thank the SUDMED project team that shared the field experiment data from the region of Marrakech, Morocco.

Figures:

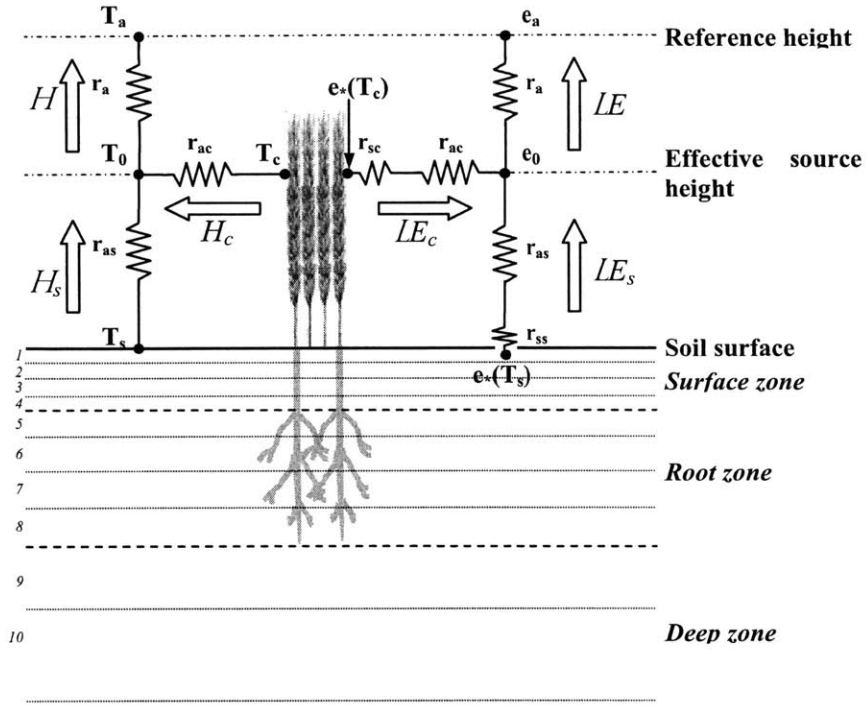

Fig. 1: Dual source (soil-canopy) resistance network. This model is coupled with a 10-layer diffusive soil model for heat and moisture transfer.

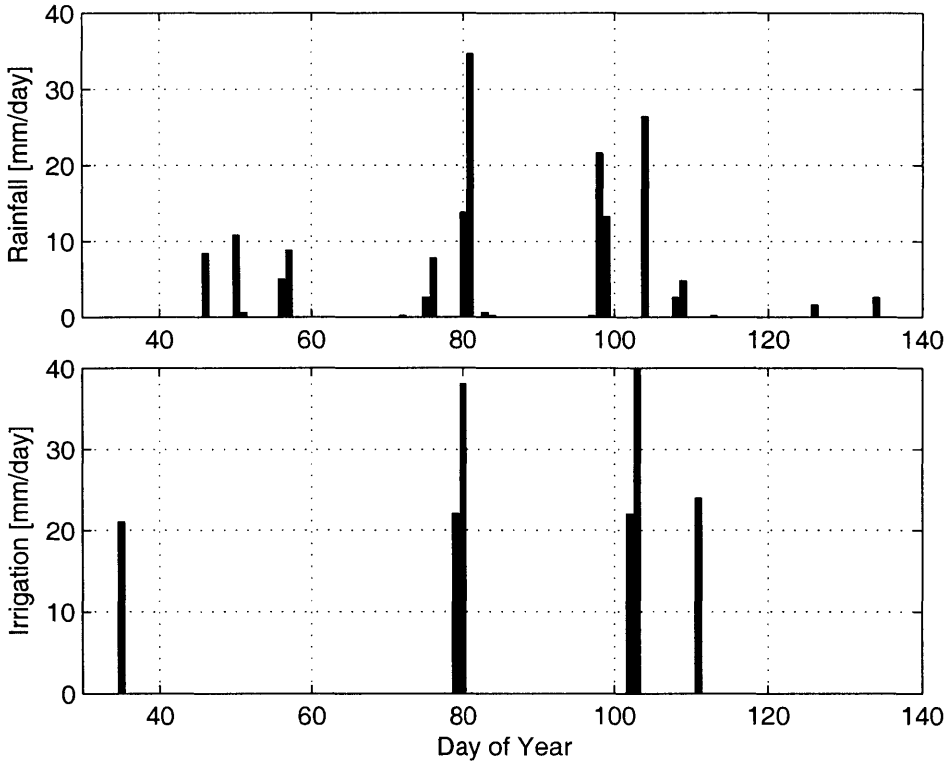

Fig. 2: Measured daily rainfall and estimated irrigation over R3 B123 in 2003

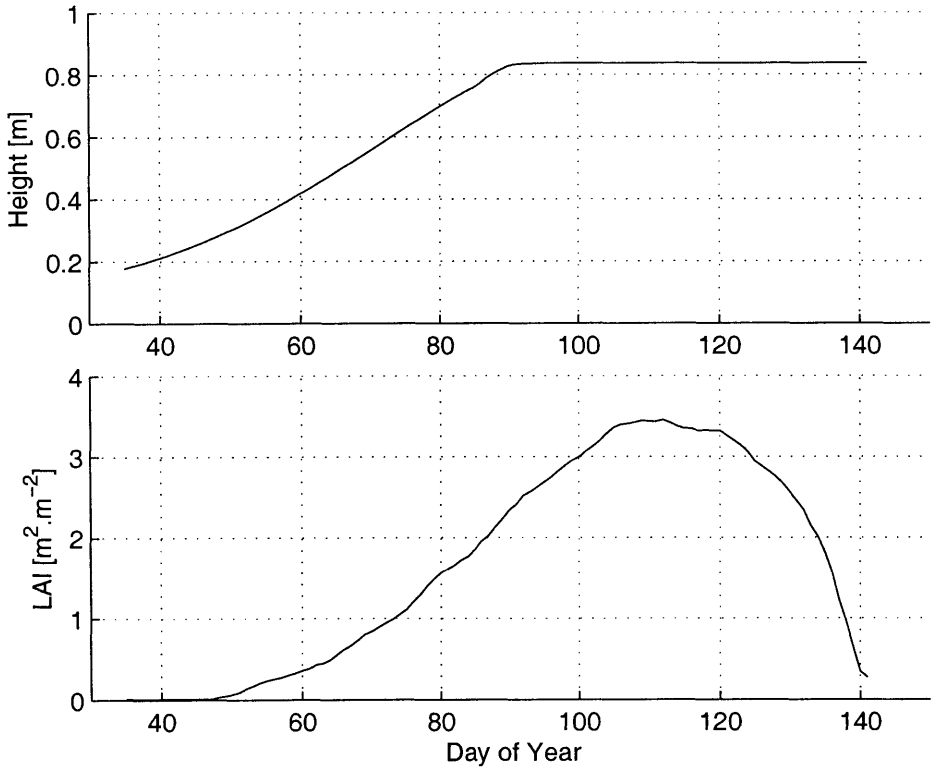

Fig. 3: Leaf Area Index and vegetation height measurements on R3B123 field in 2003

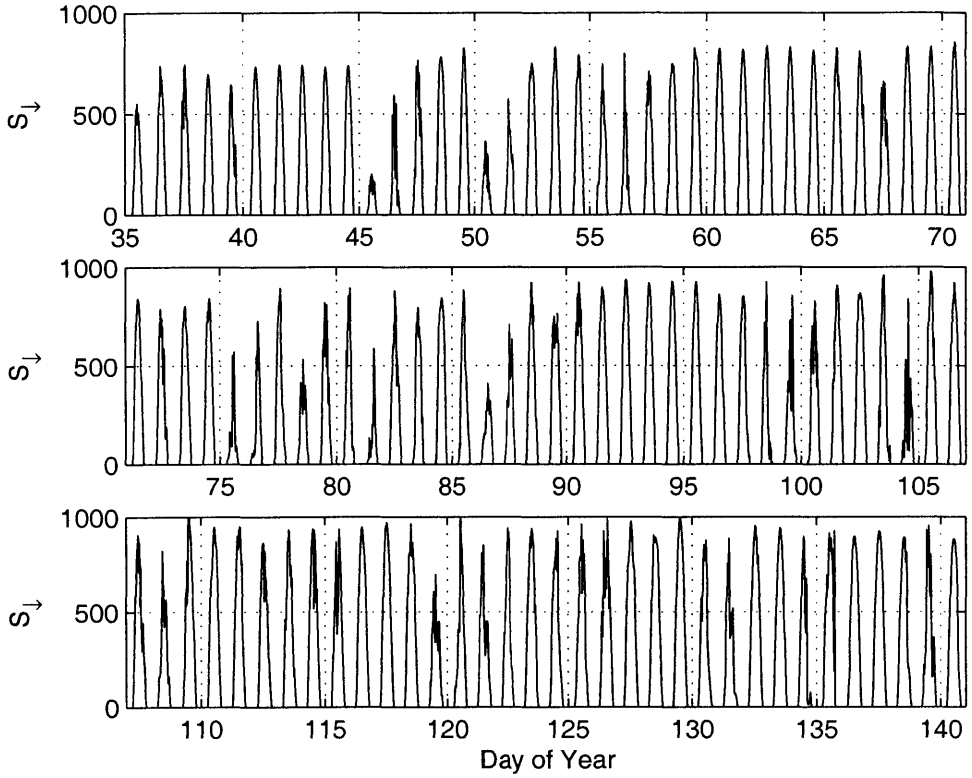

Fig. 4: Observed solar incoming shortwave radiation in W.m^{-2} over R3-B123 field in 2003

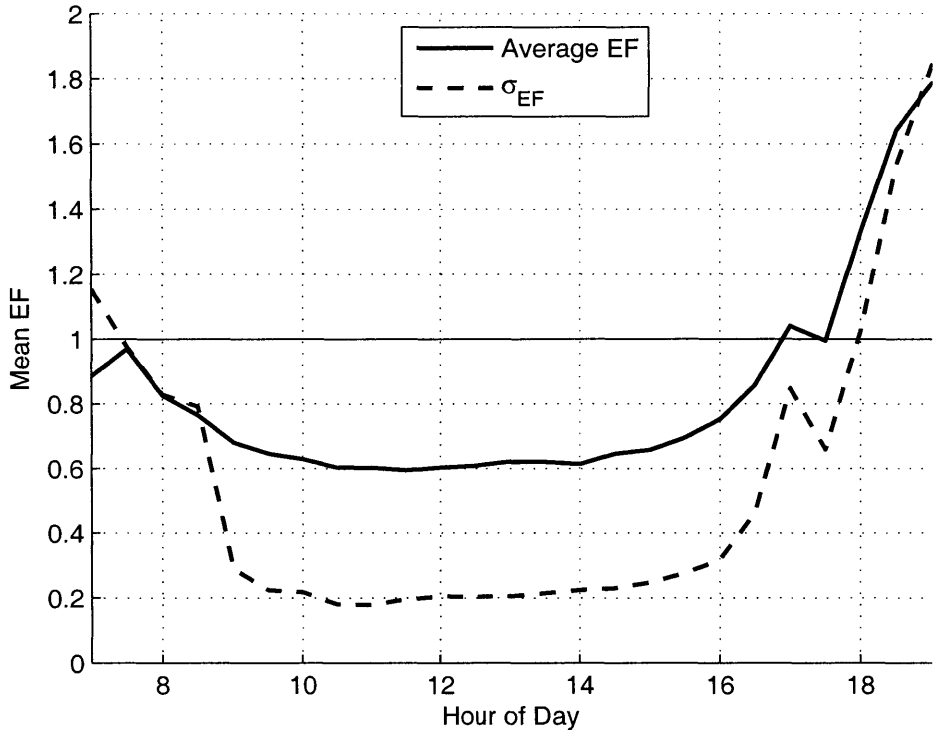

Fig. 5: Mean EF shape (solid line) and surrounding standard deviation (dashed line) using measured flux data on R3-B123 wheat parcel.

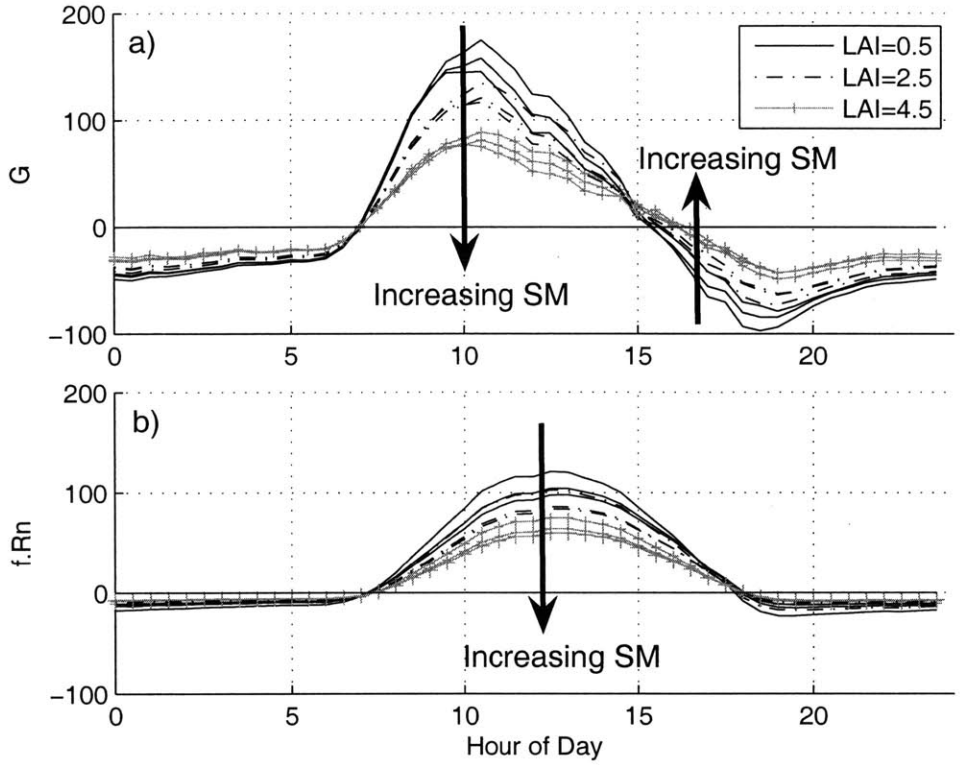

Fig. 6: Mean daily cycle of the SVAT modeled soil heat flux (a) and soil heat flux taken as fraction of the net radiation (b); for surface soil moisture (SM) values values of 0.1, 0.2, 0.3 [$m^3.m^{-3}$].

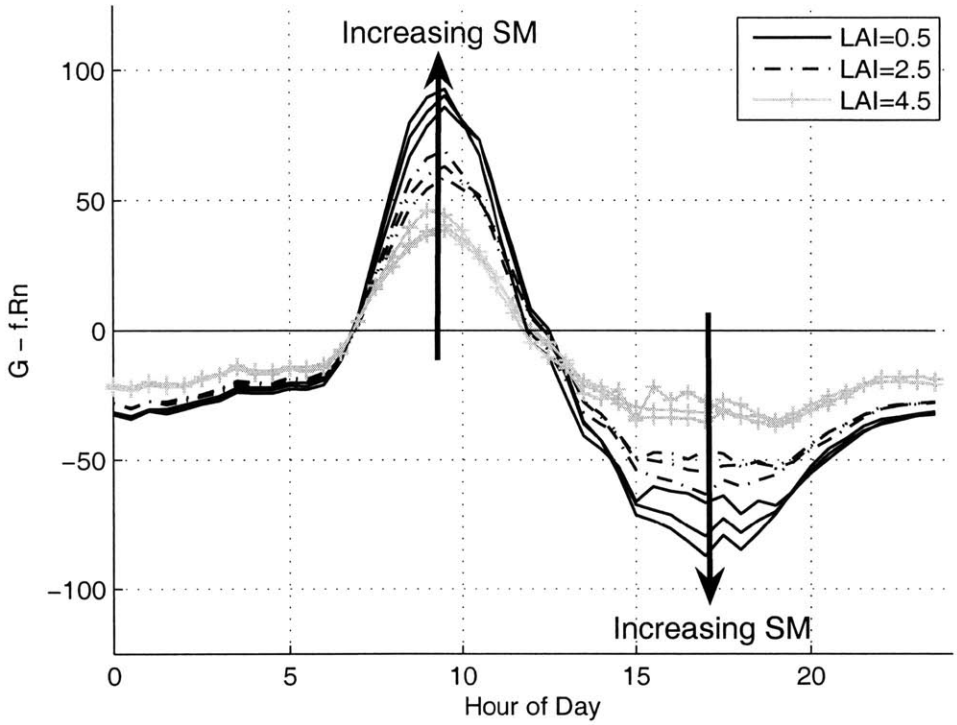

Fig. 7: Mean daily cycle of the difference between the SVAT modeled soil heat flux and the net radiation proportional heat flux; for surface soil moisture (SM) values of 0.1, 0.2, 0.3 [$m^3.m^{-3}$].

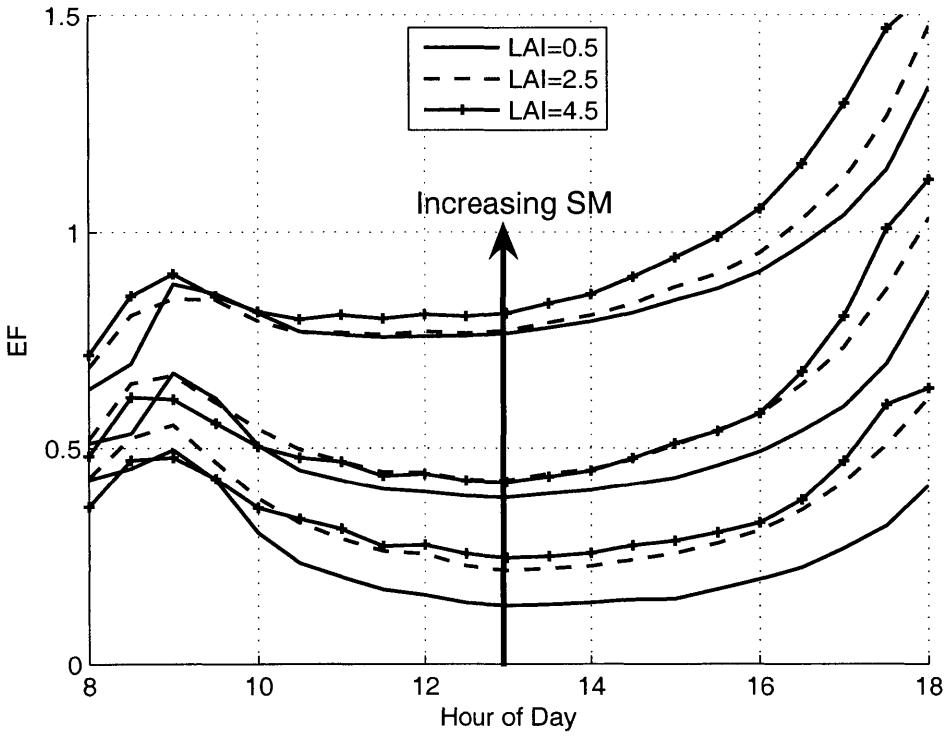

Fig. 8: Mean diurnal cycle of modeled Evaporative Fraction, from January 4th 2003 to May 21st 2003, for constant surface soil moisture (SM) values of 0.1, 0.2 and 0.3 [$m^3.m^{-3}$], and constant LAI values of 0.5, 2.5 and 4.5.

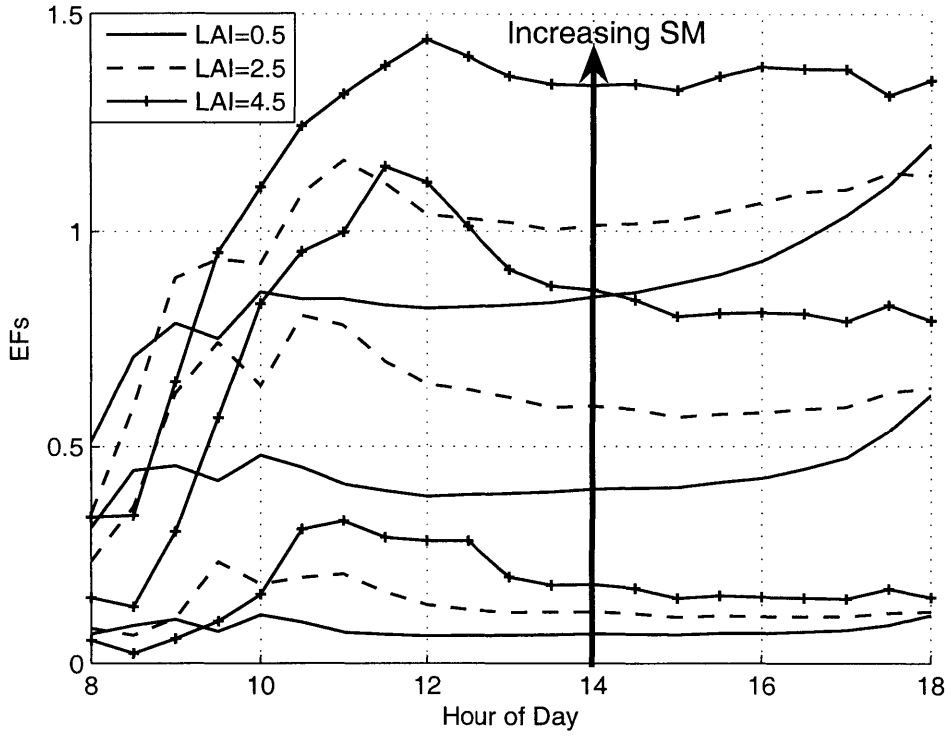

Fig. 9: Mean diurnal cycle of modeled soil Evaporative Fraction, from January 4th 2003 to May 21st 2003, for constant surface soil moisture (SM) values of 0.1, 0.2 and 0.3 [$m^3.m^{-3}$], and constant LAI values of 0.5, 2.5 and 4.5.

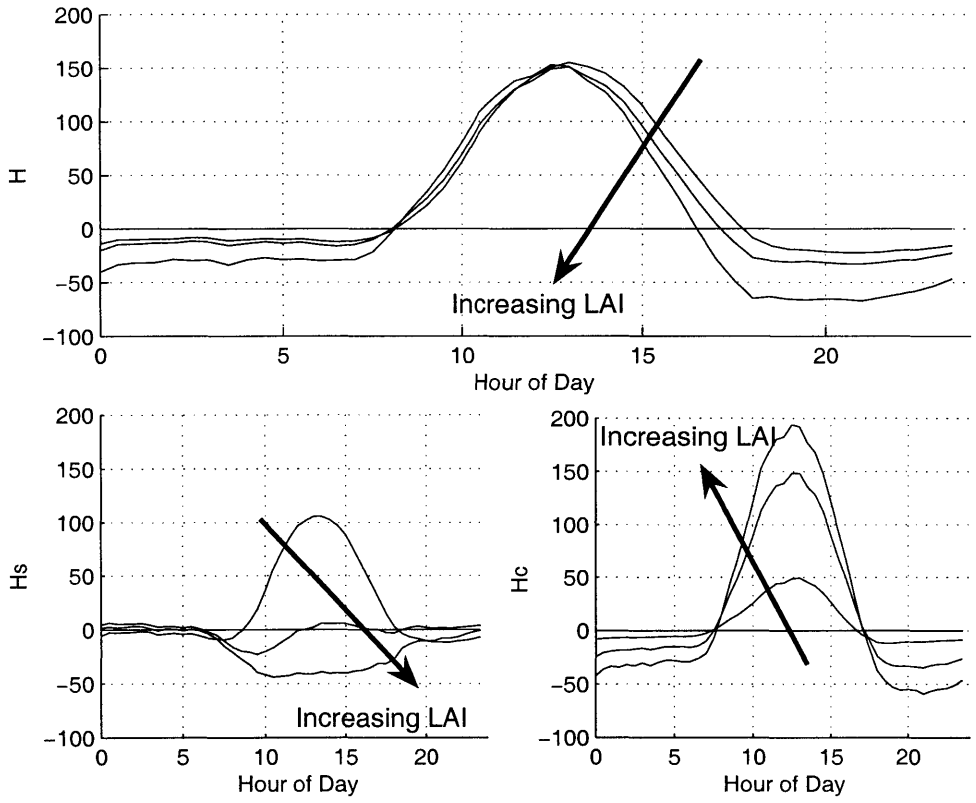

Fig. 10: Diurnal course of the total sensible heat flux (a), soil sensible heat flux (b), and canopy sensible heat flux (c) for a medium soil moisture value of 0.25 [$m^3.m^{-3}$], and constant LAI values of 0.5, 2.5 and 4.5 [$m^2.m^{-2}$].

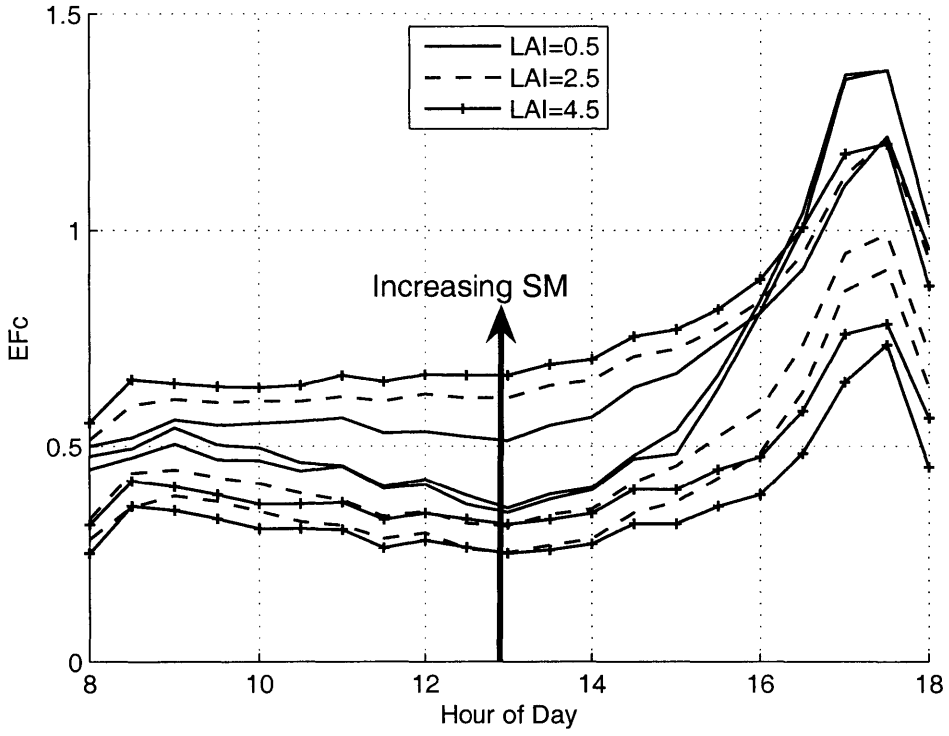

Fig. 11: Mean diurnal cycle of modeled canopy Evaporative Fraction, from January 4th 2003 to May 21st 2003, for constant surface soil moisture (SM) values of 0.1, 0.2 and 0.3 [$m^3.m^{-3}$], and constant LAI values of 0.5, 2.5 and 4.5.

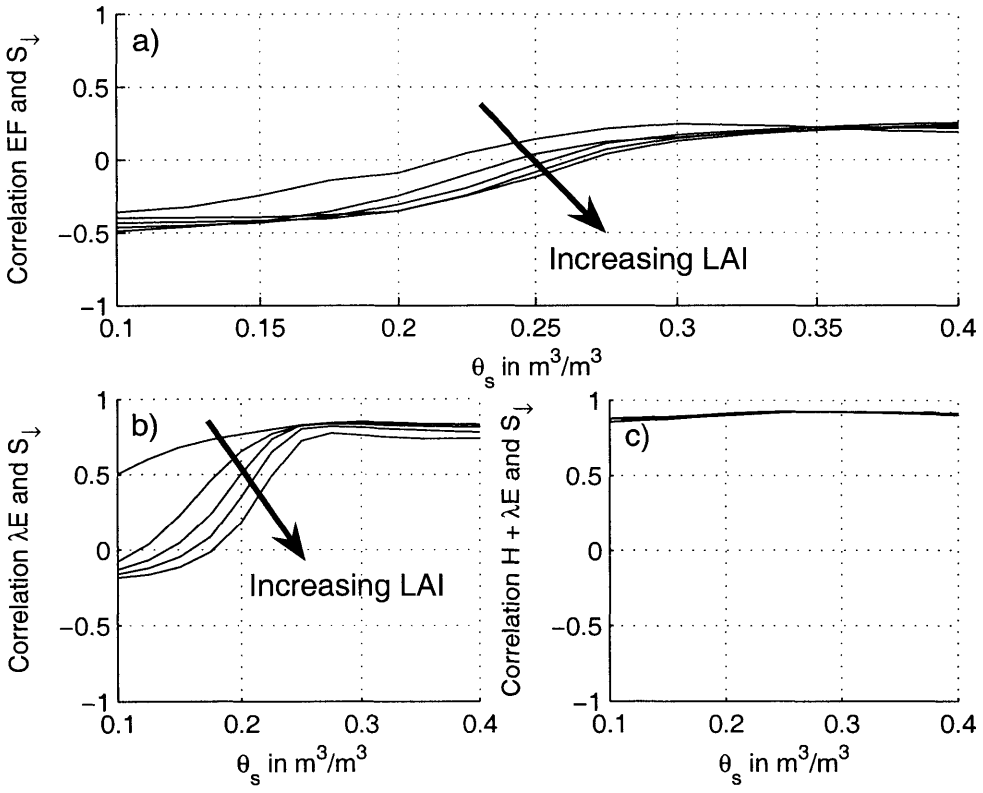

Fig. 12: Cross-correlation between (a) EF, (b) lE, (c) H+λE and solar incoming radiation over the January 4th-May 21st 2003 modeling period for constant LAI values of 0.5, 1.5, 2.5, 3.5 and 4.5.

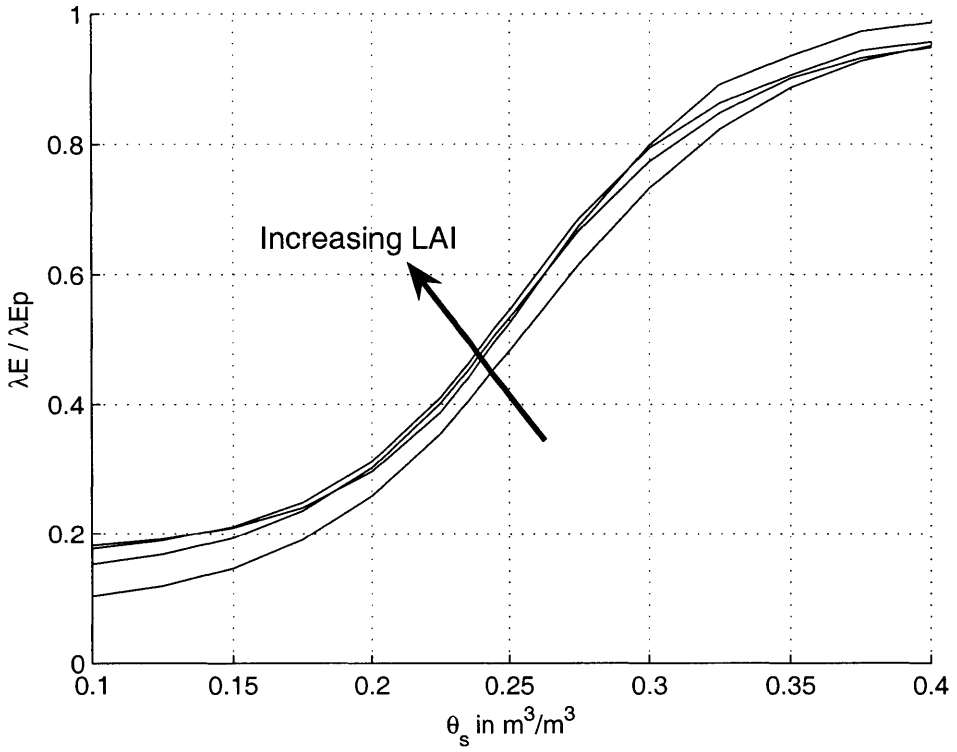

Fig. 13: Ratio of averaged daily latent heat flux over average daily potential latent heat flux for LAI=1, 2, 3 and 4.

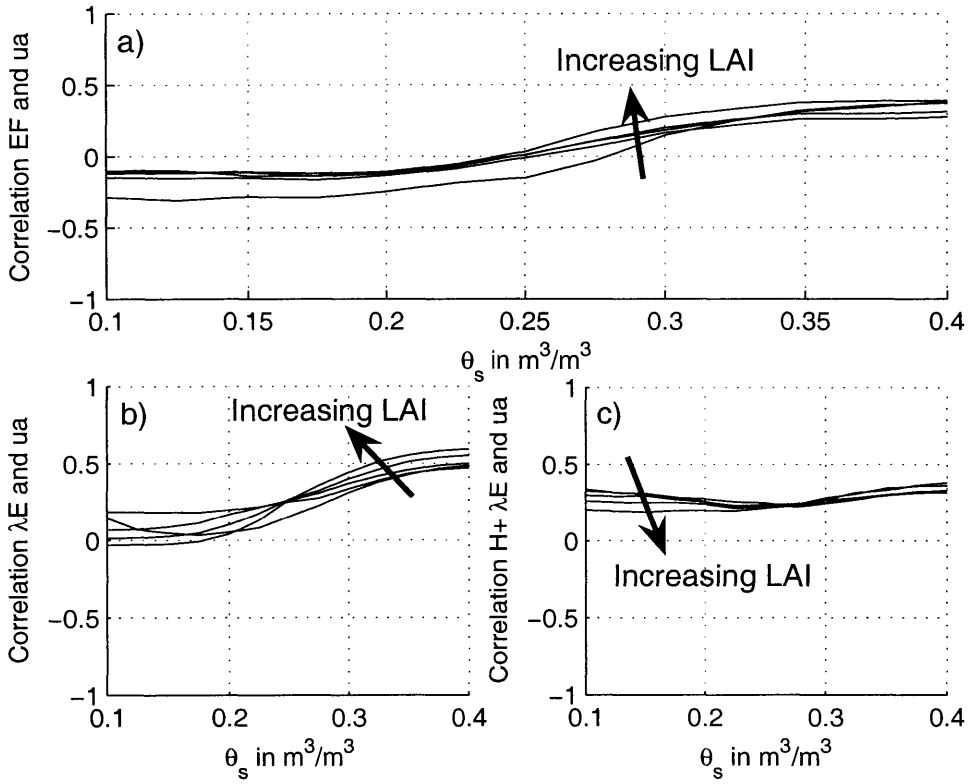

Fig. 14: Cross-correlation between (a) EF, (b) λE, (c) H+λE and wind speed over the January 4th-May 21st 2003 modeling period for constant LAI values of 0.5, 1.5, 2.5, 3.5 and 4.5.

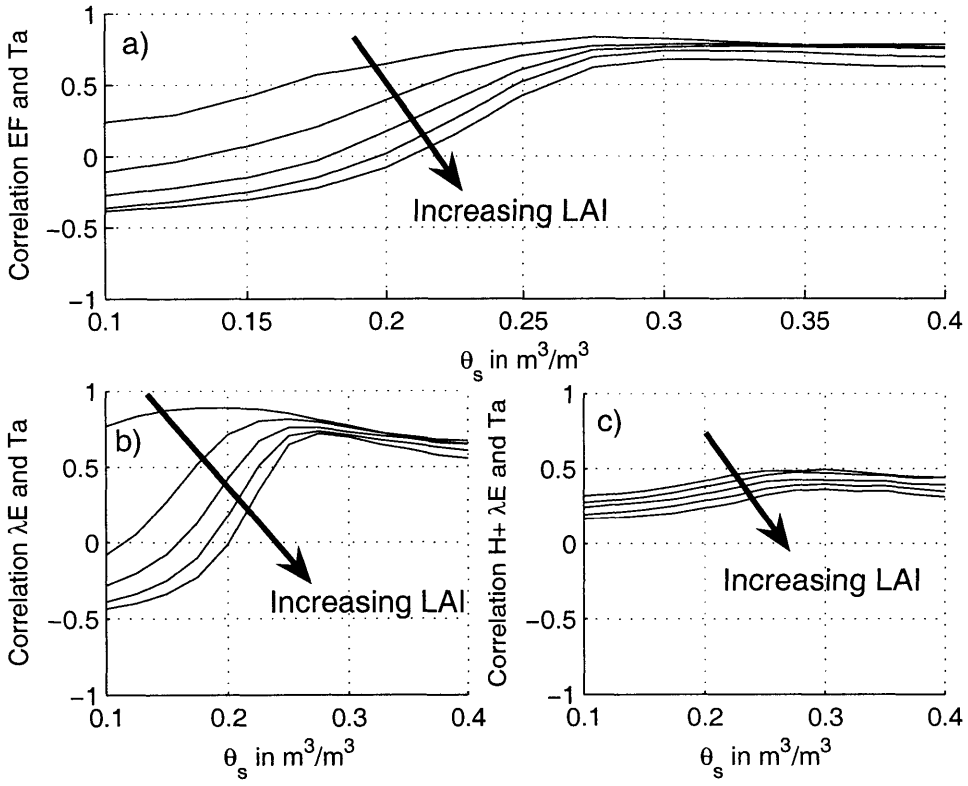

Fig. 15: Cross-correlation between (a) EF, (b) λE, (c) H+ λE and air temperature over the January 4th-May 21st 2003 modeling period for constant LAI values of 0.5, 1.5, 2.5, 3.5 and 4.5.

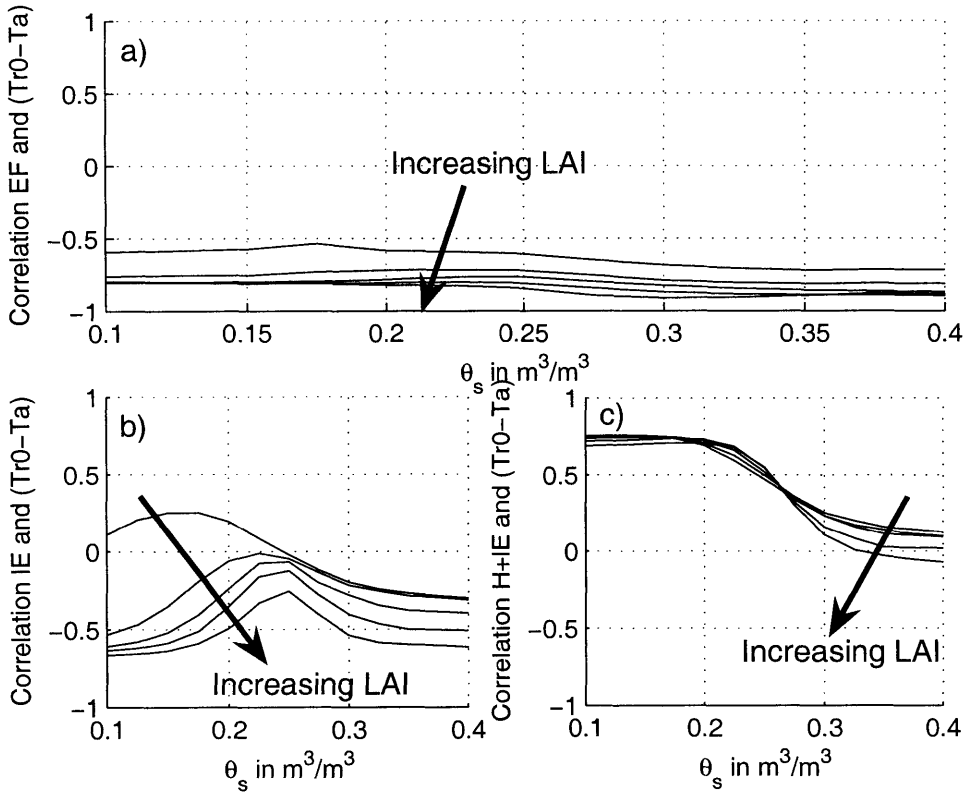

Fig. 16: Cross-correlation between (a) H, (b) λE, (c) H+ λE, (d) EF and the difference between the radiative and air temperatures over the January 4th-May 21st 2003 modeling period for constant LAI values of 0.5, 1.5, 2.5, 3.5 and 4.5.

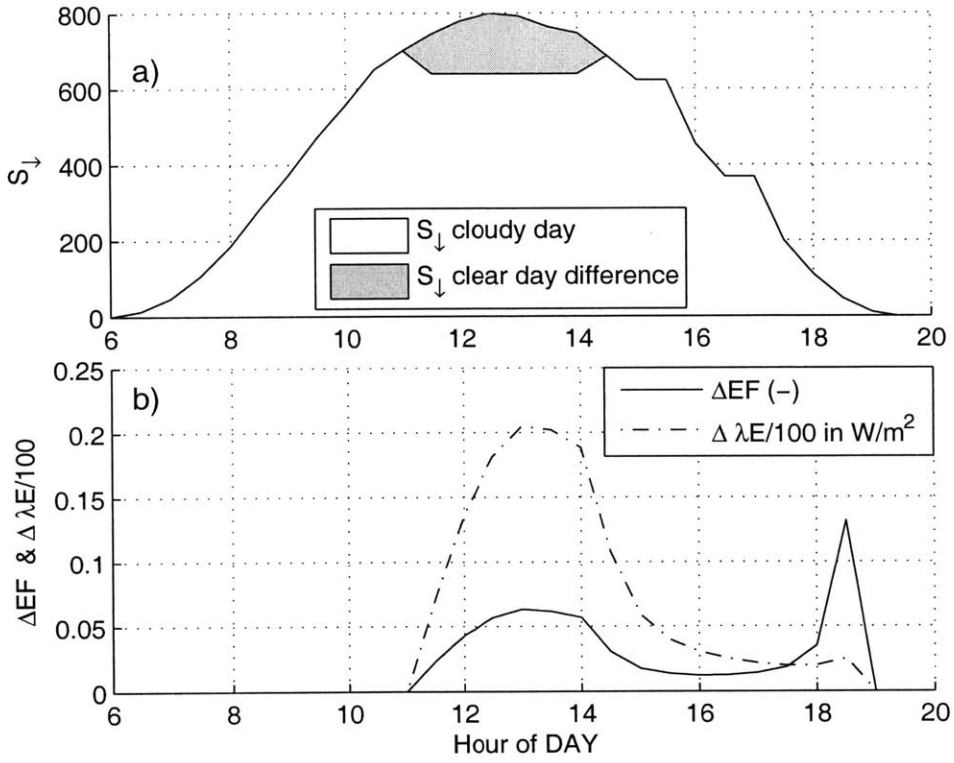

Fig. 17: Theoretical cloud event repercussion (a) on the solar incoming radiation and (b) resulting increased EF value, and its implication on the latent heat flux [W.m^2] estimation error.

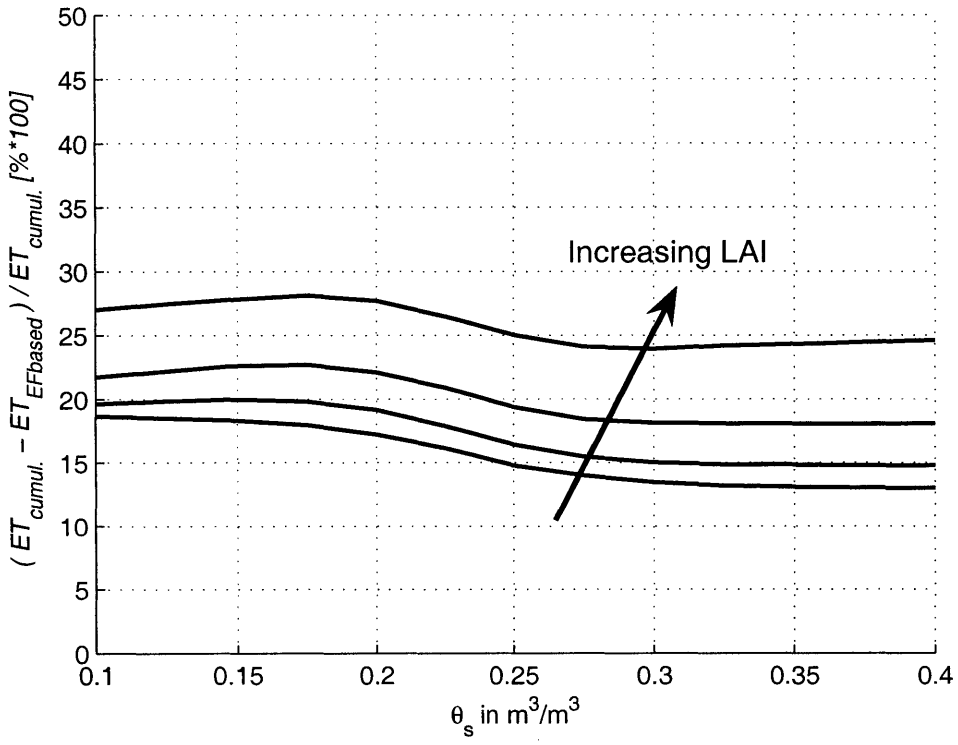

Fig. 18: Relative cumulative evapotranspiration error [%*100] from DAY 35 to DAY 141 using the daily mean EF value, for LAI equals to 0.5, 1.5, 2.5, 3.5 and 4.5.

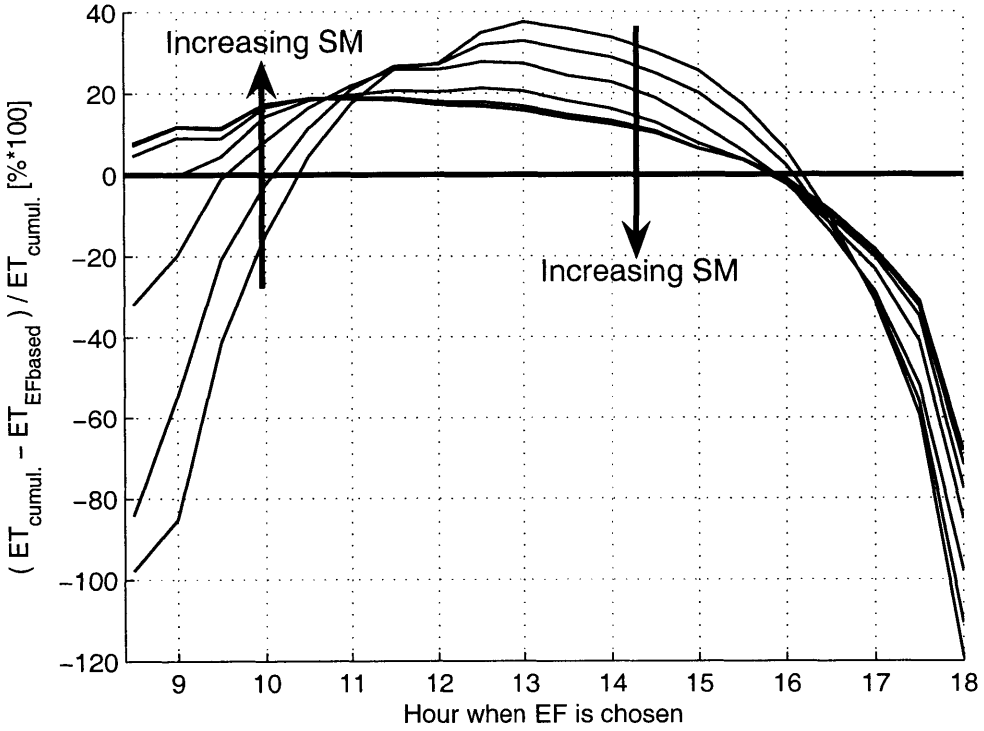

Fig. 19: Relative cumulative evapotranspiration error [%*100] from DAY 35 to DAY 141 using the EF value determined for different hours of the day, for constant surface soil moisture (SM) values of 0.1, 0.15, 0.2, 0.25, 0.3, 0.35 and 0.4 [$m^3.m^{-3}$].

Appendix A: Model Description

This study is based on the soil-vegetation-atmosphere-transfer (SVAT) model called ICARE-SVAT. This model is calibrated and tested on two wheat parcels and one olive tree orchard during the 2002 and 2003 SUDMED field experiments.

A.1. Soil module

The evolution of ground temperatures is characterized by a classical heat diffusion equation following the approach introduced by DeVries (1958). The soil horizon is divided into different layers with their own soil properties and soil water content and temperature states. The horizontal diffusion is neglected leading to a one-dimensional vertical diffusive equation

$$\begin{cases} c\dfrac{\partial T}{\partial t} = \dfrac{\partial G}{\partial z} \\ G = k_T \dfrac{\partial T}{\partial z} \end{cases} \tag{A1}$$

Appendix B presents lists of symbols and their units.

The evolution of the soil moisture content is based on Boone (2002) diffusive moisture scheme in a snow-free case

$$\begin{cases} \dfrac{\partial w}{\partial t} = -\dfrac{\partial F}{\partial z} \quad when \quad 0 < w \le w_{sat} \\ F = -k\dfrac{\partial}{\partial z}(\psi + z) - \dfrac{D}{\rho_w}\dfrac{\partial \psi}{\partial z} - K_d \end{cases} \tag{A2}$$

The soil water content is the water state variable of the SVAT model. To calculate the water matric potential ψ the Brooks & Corey (1966) relationship between the soil water content and the soil matric potential is used

$$\psi_2(w_2) = \psi_{sat}\left(\frac{w_2}{w_{sat}}\right)^{-B} \tag{A3}$$

Where B is the shape parameter of the retention curve. The parameters of the curves were calibrated based on soil samples from SUDMED.

The discretized equations are solved using a Crank-Nicholson algorithm, with a Crank-Nicholson parameter $CN = 1/2$ with 16 nodes.

A2. Dual-Source Energy Fluxes

The approach used for the soil and vegetation exchange of heat and water with the atmosphere is the one-dimensional, two-layer resistance network introduced by Shuttleworth and Wallace (1985) (see Fig. 1), in which soil and vegetation are independent sinks/sources of heat fluxes. In this field experiment case (sparse vegetation) the series resistance approach performed better than the parallel formulation of Boulet (1999). The net radiation available above the canopy is divided into a soil and canopy radiation

$$R_n = R_n^s + R_n^c \tag{A4}$$

$$\begin{aligned} R_n^c = {} & (1-b_0)(1-\alpha_c)\left[\frac{1+\alpha_s b_0}{1-(1-b_0)\alpha_s\alpha_c}\right]S_\downarrow + \left[(1-b_0)\varepsilon_c + \frac{(1-b_0)b_0(1-\varepsilon_s)\varepsilon_c}{1-(1-b_0)(1-\varepsilon_s)(1-\varepsilon_c)}\right]L_\downarrow \\ & -(1-b_0)\varepsilon_c\left[1+\frac{b_0(1-\varepsilon_s)+\varepsilon_s}{1-(1-b_0)(1-\varepsilon_s)(1-\varepsilon_c)}\right]\sigma T_c^4 + \left[\frac{(1-b_0)\varepsilon_s\varepsilon_c}{1-(1-b_0)(1-\varepsilon_s)(1-\varepsilon_c)}\right]\sigma T_s^4 \end{aligned} \tag{A5}$$

$$\begin{aligned} R_n^s = {} & \frac{b_0(1-\alpha_s)}{1-(1-b_0)\alpha_s\alpha_c}S_\downarrow + \left[\frac{(1-b_0)\varepsilon_s\varepsilon_c + b_0\varepsilon_s}{1-(1-b_0)(1-\varepsilon_s)(1-\varepsilon_c)}\right]L_\downarrow \\ & -\left[\frac{(1-b_0)\varepsilon_s\varepsilon_c + \varepsilon_s b_0}{1-(1-b_0)(1-\varepsilon_s)(1-\varepsilon_c)}\right]\sigma T_s^4 + \left[\frac{(1-b_0)\varepsilon_s\varepsilon_c}{1-(1-b_0)(1-\varepsilon_s)(1-\varepsilon_c)}\right]\sigma T_c^4 \end{aligned} \tag{A6}$$

which follows Taconet et al. (1986). The energy budget is closed for both the canopy and the soil compartments

$$R_n^s - H_s - \lambda E_s - G = 0 \tag{A7}$$

$$R_n^c - H_c - \lambda E_c = 0 \tag{A8}$$

As proposed by Shuttleworth and Wallace (1985), a mean air flow at the source level is used. Energy exchange is located between this source and the soil, the canopy, or the above canopy reference height. The heat fluxes are expressed as a function of the resistances, temperatures and vapour pressures at the different nodes of interest.

The latent heat fluxes can be expressed with those resistances as

$$\lambda E_s = \frac{\rho . c_p}{\gamma}\frac{e^*(T_s) - e_0}{r_{as} + r_{ss}} \tag{A9}$$

$$\lambda E_c = \frac{\rho.c_p}{\gamma} \frac{e^*(T_c) - e_0}{r_{ac} + r_{sc}} \tag{A10}$$

$$\lambda E = \frac{\rho.c_p}{\gamma} \frac{e_0 - e_a}{r_a} \tag{A11}$$

Similarly the sensible heat fluxes are expressed as

$$H_s = \rho.c_p \frac{T_s - T_0}{r_{as}} \tag{A12}$$

$$H_c = \rho.c_p \frac{T_c - T_0}{r_{ac}} \tag{A13}$$

$$H = \rho.c_p \frac{T_0 - T_a}{r_a} \tag{A14}$$

Where T_0 is the mean temperature value at the source level within the canopy. Based on (A12-A14) T_0 can be explicitly written as

$$T_0 = \frac{T_a / r_a + T_s / r_{as} + T_c / r_{ac}}{1/r_a + 1/r_{as} + 1/r_{ac}} \tag{A15}$$

Similarly based on (A9-A11), e_0 can be explicitly written as

$$e_0 = \frac{e_a / r_a + e^*(T_s)/(r_{as} + r_{ss}) + e^*(T_c)/(r_{ac} + r_{sc})}{1/r_a + 1/(r_{as} + r_{ss}) + 1/(r_{ac} + r_{sc})} \tag{A16}$$

All aerodynamic resistances are based on Choudhury and Monteith (1988) with inclusion of atmospheric static-stability correction. The aerodynamic resistance r_a (for heat and water vapour) is calculated as in Brutsaert (1982)

$$r_a = \frac{\ln\left(\frac{z_r - d}{z_{0_h}}\right) - \psi_h\left(\frac{z_r - d}{L_{mo}}\right)}{K.u^*} \tag{A17}$$

where

$$u^* = \frac{Ku_a}{\ln\left(\frac{z_r - d}{z_0}\right) - \psi_m\left(\frac{z_r - d}{L_{mo}}\right)} \tag{A18}$$

ψ_h and ψ_m represent the integral adiabatic correction functions, respectively, for heat and momentum given by Paulson (1970). The stability correction is computed using the Monin-Obukhov length scale

$$L_{mo} = -\rho c_p T_a u_*^3 / K g_0 H \tag{A19}$$

The zero displacement height and the roughness length for momentum z_0 are determined following Choudhury and Monteith (1988) for wheat

$$d = 1.1h \ln(1 + X^{1/4}) \tag{A20}$$

$$X = C_d.(LAI_{green} + LAI_{dry}) \tag{A21}$$

$$z_0 = \begin{cases} z_{0_s} + 0.3hX^{1/2}, 0 < X \le 0.2 \\ 0.3h(1 - d/h), 0.2 < X \le 1.5 \end{cases} \tag{A22}$$

where C_d is the main drag coefficient assumed to be uniform within the canopy.

The aerodynamic resistance between ground surface and within canopy source height is estimated using the approach proposed by Shuttleworth and Gurney (1990)

$$r_{as} = \frac{h.\exp(\alpha)}{\alpha K_h}\left[\exp\left(-\frac{\alpha.z_{0_s}}{h}\right) - \exp\left(-\frac{\alpha.(z_0 + d)}{h}\right)\right] \tag{A23}$$

where

$$K_h = K.u^*(h - d) \tag{A24}$$

The bulk boundary layer resistance to heat and water vapour in the canopy, is computed following Choudhury and Monteith (1988)

$$r_{ac} = \frac{100\alpha'}{2(LAI_{green} + LAI_{dry})}\sqrt{\frac{W}{u_h}}\frac{1}{1 - e^{-\alpha'/2}} \tag{A25}$$

The soil resistance to evaporation is an empirical resistance whose parameters are calibrated based on the bare soil observations during SUDMED field experiment. The exponential formulation of Passerat De Silans (1986) is used

$$r_{ss} = \exp(A - B \times w_s / w_{fc}) \tag{A26}$$

where A and B are calibrated empirical coefficients determined to be A=11 [ln(s/m)] and B=11[ln(s/m)] for the study site.

The bulk stomatal resistance r_{sc}, follows the classical Jarvis (1976) representation (as in Choudhury (1985)). Green and dry LAI are distinguished. They respectively

appears as LAI_{green} from LAI_{dry} in this resistance expression. Plant transpiration is only regulated by the green part of the plant that is photosynthetically active. Thus the stomatal resistance is taken to be

$$r_{sc} = \frac{r_{sc,\min}}{LAI_{green}} . f_1(S_\downarrow) f_2(w_2) f_3(e^*(T_a) - e_a) f_4(T_c - T_a) \qquad \text{(A27)}$$

where $f_1(S_\downarrow)$ is a stress function related to the solar incoming radiation

$$f_1(S_\downarrow) = \frac{1+f}{f + \dfrac{r_{s,\min}}{r_{s,\max}}}, \quad where \quad f = 0.011 \frac{2S_\downarrow}{LAI_{green}} \qquad \text{(A28)}$$

The water stress is expressed as in Noilhan and Planton(1989)

$$f_2(w_2) = \begin{cases} 1 & when \quad w_2 > w_{fc} \\ \dfrac{w_{fc} - w_{wilt}}{w_2 - w_{wilt}} & when \quad w_{fc} \geq w_2 \geq w_{wilt} \\ +\infty & when \quad w_2 < w_{wilt} \end{cases} \qquad \text{(A29)}$$

The water vapor stress factor depends on the vapour pressure deficit

$$f_3(e^*(T_a) - e_a) = \frac{1}{1 - D_P\left(e^*(T_a) - e_a\right)} \qquad \text{(A30)}$$

The temperature stress factor depends on the canopy and air temperature difference

$$f_4(T_c - T_a) = \frac{1}{1 - D_T\left(T_c - T_a\right)^2} \qquad \text{(A31)}$$

Calibrations at the study site resulted in minimum stomatal resistance rs_{min}=90 [$s.m^{-1}$], vapor pressure deficit coefficient D_P=1.5 [Pa^{-1}] and temperature stress coefficient D_T=1.5 [K^{-2}].

Appendix B: List of Variables and Their Units

Greek Letters

α_c	*Canopy albedo (0.22 dimensionless)*
α_s	*Bare soil albedo (0.20 dimensionless)*
γ	*Psychrometric constant (0.66e-3 bar.K^{-1})*
ε_c	*Canopy emissivity (0.98 dimensionless)*
ε_s	*Bare soil emissivity (0.96 dimensionless)*
λ	*Latent heat of vaporisation at the triple point Tt=273.16K (2.45e6 J.kg^{-1})*
λEc, λEs, λE	*Latent heat fluxes respectively above the canopy, from the bare soil and from the ground (W.m^{-2})*
ρ	*Density of air (1.2 kg.m^{-3})*
ρ_w	*Density of water (1000 kg.m^{-3})*
σ	*Stefan-Boltzmann constant (5.6705e-8 W.m^{-2}.K^{-4})*
ψ_2	*Soil water potential in the root zone (m)*
ψ_f	*Water foliar potential (m)*
ψ_{fc}	*Soil water potential at field capacity depending on soil characteristics (m)*
ψ_{sat}	*Soil water potential at saturation depending on soil characteristics (m)*
ψ_{wilt}	*Soil water potential at wilting point depending on soil characteristics (m)*

Latin letters

B	*Slope of the retention curve depending on the soil characteristics- exponent relating soil matric potential to soil moisture content (dimensionless)*
c	*Soil heat capacity (J m^{-3}.K^{-1})*
c_p	*Specific heat of air at constant pressure (1012 J.kg^{-1}.K^{-1})*
D	*Isothermal vapour conductivity (kg.m^{-2}.s^{-1})*
$e^*(T)$	*Saturated vapour pressure at temperature T (mbar)*
e_0	*Vapour pressure at within canopy source height (mbar)*

e_a	*Vapour pressure at above canopy reference height (mbar)*
g	*Gravity acceleration (9.81 $m.s^{-2}$)*
G	*Ground heat flux($W.m^{-2}$)*
h	*Vegetation height (m)*
Hc, Hs, H	*Sensible heat fluxes respectively above the canopy, from the bare soil and from the ground ($W.m^{-2}$)*
k	*Hydraulic conductivity ($m.s^{-1}$)*
k_T	*Soil thermal conductivity ($W.K^{-1}.m^{-2}$)*
K	*Von Karman's constant (0.4 dimensionless)*
$L\downarrow$	*Longwave incoming solar flux at the top of the canopy ($W.m^{-2}$)*
LAI_{dry}	*Dry Leaf Area Index (dimensonless)*
LAI_{green}	*Green Leaf Area Index (dimensionless)*
P	*Precipitation reaching the soil per unit ($mm.s^{-1}$)*
r_a	*Aerodynamic resistance between within canopy source height and above canopy reference height ($s.m^{-1}$)*
r_{ac}	*Aerodynamic resistance between canopy and within canopy source height ($s.m^{-1}$)*
r_{as}	*Aerodynamic resistance between ground surface and within canopy source height ($s.m^{-1}$)*
r_{sc}	*Bulk stomatal resistance of the canopy ($s.m^{-1}$)*
r_{ss}	*Surface resistance of the ground to evaporation ($s.m^{-1}$)*
r_{smin}	*Minimum stomatal resistance ($50\ s.m^{-1}$ for wheat and $150\ s.m^{-1}$ for olive trees)*
Rnc, Rns, Rn	*Net radiation respectively above the canopy, from the bare soil and from the ground ($W.m^{-2}$)*
$S\downarrow$	*Shortwave incoming solar flux at the top of the canopy ($W.m^{-2}$)*
T_0	*Mean air temperature at within canopy source height (K)*
T_2	*Mean temperature of the soil in the root zone (K)*
T_a	*Temperature of the air above the canopy at the reference height (K)*
T_c	*Mean temperature of the canopy (K)*
T_s	*Soil surface temperature (K)*

u^*	*Friction velocity ($m.s^{-1}$)*
u_0	*Wind speed at source height ($m.s^{-1}$)*
u_a	*Wind speed at reference level z_{ref} ($m.s^{-1}$)*
u_h	*Wind speed at top of the canopy: height h ($m.s^{-1}$)*
w_s	*Volumetric surface water content (dimensionless)*
w_2	*Mean volumetric soil moisture content in the root zone (dimensionless)*
w_{fc}	*Volumetric soil moisture content at field capacity (dimensionless)*
w_{sat}	*Volumetric soil moisture content saturation (dimensionless)*
w_{wilt}	*Volumetric soil moisture content at wilting point (dimensionless)*
W	*Characteristic leaf width (m)*

References:

Anderson M.C., Norman J.M., Diak G.R., 1997.

A two-source time-integrated model for estimating surface fluxes using thermal infrared remote sensing. Remote Sensing of Environment. 60 (2), 195-216.

Bastiaanssen W.G.M., Pelgrum H., Droogers P., 1997.

Area-average estimates of evaporation, wetness indicators and top soil moisture during two golden days in EFEDA. Agricultural and Forest Meteorology. 87 (2-3), 119-137.

Bastiaanssen W.G.M., Menenti M., Feddes R.A., 1998.

A remote sensing surface energy balance algorithm for land (SEBAL) - 1. Formulation. Journal of Hydrology. 213 (1-4), 198-212.

Bastiaanssen W.G.M., Pelgrum H., Wang J., 1998.

A remote sensing surface energy balance algorithm for land (SEBAL) - 2. Validation. Journal of Hydrology. 213 (1-4), 213-229.

Bastiaanssen W.G.M., Noordman E.J.M., Pelgrum H., 2005.

SEBAL model with remotely sensed data to improve water-resources management under actual field conditions. Journal of Irrigation and Drainage Engineering –ASCE. 131 (1), 85-93

Betts A.K., Viterbo P., Wood E., 1998. Surface energy and water balance for the Arkansas Red River basin from the ECMWF reanalysis. Journal of Climate. 11 (11), 2881-2897.

Boni, G., Castelli F., and Entekhabi D., 2000.

Sampling strategies and assimilation of ground temperature for the estimation of surface energy balance components. IEEE Trans. Geosci. Remote Sens. 39, 165–172.

Boni, G., Entekhabi D., and Castelli F., 2001.

Land data assimilation with satellite measurements for the estimation of surface energy balance components and surface control on evaporation. Water Resour. Res. 37, 1713– 1722.

Boone A., 2002. Description du Schéma explicite du sol : ISBA-DIF (ISBA-DIFfusion). CNRM-Météo-France, Internal note, July.

Boulet G., Chehbouni A., Braud I., 1999.

Mosaic versus dual source approaches for modelling the surface energy balance of a semi-arid land. Hydrology and Earth System Sciences. 3 (2), 247-258.

Brooks, R.H. and Corey A.T., 1966.

Properties of porous media affecting fluid flow. Journal Irrig. Drain. Div. Am. Soc. Civil Eng. 92 (IR2), 61-88.

Brutsaert W., 1975.

On a derivable formula for long-wave radiation from clear skies. Water Resources Research. 11 (5), 742-744.

CampbellG.S., 1974.

A simple method for determining unsaturated conductivity from moisture retention data. Soil Sci. 117, 311-314.

Castelli F., Entekhabi D., Caporali E., 1999.

Estimation of surface heat flux and an index of soil moisture using adjoint-state surface energy balance. Water Resources Research. 35 (10), 3115-3125.

Caparrini F., Castelli F., Entekhabi D., 2003.

Mapping of land-atmosphere heat fluxes and surface parameters with remote sensing data. Boundary-Layer Meteorology. 107 (3), 605-633.

Caparrini F., Castelli F., Entekhabi D., 2004.

Estimation of surface turbulent fluxes through assimilation of radiometric surface temperature sequences. Journal of Hydrometeorology. 5 (1), 145-159.

Caparrini F., Castelli F., Entekhabi D., 2004.

Variational estimation of soil and vegetation turbulent transfer and heat flux parameters from sequences of multisensor imagery.Water Resources Research. 40 (12) Paper No. 10.1029/2004WR003358.

Choudhury B.J. and Idso S.B. , 1985.

An empirical model for stomatal resistance of field-grown wheat. Agric. For. Meteorol. 36, 65-82.

Choudhury B.J. and Monteith J.L., 1988.

A four-layer model for the heat budget of homogeneous land surfaces. Royal Meteorological Society, Quarterly Journal. 114, 373-398.

Clothier B. E., Clawson K.L., Pinter P.J. Jr., Moran M.S., Reginato R.J., and Jackson R.D., 1986.

Estimation of soil heat flux from net radiation during the growth of alfalfa. Agric. For. Meteor., 37, 319–329.

Crago R., Brutsaert W., 1996.

Daytime evaporation and the self-preservation of the evaporative fraction and the Bowen ratio. Journal of Hydrology. 178 (1-4), 241-255.

Crago R., 1996.

Conservation and variability of the evaporative fraction during the daytime. Journal of Hydrology. 180 (1-4), 173-194.

Crago R., 1986.

Comparison of the evaporative fraction and the Priestley-Taylor alpha for parameterizing daytime evaporation. Water Resources Research. 32 (5), 1403-1409.

De Vries D. A., 1958.

Simultaneous transfer of heat and moisture in porous media. Eos, Trans. Amer. Geophys. Union. 39 (5), 909–916.

Deardorff J.W., 1978.

Efficient prediction of ground surface temperature and moisture with inclusion of a layer of vegetation. Journal of Geophysical Research. 83 (C4), 1887-1903.

Duchemin B, Hadria R, Erraki S, et al. 2006.

Monitoring wheat phenology and irrigation in Central Morocco: On the use of relationships between evapotranspiration, crops coefficients, leaf area index and remotely-sensed vegetation indices. Agricultural Water Management. 79 (1), 1-27.

Dunne S. and Entekhabi D., 2006.

Land surface state and flux estimation using the ensemble Kalman smoother during the Southern Great Plains 1997 field experiment. Water Resources Research, 42 (1), W01407, doi:10.1029/2005WR004334.

Fuchs M., and Hadas A., 1972.

The heat flux density in a nonhomogeneous bare loessial soil. Bound-Layer Meteor. 3, 191–200.

Gilles R.R., Cui J., Carlson T.N., Kustas W.P., and Humes K.S., 1997.

Verification of the ''triangle'' method for obtaining surface soil water content and energy fluxes from remote measurements of NDVI and surface radiant temperature. Int. J. Remote Sens. 18, 3145– 3166.

Idso J., Aase K., and Jackson R.D., 1975.

Net radiation–soil heat flux relations as influenced by soil water content variations. Bound.-Layer Meteor. 9, 113–122.

Jarvis P.G., 1975.

Water transfer in plants. In: de Vries, D.A., Afgan, N.G. (Eds.), Heat and Mass Transfer in the Plant Environment. Scripta, Washington, DC, 369–394.

Jarvis P.G., 1976.

The interpretation of leaf water potential and stomatal conductance found in canopies in the field. Phil. Trans. R. Soc. London, Ser. B. 273, 593-610.

Kustas W.P., and Daughtry C.S.T., 1990.

Estimation of the soil heat flux/net radiation ratio from spectral data. Agric. For. Meteor. 49, 205–233.

Lhomme J.P. and Elguero E., 1999.

Examination of evaporative fraction diurnal behaviour using a soil-vegetation model coupled with a mixed-layer model. HYDROLOGY AND EARTH SYSTEM SCIENCES. 3 (2), 259-270.

LoSeen D., Chehbouni A., Njoku E., 1997.

An approach to couple vegetation functioning and soil-vegetation-atmosphere-transfer models for semiarid grasslands during the HAPEX-Sahel experiment. Agricultural and Forest Meteorology. 83 (1-2), 49-74.

Y. Ma, Z. Su, Z.-L. Li, T. Koike, M. Menenti, 2002.

Determination of regional net radiation and soil heat flux over a heterogeneous landscape of the Tibetan Plateau. Hydrological Processes. 16 (15), 2963-2971.

Moran M. S., Clarke T.R., Inoue Y., and Vidal A., 1994.

Estimating crop water deficit using the relation between surface-air temperature and spectral vegetation index. Remote Sens. Environ. 49, 246–263.

Mecikalski J.R., Diak G.R., Anderson M.C., and Norman J.M., 1999.

Estimating fluxes on continental scales using remotely-sensed data in an atmospheric-land exchange model. J. Appl. Meteorol. 35, 1352-1369.

Monteith J.L., 1981.

Evaporation and surface temperature. Quart. J. R. Meteorol. Soc. 107, 1-27.

Nichols W.E., Cuenca R.H., 1993.

Evaluation of the evaporative fraction for parameterization of the surface, energy-balance. Water Resources Research. 29 (11), 3681-3690.

Noilhan J. and Planton S., 1989.

A simple parameterization of land surface processes for meteorological models. Mon. Weather Rev. 117, 536-549.

Pellenq J. and Boulet G., 2004.

A methodology to test the pertinence of remote-sensing data assimilation into vegetation models for water and energy exchange at the land surface. Agronomie. 24, 197-204, DOI: 10.1051/agro:2004017.

Reichle, R., McLaughlin, D., and D. Entekhabi, 2002.

Hydrologic data assimilation with the ensemble Kalman filter. Monthly Weather Review. 130 (1), 103-114.

Santanello J.A., Friedl M.A., 2003.

Diurnal covariation in soil heat flux and net radiation. Journal of Applied Meteorology. 42 (6), 851-862.

Shuttleworth W.J., and Wallace J.S., 1985.

Evaporation from sparse crops - an energy combination theory. Quart J Royal Meteorol Soc. 111: 839-855, 1985.

Shuttleworth W.J., Gurney R.J., Hsu A.Y., Ormsby J.P., 1989.

FIFE: The variation in energy partition at surface flux sites. IAHS Publ. 1989. 186, 67-74.

Shuttleworth W.J., and Gurney R.J., 1990.

The theoretical relationship between foliage temperature and canopy resistance in sparse crops. Quart J Royal Meteorol Soc. 116, 497-519.

Shuttleworth W.J., 1991.

Evaporation models in hydrology. In T.J. Schmugge and J. André, eds. Land surface evaporation, Springer, New York. 93-120.

Taconet, O., Bernard R, Vidalmadjar D., 1986.

Evapotranspiration over an agricultural region using a surface flux temperature model based on NOAA AVHRR data. Jounal of Climate and Applied Meteorology. 25 (3), 284-307, 1986.

Taconet O., Carlson T., Bernard R., 1986.

Evaluation of a surface vegetation parameterization using satellite measurements of surface temperature. Jounal of Climate and Applied Meteorology. 25 (11), 1752-1767.

3.2 Complementary results and discussion

3.2.1 Comparison with Lhomme 1999 results

The mean value of evaporative fraction during daytime EF_m and the mid-day evaporative fraction EF_m were plotted as function of different environmental factors, as done in Lhomme 1999 [32]. We have to notice that our definition of the mean diurnal value of EF is slightly different than Lhomme's:

$$EF_m = \frac{\int_{sunrise}^{sunset} \lambda E(\tau) d\tau}{\int_{sunrise}^{sunset} [H(\tau) + \lambda E(\tau)] d\tau}$$

So that if we know the total daily available energy at the surface, we can easily get the total daily evapotranspiration.

As seen on Figure B-12, EF is a decreasing function of maximum solar incoming radiation. Lhomme obtained pretty similar results in his paper with a decrease of the order of a third for a maximum solar incoming radiation between 500 W/m^2 and 1000 W/m^2. We have to notice that in our case EF decreases faster than in Lhomme's case, as the soil evaporative fraction is much more dependent on the solar incoming radiation and Lhomme only modeled the canopy component. Therefore, when solar incoming radiation doubles, EF lost is larger in our case: a half of its initial value. We can also notice that EF_m is always lower than EF_d, because of the concave-up diurnal shape of EF, with a minimum generally reached in the midday.

Surprisingly, EF is almost independent of the wind speed value as depicted on figure B-13. This constitutes an extremely important result, as it means that the repercussion of a change in wind speed on the sensible heat flux and the latent heat flux is equivalent. Physically, this means that the removal of thermal energy (through H), and water vapor (through λE) away from the surface are of the same order. This result wasn't intuitive at first. This is also a very important result for EF modeling, as the wind speed is clearly the most variable environmental factor in both space and time. As the meteorological station may not necessary be exactly at the location of interest, this wind speed decorrelation will be extremely useful. If one wants to

use remote sensing images to estimate evapotranspiration, it is difficult to directly estimate λE, because of the repercussion of the temporal and spatial wind speed variations on λE. It will be much easier to estimate EF, which does not depend much on the wind speed, provided that we can have a good estimate of the total energy available at the land surface to easily derive the latent heat flux.

One of the plots that could not fit the article required length is the cross-correlation between the air relative humidity and the Evaporative Fraction, see Figure B-14. This plot is very informative. First of all, the left-bottom plot depicts the correlation between the latent heat flux and air relative humidity. When soil water content is sufficient, in our case larger than 0.25 m^3/m^3 ($\theta_{fc} = 0.375\ m^3/m^3$), soil moisture is not anymore a limiting factor to evapotranspiration and the latent heat flux is directly limited by the water vapor pressure deficit.

$$\lambda E = \frac{\rho C_p}{\gamma} \frac{e_0 - e_a}{r_a} = \frac{\rho C_p}{\gamma} \frac{e_0 - RH_a e^*(T_a)}{r_a}$$

So we can understand the pretty strong negative correlation between air relative humidity and latent heat flux through the factor $RH_a e^*(T_a)$. The influence of this factor is diminished by the dependence of e_0, the air water vapor pressure at canopy level with the air relative humidity. Yet, a pretty strong negative correlation exists. When soil moisture is limited, i.e. in our case $\theta_s < 0.25\ m^3/m^3$, soil moisture becomes the most limiting factor, hence a decorrelation with λE occurs. This phenomenon is clearly depending on LAI, as transpiration can barely occurs close to wilting point, whereas soil evaporation can exists even for very low soil moisture contents. Therefore, for low LAI values, the latent heat flux will still be correlated with the air relative humidity, because of soil evaporation. For high LAI values, transpiration can hardly occur, leading to a decorrelation between latent heat flux and air relative humidity. The mean daily value of EF and its value at noon are also described as a function of air specific moisture q_a on figure B-16. We can see that EF is a slowly decreasing function of specific moisture. The soil evaporative fraction is almost insensitive to air specific moisture, contrary to the canopy evaporative fraction. Indeed, transpiration

is extremely dependent on the humidity contained in the air, whereas bare soil evaporation is not as much dependent on this factor. Finally, the global EF is only weakly dependent on air specific moisture at least for medium LAI values, in our case a LAI of 2 was used. The right-bottom plot shows the correlation between available energy and air relative humidity. As the sensible heat flux is not very dependent on relative air temperature, we finally just have a lower correlation for $H + \lambda E$, than for λE. Finally, the top plot shows the correlation between EF and air relative humidity. The compensating effects between the latent heat flux and the relative humidity leads to a small correlation for low soil water content and a very high negative correlation for high soil moisture, i.e. far away from water content at wilting point.

The last environmental factor influencing EF is the air temperature. Figure B-17 presents the link between EF_m, EF_d and the air temperature. EF ranges from 0.3 to 0.9 for temperature ranging from 10 to 30 $°C$. So it is clear from here on that air temperature is the most important environmental parameter determining the value of EF.

Another interesting study is the response of EF to the vegetation and soil characteristics. The variation of EF to a change in Leaf Area Index (LAI) is described on figure B-18. Surprisingly, EF is weakly sensitive to any change in LAI, wether EF is chosen at midday or on daily average. It is surprising as we know that transpiration is a more "efficient" process than soil evaporation. However, we have to notice that for high LAIs, the soil heat flux is very small compared to low vegetation cover. Hence, even for constant EF values, transpiration of a fully covering vegetation will be higher than soil evaporation over bare ground because of the difference in soil heat flux. Finally, when LAI increases a more important fraction of the incident energy will lead to evapotranspiration and a smaller fraction of it will propagate into the ground. This is a very interesting result, as the soil and canopy evaporative fractions are clearly depending on the LAI values. There is a positive compensative effect between the soil and canopy evaporative fractions that lead to an almost constant EF, with regards to LAI variations. This suggests that it will be easier to obtain a good estimate of evapotranspiration using the global EF value and not separated soil and

canopy components: EFs and EFc.

EF is also almost insensitive to any change in vegetation height, as seen on Figure B-19. And both the soil and vegetation components of the evaporative fraction are insensitive to a change in vegetation height. This a very important result for remote sensing applications, as the vegetation height is very difficult to estimate using remote sensing images. EF depends on LAI and not vegetation height, and LAI can be easily estimated from remote sensing.

Two important factors determining the value of the sensible and latent heat flux are the substrate roughness length z_{0s} and the ratio between the momentum and heat roughness lengths $\frac{z_{0m}}{z_{0h}}$. Surprisingly, the roughness length of the substrate z_{0s} has almost no influence on EF as seen on Figure B-20. This means that the contribution of the substrate roughness length on the sensible heat flux is proportional to its contribution on the latent heat flux. This is extremely useful as the knowledge of z_{0s} is very important to determine H and λE, but not EF. This constitutes a drastic advantage as z_{0s} is extremely difficult to measure, and can usually only be obtained by inversion of the sensible heat flux over bare soil. The results of the ratio between the momentum and heat roughness lengths $\frac{z_{0m}}{z_{0h}}$ are very equivalent and are described on Figure B-21. Once again there is almost no sensitivity of EF to a change in $\frac{z_{0m}}{z_{0h}}$. This also constitutes an interesting result, as this ratio is usually badly known and difficult to determine.

3.2.2 Variation of sensible and latent heat fluxes with soil moisture and LAI

It is very interesting to understand the dependency of the energy fluxes on soil moisture and LAI. This gives much insight on the behavior of EF, and its dependency on soil and vegetation conditions. The mean daily value of the sensible, latent and soil heat fluxes were plotted for different values of surface soil moisture and LAI.

As seen on Figure B-22, sensible heat flux is high for low soil moisture content and very low for high soil moisture content, this follows the intuitive concept on sensible

heat flux. It is also worth looking at the the soil and canopy fluxes independently. The soil sensible heat flux is pretty high for low LAIs, but when LAI increases, it can even become negative for most soil water conditions. When LAI increases at some point most energy will be received by the canopy and transpiration won't be large enough to avoid a temperature inversion between the soil and the canopy. Indeed, the canopy temperature becomes higher than the soil temperature, and sensible heat flux goes downward from the canopy to the soil. Hence, the soil sensible heat flux is negative, as the positive convention is directed upward. The daily mean canopy sensible heat flux is never negative, as it is almost impossible that the canopy temperature would be lower than the air temperature during the midday period. Canopy sensible heat flux is naturally very dependent upon LAI, and is much higher for high LAI values.

Latent heat flux has a very different behavior as it cannot become negative (see Figure B-24). Latent heat flux is clearly increasing when soil water content increases, as more water is available for evapotranspiration. We can also see that transpiration is very slightly more efficient than evaporation of the ground, and that they are both increasing when soil moisture increases.

Negative values of sensible heat fluxes will have an important repercussion on EF. Indeed, we saw that the soil sensible heat flux can easily become negative. Moreover, the sensible heat flux may also be negative at the beginning of the day and in the late afternoon before sunset, as the air temperature at reference height is then higher than the air temperature at canopy level, see B-23. Evaporative Fraction will hence be larger than one, in the early morning and late afternoon. At those times the evapotranspiration process is very efficient as it is reinforced by the added heat flux provided by the sensible heat flux: our soil-vegetation system becomes a sink of sensible heat flux i.e. a sink of thermal energy that can be converted into latent heat flux.

The soil heat flux is clearly very dependent on LAI as already discussed before. A lower soil heat flux will not necessary change the EF value as seen previously, but it will increase evapotranspiration, as EF remains almost constant as a function of LAI. So this emphasizes the importance of soil heat flux to evapotranspiration. Contrary

to what was stated by many papers, soil heat flux cannot be overlooked, and only its accurate determination will lead to an accurate estimation of evapotranspiration.

Finally, it is also interesting to understand the difference in evapotranspiration estimated with ICARE SVAT and the ET estimated using the mean daily value of EF. On figure B-26, the cumulative absolute error is plotted. The absolute error was plotted to avoid compensative effects of a poor evapotranspiration estimate. We see that the estimation error is clearly increasing with soil moisture and LAI. Indeed when soil moisture increases, more water is available for evapotranspiration, leading to generally larger evapotranspiration errors. It is also interesting that for a given soil moisture content, the error is increasing with LAI. This might be due to the fact that transpiration is larger than bare soil evaporation for the same soil conditions.

The second Figure B-27, represents this absolute error as a percentage of the total cumulated SVAT evapotranspiration. We can see that the relative error decreases with soil moisture, even if the amount of evapotranspiration error in [mm] is getting higher. In general, we are more interested in errors given in [mm] but the relative plot can give an idea of the relative degree of confidence in our evapotranspiration estimation.

Chapter 4

EF models

In order to improve the estimation of evapotranspiration, different models of Evaporative Fraction are defined and tested on our site. The results of the EF models were compared to a reference dual-source, diffusive soil model: ICARE-SVAT, that was calibrated and tested in 2002 on the SUDMED project, in Marrakech, Morocco. The model was calibrated and validated on two wheat field parcels, namely R3-B123 and R3-B130. Both the meteorological and phenological conditions were pretty different during this period leading to a very resistant calibration of the SVAT model. In the first part of the study, the EF models were tested using a combined-source formulation. Then a double-source formulation was being used and the EF values were determined at the same time for the canopy and soil components. The different EF models will be discussed and compared in the following parts.

4.1 Combined-source EF modeling

In this section, to estimate the total evapotranspiration (ET) different EF models were compared for different LAIs and soil moisture (SM) conditions. Combined-source models do not differentiate between the soil and canopy components of the fluxes, and only one parameter which is a mixture of vegetation transpiration and soil evaporation is estimated. As seen in the previous chapter, using only one EF and no separation between EF soil and EF canopy should be much easier and lead to a reasonable estimate of evapotranspiration. Indeed most environmental parameters and vegetation conditions have a small influence on EF, contrary to EFs and EFc. This is due to a compensating effect between EFs and EFc.

The first model uses the constant daily EF assumption and is named model O1. The second model uses a daily constant EF' assumption, which is defined as $EF' = \frac{EF}{EF_p}$. EF_p being the instantaneous potential evaporative fraction calculated using the micro-meteorological data. This model is named O2. The parameters (either EF or EF') were estimated at different hours of the day, as would be the case whith using remote sensing. Indeed the evapotranspiration parameters can only be estimated when a satellite is passing over the land, the passing time depending on the path of

the satellite.

Next, two following models use a weighted EF to compensate for the typical-concave up shape of EF, which generally leads to underestimation of evapotranspiration when using a daily constant EF assumption. In the A1 case, the weighting function is the net radiation, whereas the solar incoming radiation is used for the A2 model. Both net radiation and solar incoming radiation can be easily calculated and estimated.

The last two models use a very simple hyperbolic representation of EF to reproduce the concave-up diurnal cycle of EF. In these models, EF cannot exceed 1 and reaches is minimum, when the net radiation is maximum for model B1, or when the solar incoming radiation is maximum for model B2. A summary of the different EF models is presented in Table A.1. The comparison of the resulting ET of these models to the reference SVAT model ET were calculated for different LAI and soil moisture conditions. First, the combined-source models were used. For these models there is no distinction between the soil and canopy component and only one parameter is determined at once.

Generally, the worst performing models are models B1 and B2, as shown on Figure B-28. Those models are pretty empirical and are usually not able to correctly describe the diurnal behavior of EF. Therefore those models lead to a pretty strong ET estimation error compared to the reference SVAT model. The cumulated ET estimation error ranges between -50mm for a dry soil case ($\theta_s = 0.1\ m^3/m^3$) with LAI=4 and -150mm for a wet soil case ($\theta_s = 0.4\ m^3/m^3$) with LAI=4. Those are the largest errors compared to any model. Moreover we should notice that a bias is introduced when using those models, because even for a pretty dry soil case we have a systematic estimation error of about 50mm for a LAI of 4 and 30mm for lowest LAI values, this represents 30 to 50 percents of the total evapotranspiration, which is a very important ratio. This means that those models are always underestimating EF.

Then the second best group of models is the A group: A1 and A2. These models perform reasonably well in most cases as seen on B-28. They use an evaporative fraction weighted by respectively the solar incoming radiation and the net radiation

at the surface. For LAI=1, the cumulated evapotranspiration error ranges between 0 and -40mm and for LAI=4, this ranges between -20 and -100mm. Moreover for low soil moisture values the bias of the cumulated evapotranspiration error is almost zero. We may also notice that model A1 is generally slightly more accurate then model A2. Indeed the diurnal behavior of EF is depending on the net radiation through its denominator. EF is only indirectly related to the solar incoming radiation, and net radiation and solar incoming radiation may sometimes not be exactly in phase.

The most interesting models are O1 and O2. The O1 model is based on the diurnal constant EF assumption and O2 assumes that the ratio between potential evaporative fraction for zero bulk resistance, i.e. non stressed plant, is a daily constant. The value of EF or $EF' = \frac{EF}{EF_p}$ are determined at a given time of day, usually when a satellite is passing over the region of interest. Therefore, those models were tested choosing different hours of the day to estimate EF or EF'. Those parameters were estimated from 10AM to 4PM every hour. This variation of the time of measurement can lead to dramatic changes in the estimated evapotranspiration. As already seen, EF in the mid-day is generally underestimating the mean daily value of EF, as EF is becoming higher in the early morning and late afternoon. Thereby, when EF or EF' are estimated between 10AM and 4PM, it will most probably underestimate the diurnal ET, and therefore the cumulated ET. This will produce a general bias.

The performances of model O1 are shown on Figure B-29. The minimum and maximum ET estimation errors are plotted in dotted line, and the average ET error, over the range of hours of measurements, is plotted in bold line. We can see that if the time of measurements is correctly chosen, the ET estimation error can be very small with just a few millimeters of error. Moreover, we may also notice that the higher the LAI, the larger the ET error made. This plots emphasizes the importance of the time of EF estimation. The resulting ET can be extremely good in some cases, and very bad in some other cases. When a satellite is passing over the land surface, it allows estimation of EF, using for instance radiative temperature measurements. However, the passing time of the satellite depends on its path, so in most cases this will not correspond to the time leading to the smallest ET error. Therefore, we understand

that the application of the constant EF assumption is limited, in most cases this won't give a good estimate of ET.

The results of Model O2 are depicted on Figure B-29. We can see that generally model O2 gives pretty good ET estimation results, for any LAI and soil moisture conditions. Moreover, any time of EF' estimation leads to good results, and any time of measurements gives pretty good ET estimation. The time of EF' estimation only has a small repercussion on the quality of the estimated ET. However, this model can never achieve the best results obtained by model O1 when the measurements are made at the most appropriate time of the day. This model is therefore pretty interesting if we want to have a pretty accurate ET estimation valid in any case and if we don't need to have a perfect ET estimation. This model is pretty stable and resistant with regards to the time of estimation of EF'. Depending on the application, this model can be a good alternative to model O1, in particular if we are using different remote sensing images available at different times of the day.

Finally, this study suggests that for now the best model is model O1, where a constant EF assumption is used. However, the quality of the estimated ET greatly depends on the hour of estimation of EF. The second best model is model O2, which usually does a good job in estimating ET. Moreover, this model has the neat advantage to be used with measurements available at any time of the day. For many applications, this would be the favorite model. A summary of the performances of the different models is presented on figures B-34. In bold line we can see the best performing model, and in dotted line, the second best model. But this plot assumes that we are considering the best time of the day for both model O1 and model O2. The worst performing models are shown on figure B-35. These plots assume that we are picking up the worst time of the day for both models O1 and O2.

4.2 Dual-source EF modeling

In this part, two independent EF parameters were simultaneously estimated for both the vegetation and the soil (EFc and EFs). The EF models are basically the same

as the ones presented in a combined-source case, except that they are determined for both the vegetation and soil at the same time. This was done to reduce the ET estimation error. Table A.2 summarizes the models.

First, we can see on plot B-36, that the dual-source modeling approach performs worse than the combined-source EF modeling. Although it can seem surprising, we saw in the last chapter that in many cases EF did not depend strongly on the environmental and vegetation factors, whereas EFs and EFc are changing more with the environmental conditions. Therefore, this suggests that EF will generally be a better and easier estimator of evapotranspiration than combined EFs and EFc. Moreover, as seen in the article, EFs and EFc vary daily and their shape is not symmetrical contrary to EF. Finally, models A1, A2, B1 and B2 do not perform well in a dual-source case. Models O1, O2, B1 and B2 also perform slightly worse in a dual-source case compared to a combined-source case, as seen on figures B-37 and B-38. This may be due to the diurnal non-preservation of EFs and EFc. EF is closer to a constant diurnal value and can more easily lead to a good estimate of evapotranspiration. Finally the best and worst performing models are depicted on Figures B-42 and B-43. These plots show which models obtain the best and worst evapotranspiration estimate as a function of soil water content. The models are described by their Index: O1, O2, A1, A2, B1, B2 as it is described in Table A.2.

This latter result is very important. Indeed, we have shown that there is no need of using a dual-source modeling of EF, as it will not lead to a better estimate of ET. Moreover, the estimation of EFs and EFc, might be a much harder task to perform in reality as we only have limited measurements available, such as radiative temperature seen from a satellite. Hence, the estimation of EFs and EFc may be noisy and erroneous. We finally suggest using only EF and not EFs and EFc to determine ET. We also saw in the previous chapter that EF was only slightly sensitive to LAI, so that EF won't change much with LAI contrary to EFs and EFc, which will have to be reevaluated each time the vegetation changes.

Conclusion

In this thesis, the diurnal behavior of Evaporative Fraction (EF) has been examined, as well as the influence of the environmental parameters (air temperature, wind speed, solar incoming radiation, and air humidity) and the soil and vegetation conditions. It has been shown that EF exhibits a typical concave-up shape for any soil and vegetation conditions. The phase and amplitude of the soil heat flux G play very important roles on the shape and value of EF and they cannot be overlooked, as it has often be done so far. Only a good estimation of the soil heat flux and its diurnal behavior will permit to obtain a good estimate of EF. Moreover, EF has been proved to be only slightly changing with vegetation cover change. This constitutes a very important result for EF estimation. However EF is extremely sensitive to the soil moisture conditions and the soil water content is the most important factor determining EF value. So we can state that there is a clear link between the soil water content and EF.

The environmental factors play very different roles on EF value. Hence, wind speed has almost no influence on EF, contrary to the sensible and latent heat flux. This means that the repercussion of wind speed change is of the same order on the sensible and latent heat fluxes. This also means that the influence of wind speed on the transport of energy via H is equivalent to the transport of water vapor via λE. This is very important, as wind speed is definitely the most varying environment parameter in both space and time. Therefore, estimating EF will be easier than estimating the turbulent fluxes, as the wind speed will not have much influence on EF. Second, the relative humidity only has a small influence on the EF value, which wasn't clear before this study. Third, EF is a slowly decreasing function of solar

incoming radiation. This means that sensible heat flux increases faster than latent heat flux, when the solar incoming radiation increases, and this for any soil moisture and LAI conditions.

Finally, this study suggests the strategy to estimate EF using the global value of EF and not the soil and canopy components of EF, to obtain a good estimation of evapotranspiration. It has also been shown that to estimate EF, the best measurements would be the difference between the radiative temperature measured from remote sensing and the air temperature $Tr_0 - T_a$. Indeed, $Tr_0 - T_a$ is the most correlated variable with the value of EF. Previously, the radiative temperature Tr_0 was used to estimate EF. This temperature is not as much correlated wih the value of EF as $Tr_0 - T_a$. $Tr_0 - T_a$ is clearly an indicator of the plant stress when we have a fully covering vegetation. When $Tr_0 - T_a$ is high, the plant experiences stress, which is synonymous to lack of water in the root zone and low transpiration. Similarly, for a bare soil case, the soil temperature is high when the soil is not wet enough, because of the high thermal capacity of the water. Therefore, a large $Tr_0 - T_a$ signifies that there is not much surface soil moisture, and consequently there is only a small evaporation.

This study has provided insights into the physical factors influencing EF and suggests methods for robust estimation of EF and evapotranspiration.

Appendix A

Tables

Model O1	$EF = constant_{daily}$
Model O2	$EF' = \frac{EF}{EF_p} = constant_{daily}$
Model A1	$EF^* = \frac{\int_{S_\downarrow>0} EF(\tau) S_\downarrow(\tau)\, d\tau}{\int_{S_\downarrow>0} S_\downarrow(\tau)\, d\tau}$
Model A2	$EF^* = \frac{\int_{R_n>0} EF(\tau) R_n(\tau)\, d\tau}{\int_{R_n>0} R_n(\tau)\, d\tau}$
Model B1	$EF = \frac{EF_{min} R_{n,max}}{R_n + EF_{min}(R_{n,max} - R_n)}$
Model B2	$EF = \frac{EF_{min} S_{\downarrow,max}}{S_\downarrow + EF_{min}(S_{\downarrow,max} - S_\downarrow)}$

Table A.1: EF combined-source models

Model O1	$EFs = const_{daily}$ $EFc = const_{daily}$
Model O2	$EFs' = \frac{EFs}{EFs_p} = const_{daily}$ $EFc' = \frac{EFc}{EFc_p} = const_{daily}$
Model A1	$EFs^* = \frac{\int_{S_\downarrow>0} EFs(\tau)S_\downarrow(\tau)\,d\tau}{\int_{S_\downarrow>0} S_\downarrow(\tau)\,d\tau}$ $EFc^* = \frac{\int_{S_\downarrow>0} EFc(\tau)S_\downarrow(\tau)\,d\tau}{\int_{S_\downarrow>0} S_\downarrow(\tau)\,d\tau}$
Model A2	$EFs^* = \frac{\int_{R_{n,s}>0} EFs(\tau)R_{n,s}(\tau)\,d\tau}{\int_{R_{n,s}>0} R_{n,s}(\tau)\,d\tau}$ $EFc^* = \frac{\int_{R_{n,c}>0} EFc(\tau)R_{n,c}(\tau)\,d\tau}{\int_{R_{n,c}>0} R_{n,c}(\tau)\,d\tau}$
Model B1	$EFs = \frac{EFs_{min}R_{ns,max}}{R_{n,s}+EFs_{min}(R_{ns,max}-R_{n,s})}$ $EFc = \frac{EFc_{min}R_{nc,max}}{R_{n,c}+EFc_{min}(R_{nc,max}-R_{n,c})}$
Model B2	$EFs = \frac{EFs_{min}S_{\downarrow,max}}{S_\downarrow+EFs_{min}(S_{\downarrow,max}-S_\downarrow)}$ $EFc = \frac{EFc_{min}S_{\downarrow,max}}{S_\downarrow+EFc_{min}(S_{\downarrow,max}-S_\downarrow)}$

Table A.2: EF dual-source models

Appendix B

Figures

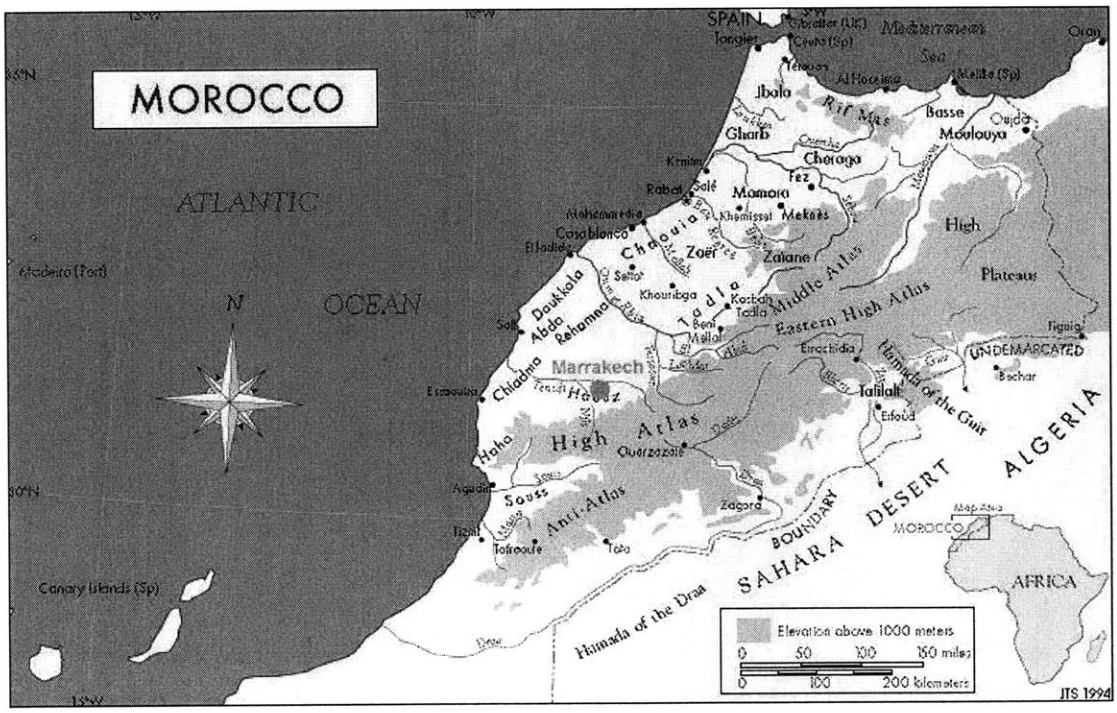

Figure B-1: Map of Morocco

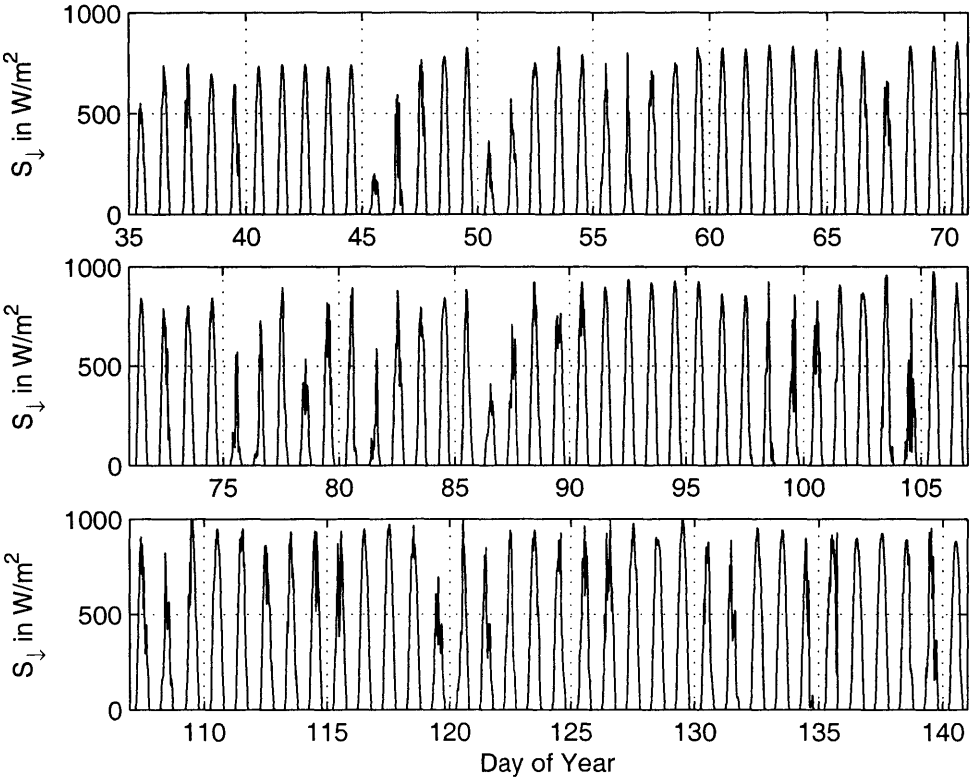

Figure B-2: Solar incoming radiation measured over parcel R3-B123 in 2003

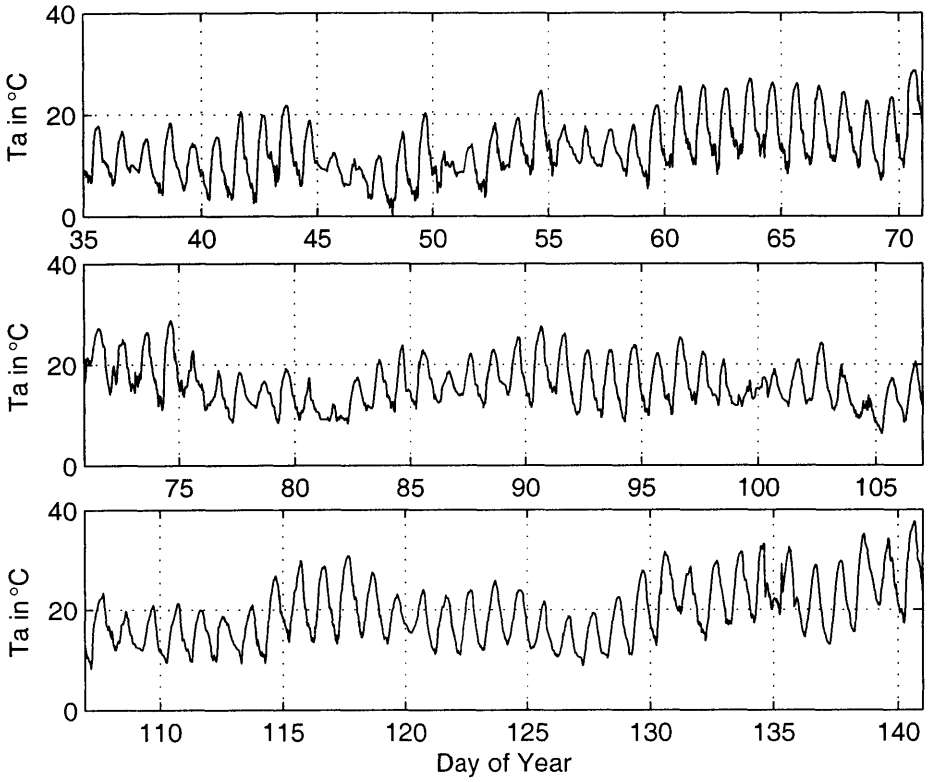

Figure B-3: Air temperature measured over parcel R3-B123 in 2003

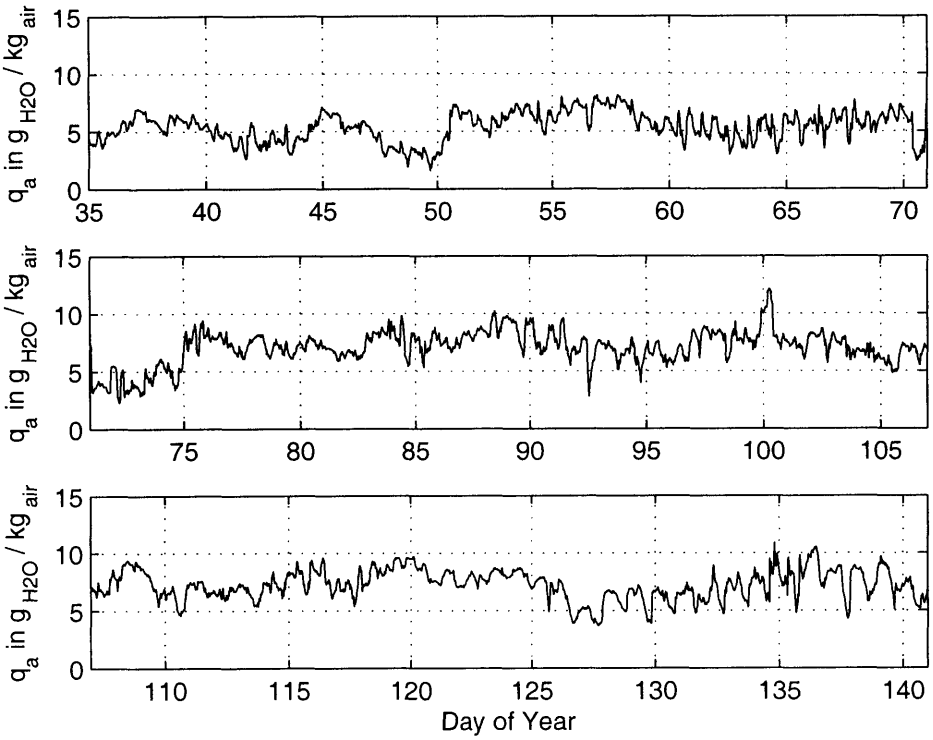

Figure B-4: Air specific humidity measured over parcel R3-B123 in 2003

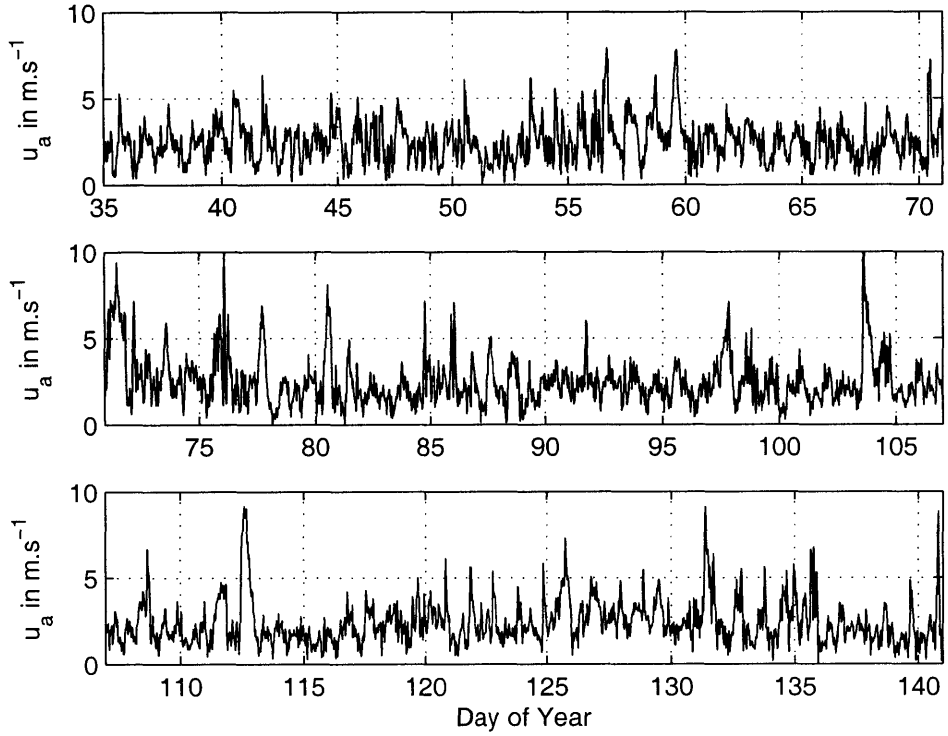

Figure B-5: Wind speed measured over parcel R3-B123 in 2003

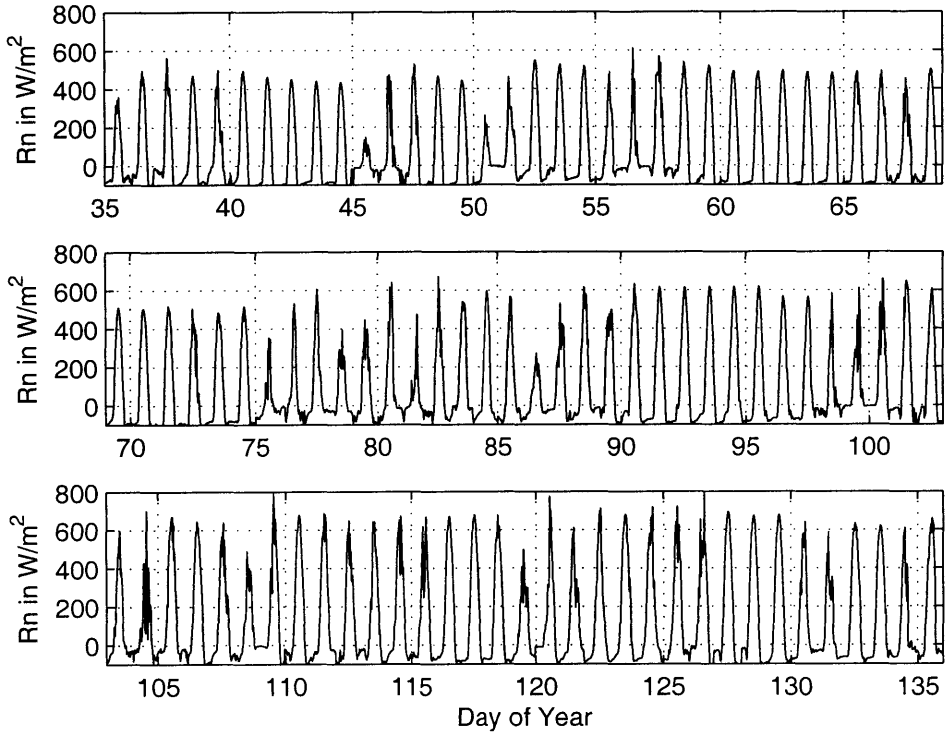

Figure B-6: Net radiation measured at 2m high over parcel R3-B123 in 2003

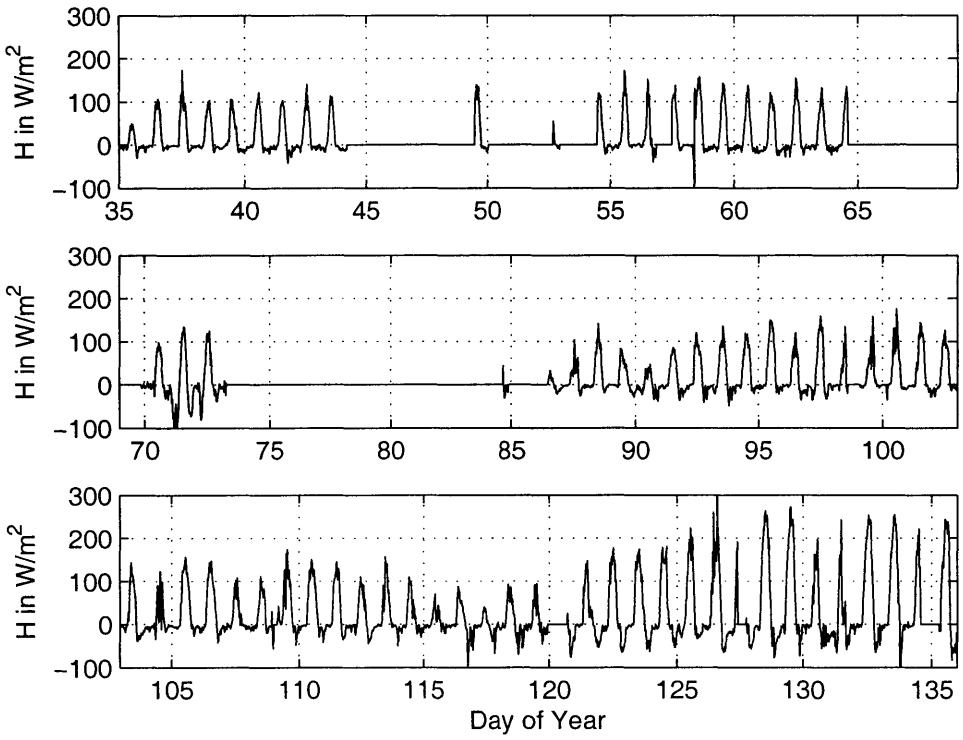

Figure B-7: Sensible Heat Flux measured using Eddy-Correlation over parcel R3-B123 in 2003

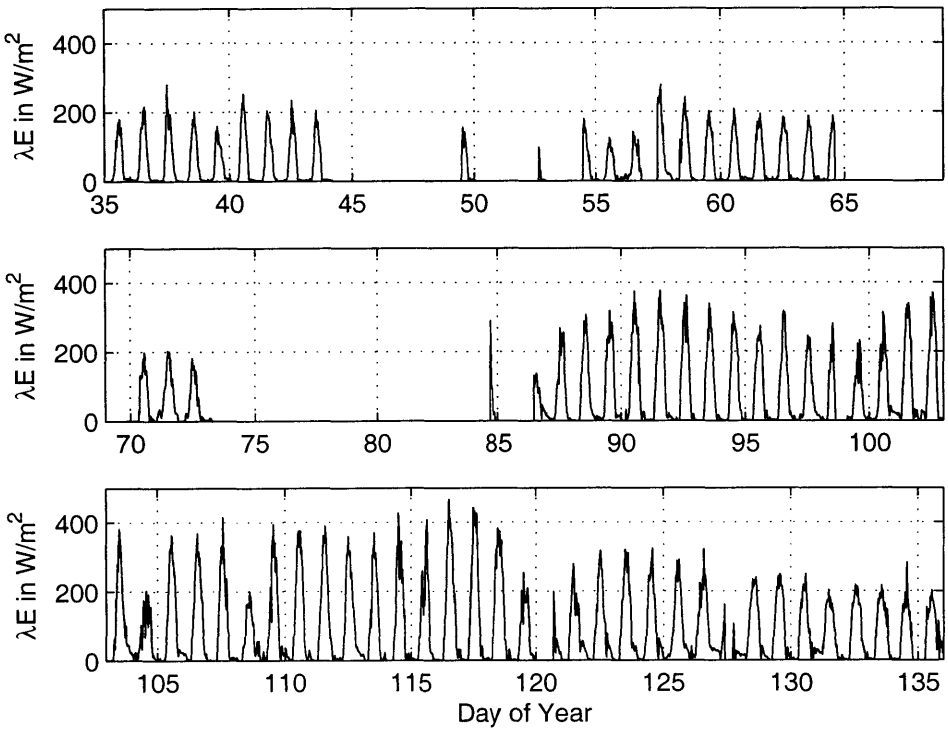

Figure B-8: Latent Heat Flux measured using Eddy-Correlation over parcel R3-B123 in 2003

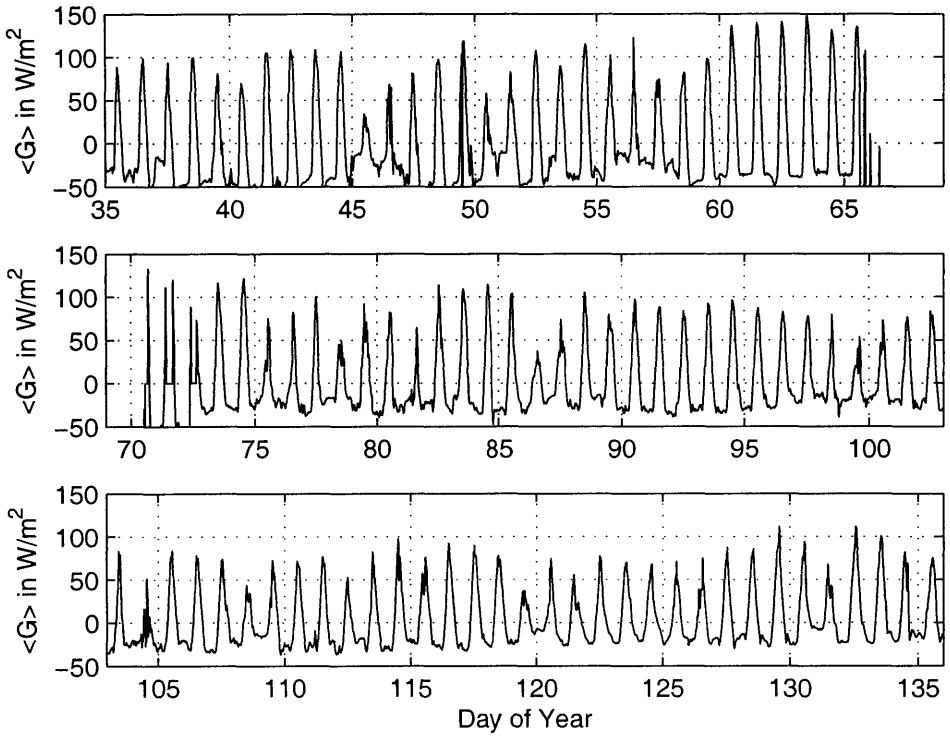

Figure B-9: Mean ground heat flux measured using 3 flux plates over parcel R3-B123 in 2003

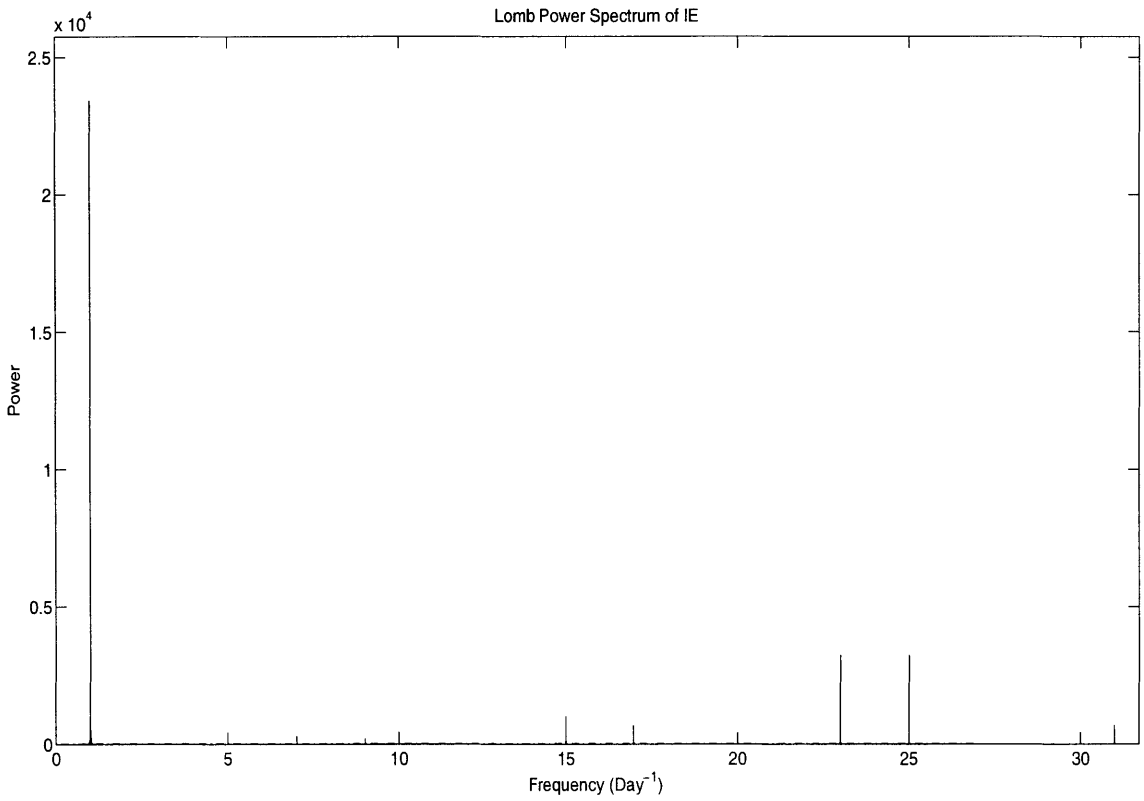

Figure B-10: Frequency analysis of latent heat flux using Lomb periodogram

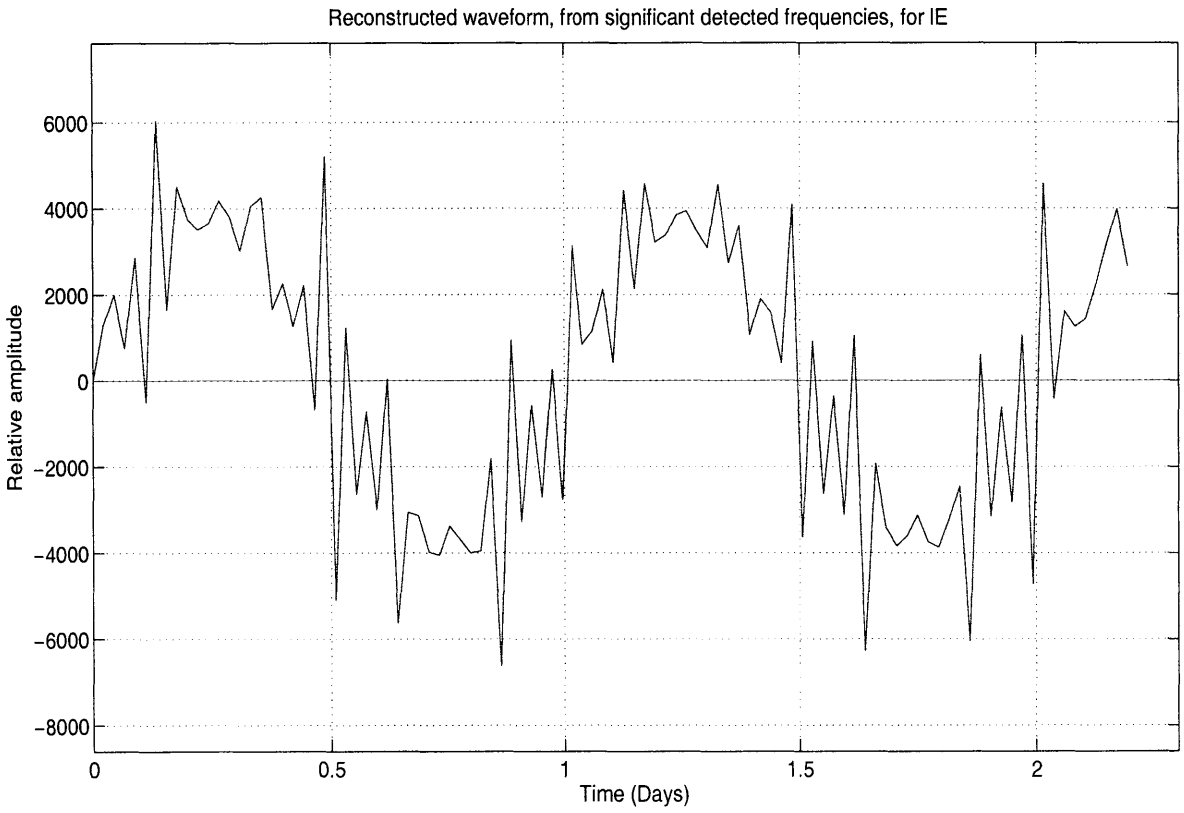

Figure B-11: Reconstructed latent heat flux using Lomb periodogram

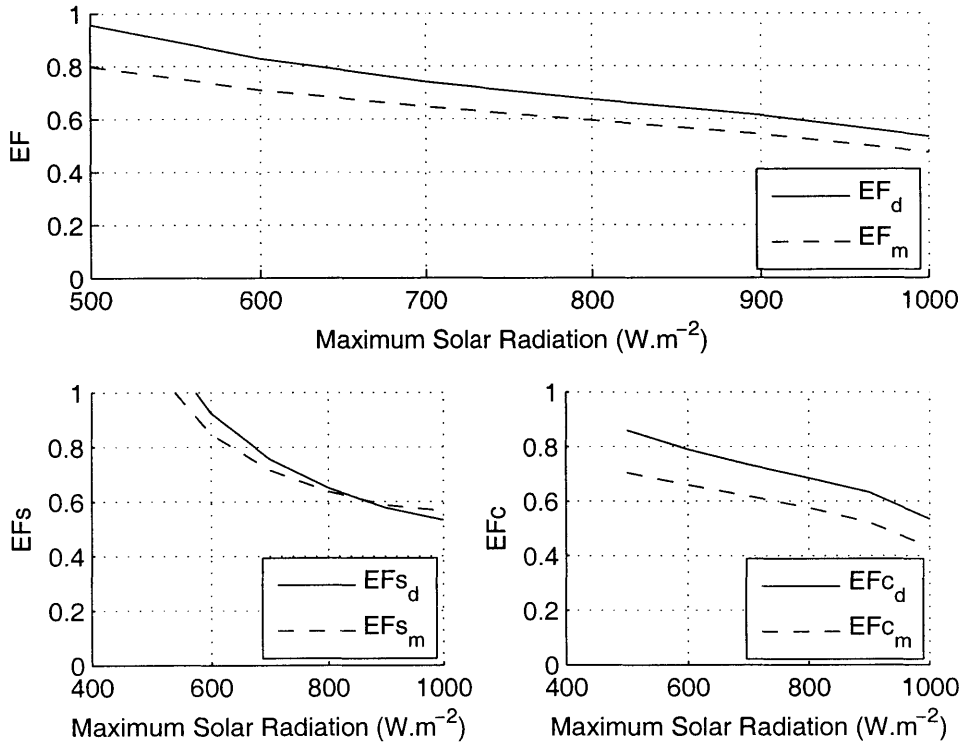

Figure B-12: Daytime and Midday Evaporative Fraction (EFd and EFm) as a function of Solar incoming radiation in $W.m^{-2}$.

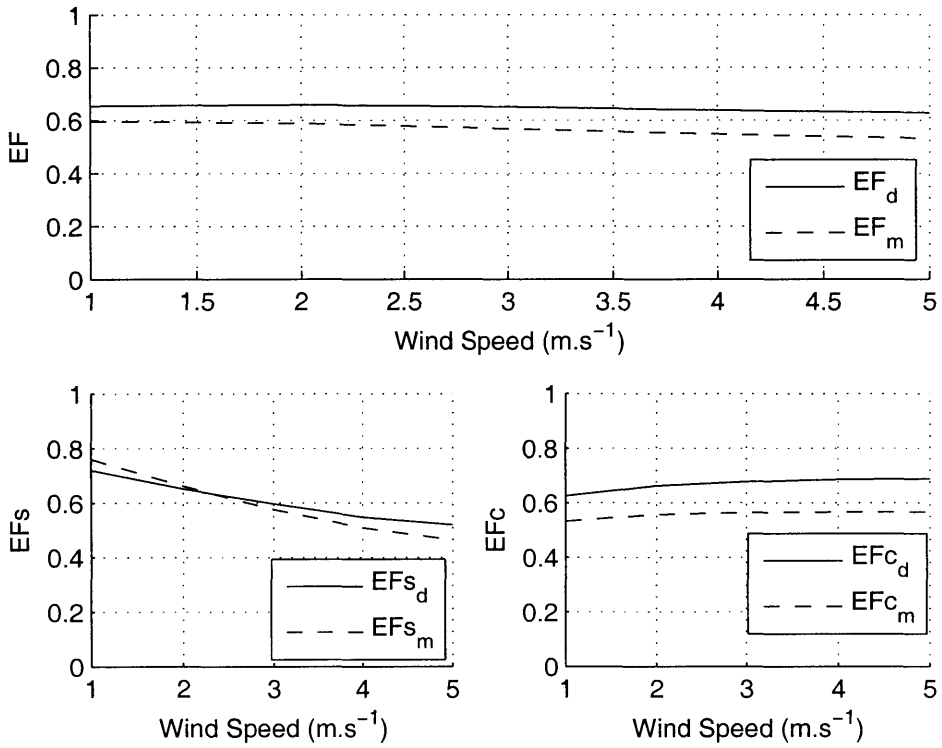

Figure B-13: Daytime and Midday Evaporative Fraction (EFd and EFm) as a function of wind speed in $m.s^{-1}$.

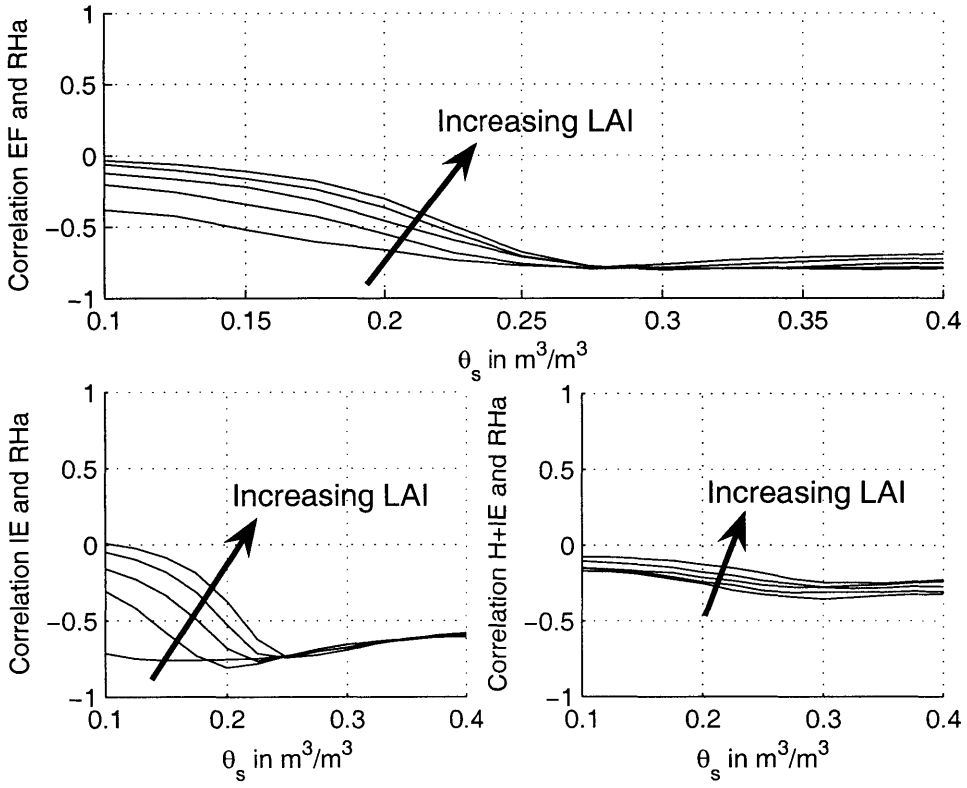

Figure B-14: Cross-correlation of EF and air relative humidity, for LAI=0.5, 1.5, 2.5 and 3.5 and surface soil moisture between 0.1 and 0.4 $m^3.m^{-3}$

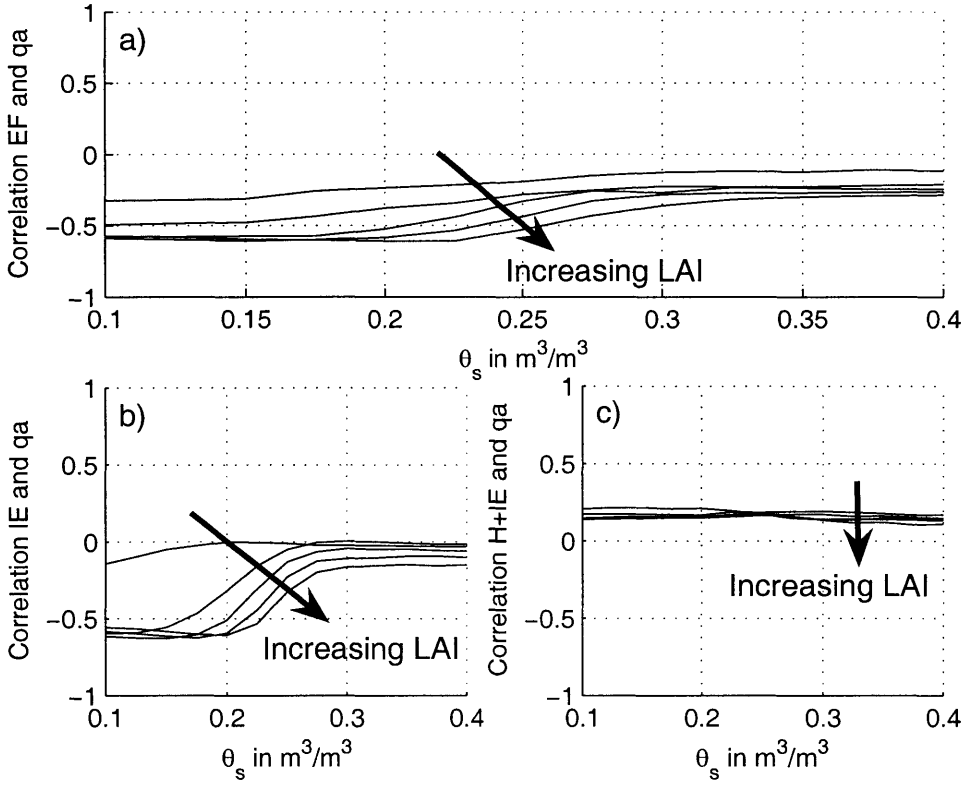

Figure B-15: Cross-correlation of EF and air specific moisture, for LAI=0.5, 1.5, 2.5 and 3.5 and surface soil moisture between 0.1 and 0.4 $m^3.m^{-3}$

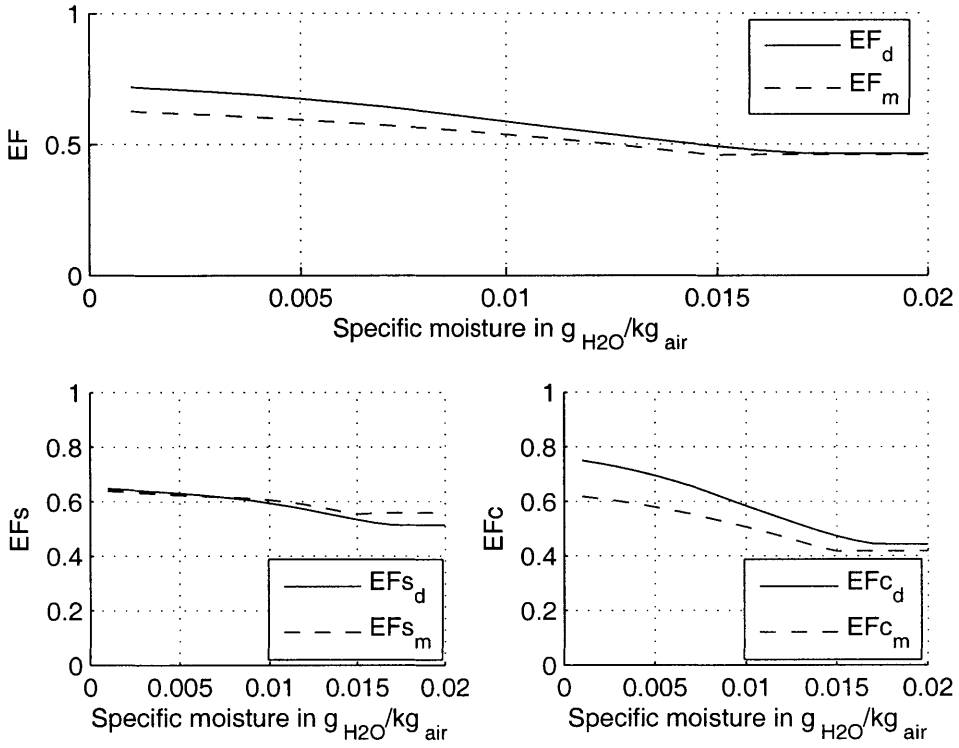

Figure B-16: Daytime and Midday Evaporative Fraction (EFd and EFm) as a function of air specific humidity in g_{H2O}/kg_{air}

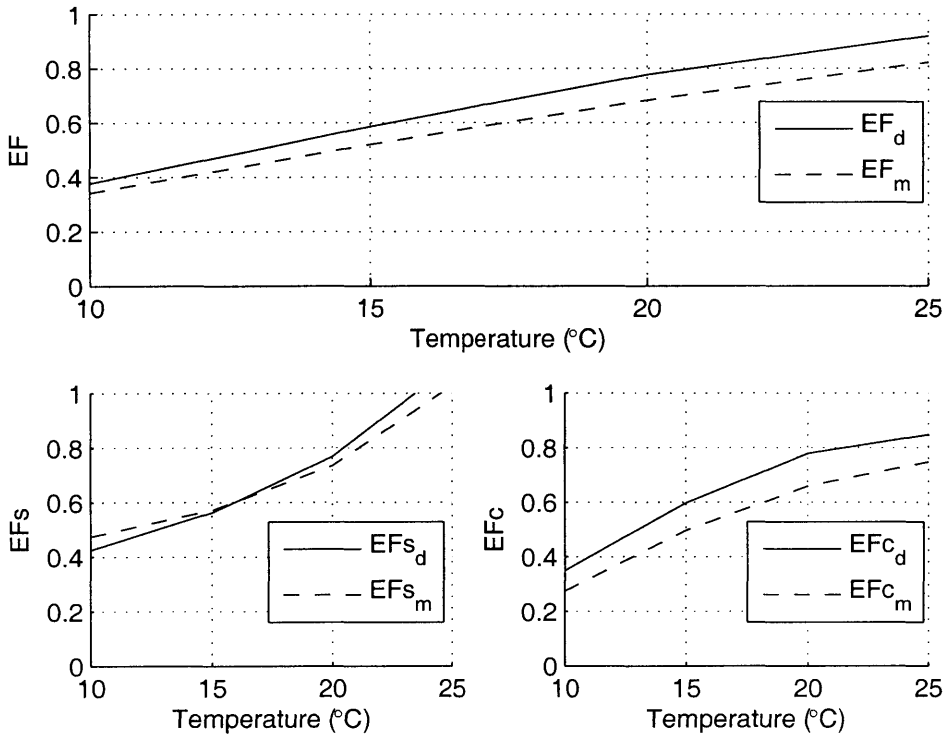

Figure B-17: Daytime and Midday Evaporative Fraction (EFd and EFm) as a function of air temperature in $^{\circ}C$.

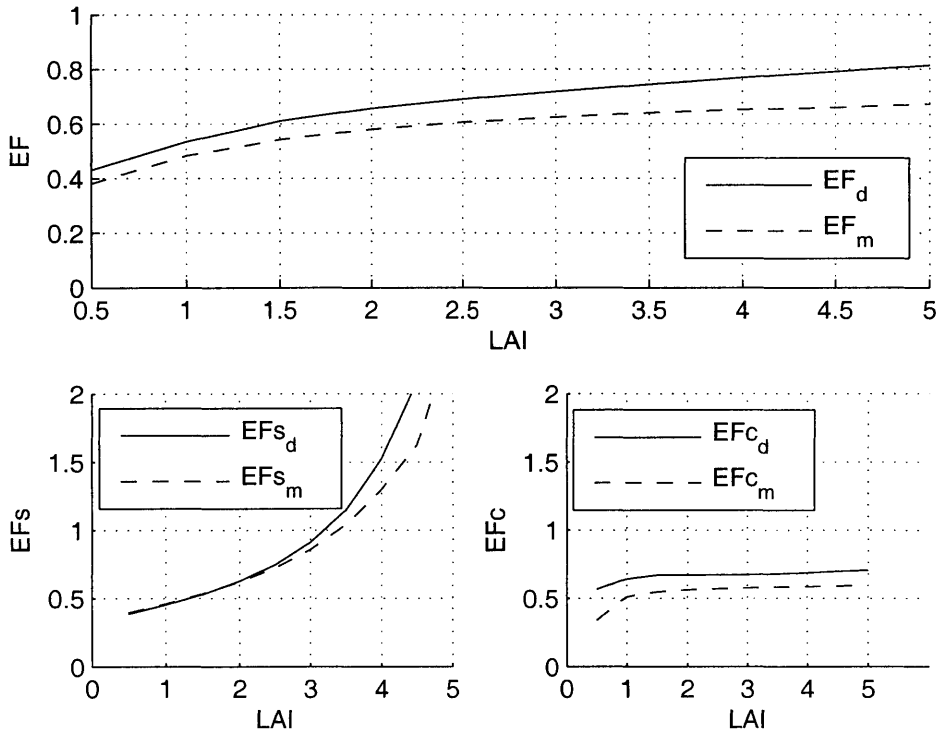

Figure B-18: Daytime and Midday Evaporative Fraction (EFd and EFm) as a function of LAI.

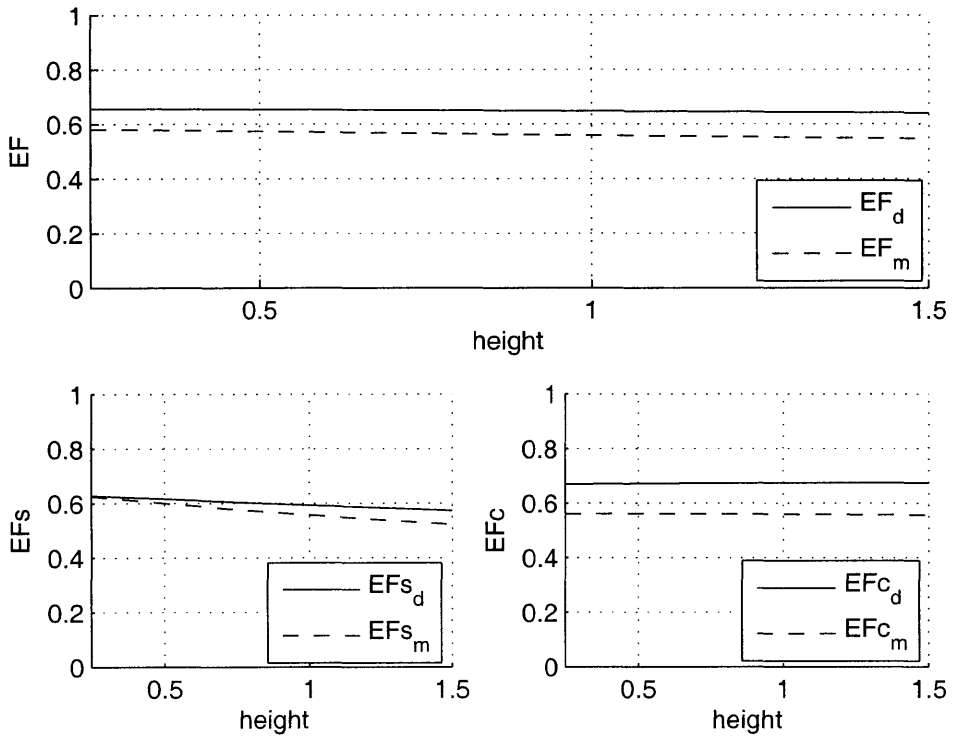

Figure B-19: Daytime and Midday Evaporative Fraction (EFd and EFm) as a function of vegetation height.

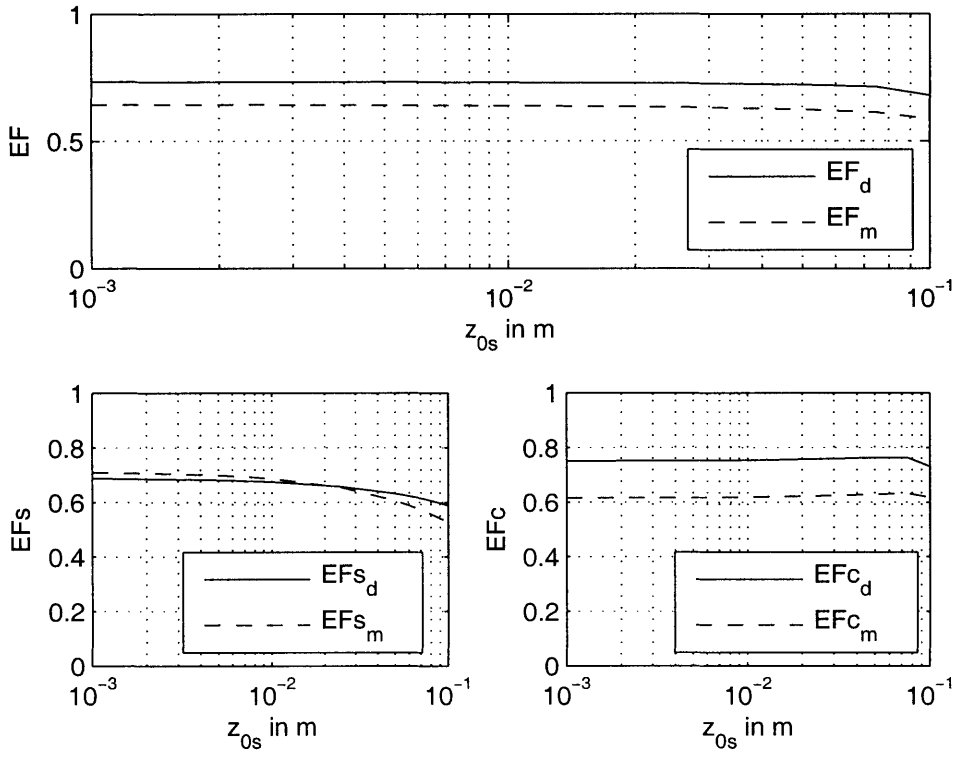

Figure B-20: Daytime and Midday Evaporative Fraction (EFd and EFm) as a function of roughness length.

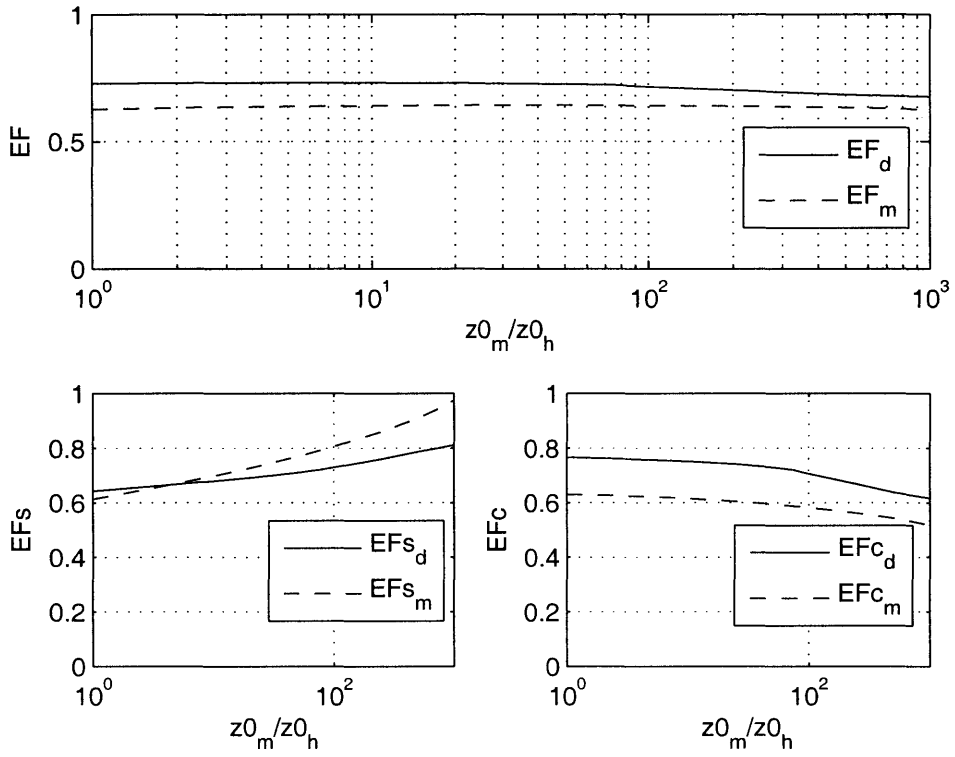

Figure B-21: Daytime and Midday Evaporative Fraction (EFd and EFm) as a function of the ratio between the momentum roughness length and the heat roughness length.

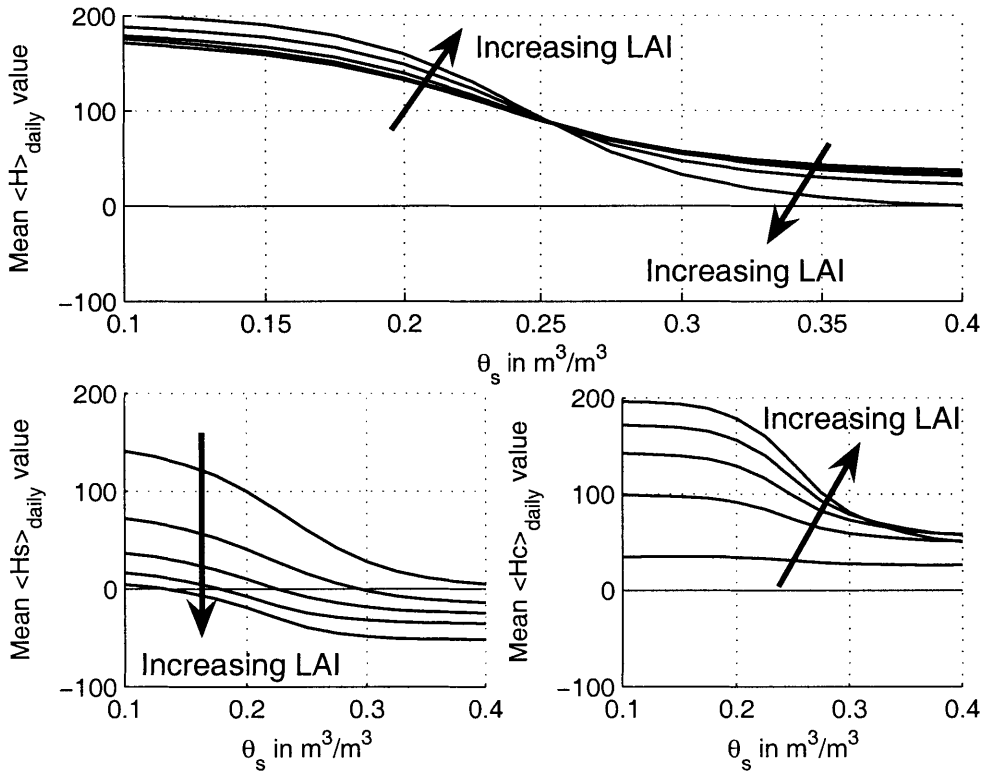

Figure B-22: Mean diurnal value of sensible heat flux H as a function of surface soil moisture for LAI=0.5, 1.5, 2.5, 3.5 and 4.5.

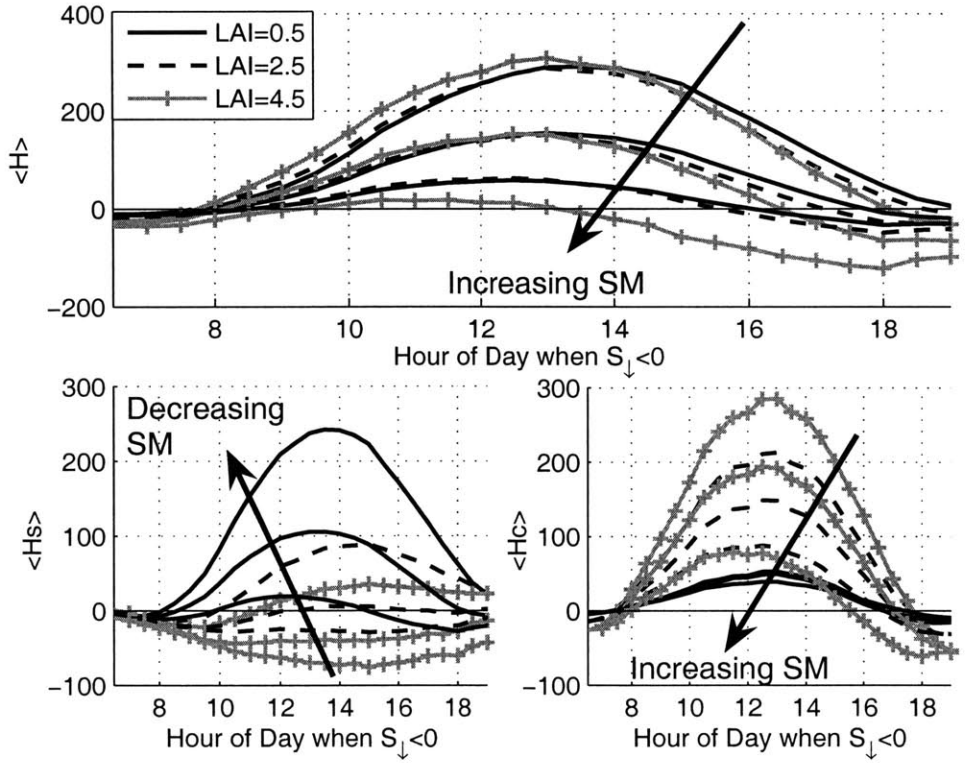

Figure B-23: Mean diurnal cycle of a) sensible heat flux, b) soil sensible heat flux and c) canopy sensible heat flux for LAI=0.5, 2.5 and 4.5 and surface soil moisture θ_s =0.1, 0.2, 0.3 $m^3.m^{-3}$

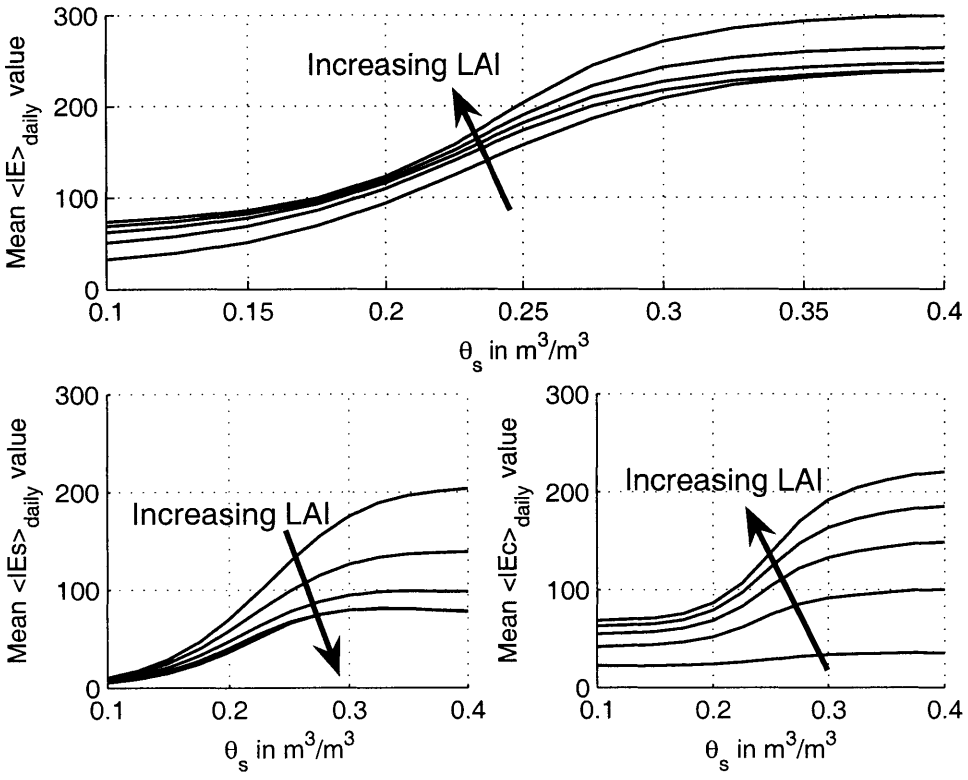

Figure B-24: Mean diurnal value of latent heat flux as a function of surface soil moisture for LAI=0.5, 1.5, 2.5, 3.5 and 4.5.

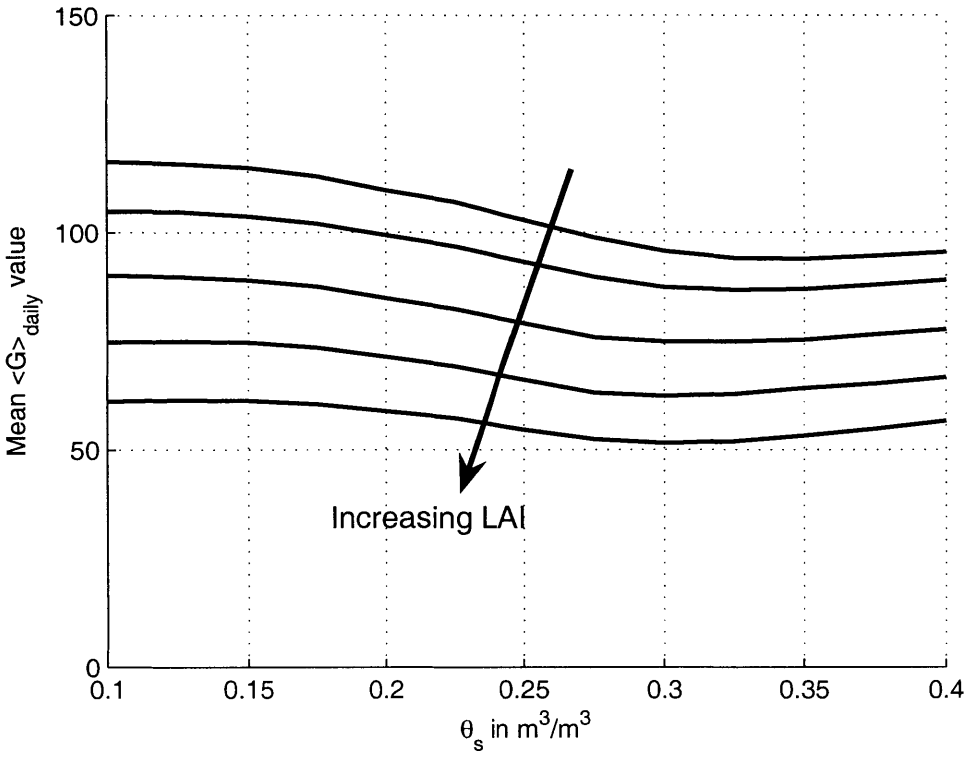

Figure B-25: Mean diurnal value of soil heat flux G as a function of surface soil moisture for LAI=0.5, 1.5, 2.5, 3.5 and 4.5.

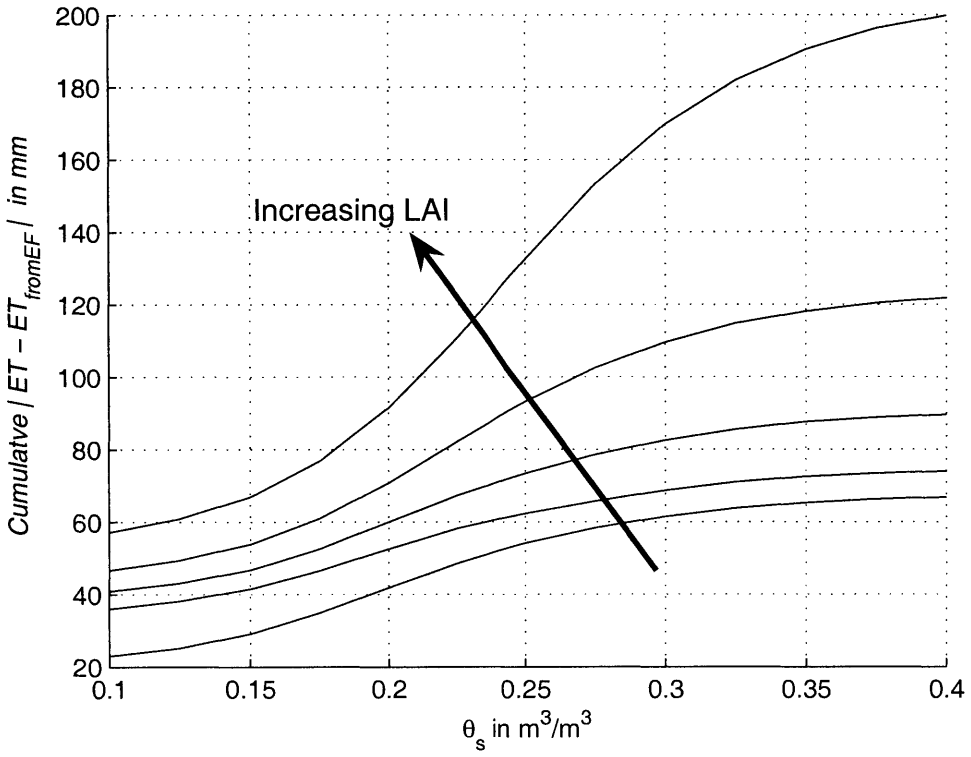

Figure B-26: Cumulative absolute ET error in mm as a function of surface soil moisture for LAI=0.5, 1.5, 2.5, 3.5 and 4.5.

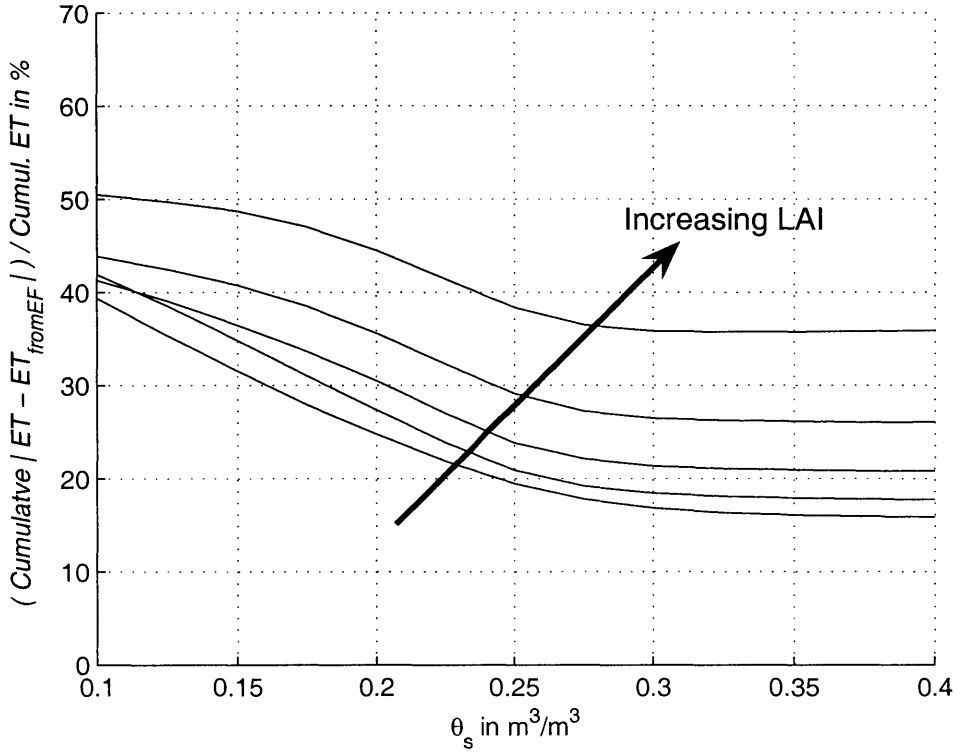

Figure B-27: Cumulative absolute ET error in percent of total cumulative ET as a function of surface soil moisture for LAI=0.5, 1.5, 2.5, 3.5 and 4.5.

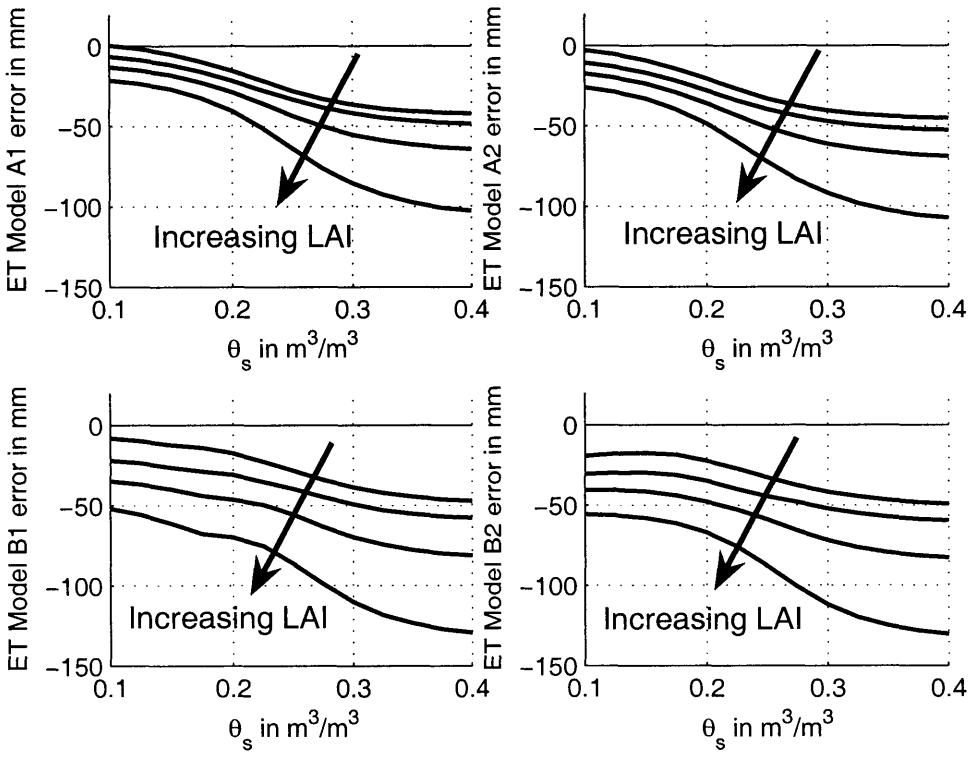

Figure B-28: Cumulated ET estimation error for different models $\int_{t_0}^{t_{end}} ET_{model}(t) - ET_{SVAT}(t)\,dt$ in mm as a function of mean surface soil moisture for LAI=1, 2, 3 and 4.

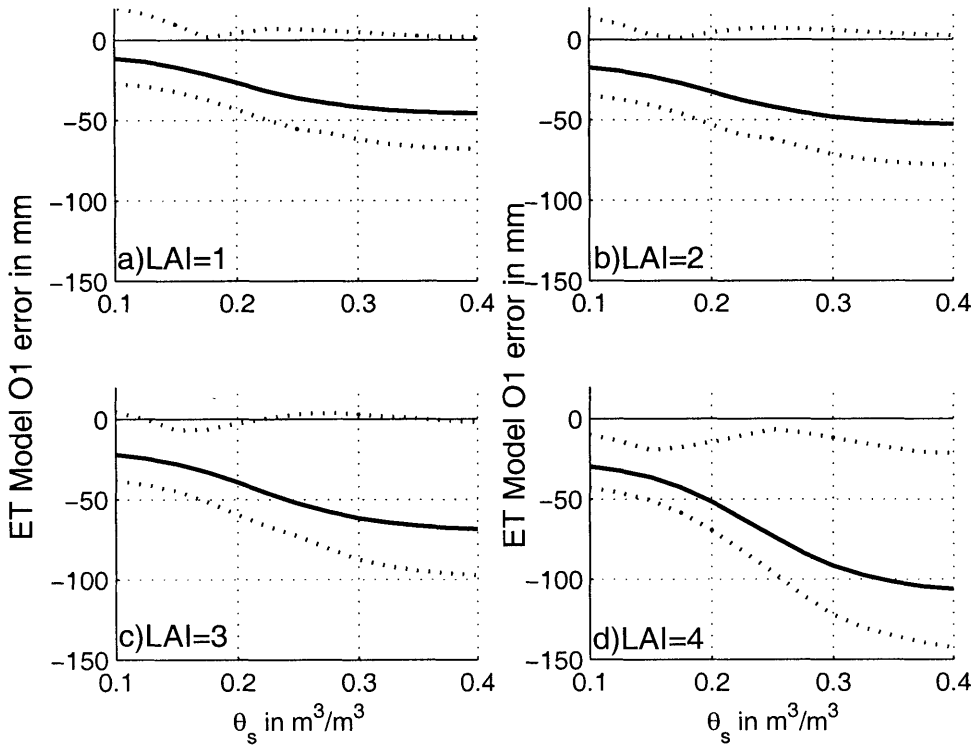

Figure B-29: Min/Max (dotted line) and mean (solid line) evapotranspiration error $\int_{t_0}^{t_{end}} ET_{O1}(t) - ET(t)\,dt$ in mm, when using the constant EF assumption and measuring EF at different hour of the day between 10AM and 4PM, as a function of mean surface soil moisture for a) LAI=1, b) LAI=2, c) LAI=3, d) LAI=4.

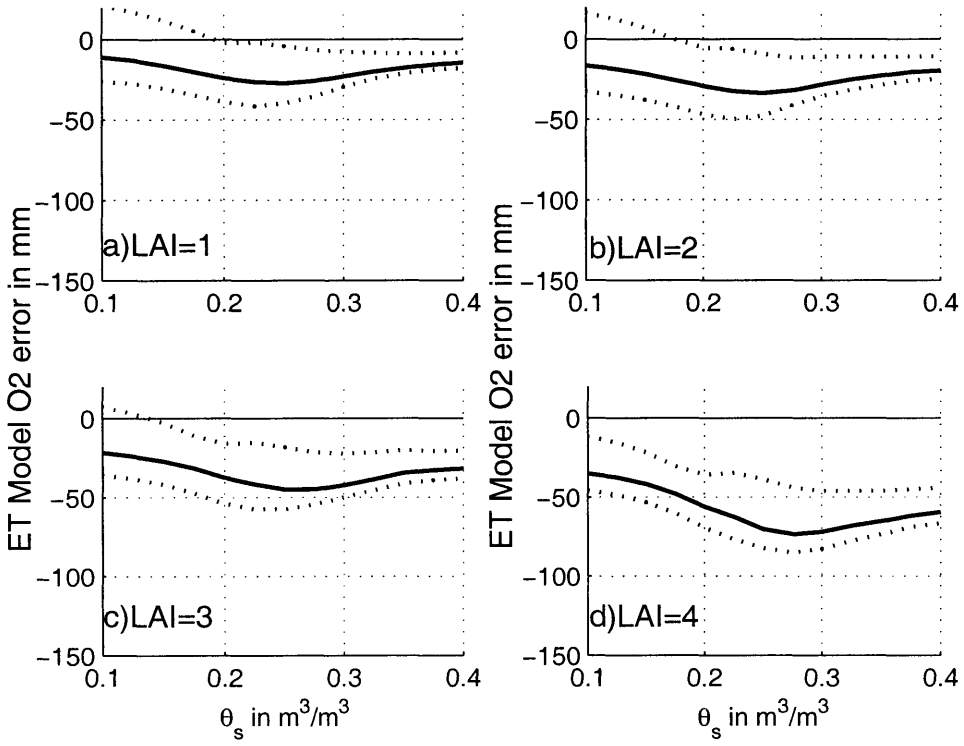

Figure B-30: Min/Max (dotted line) and mean (solid line) evapotranspiration error $\int_{t_0}^{t_{end}} ET_{O2}(t) - ET(t)\,dt$ in mm, when using the constant EF' assumption and measuring EF' at different hour of the day between 10AM and 4PM, as a function of mean surface soil moisture for a) LAI=1, b) LAI=2, c) LAI=3, d) LAI=4.

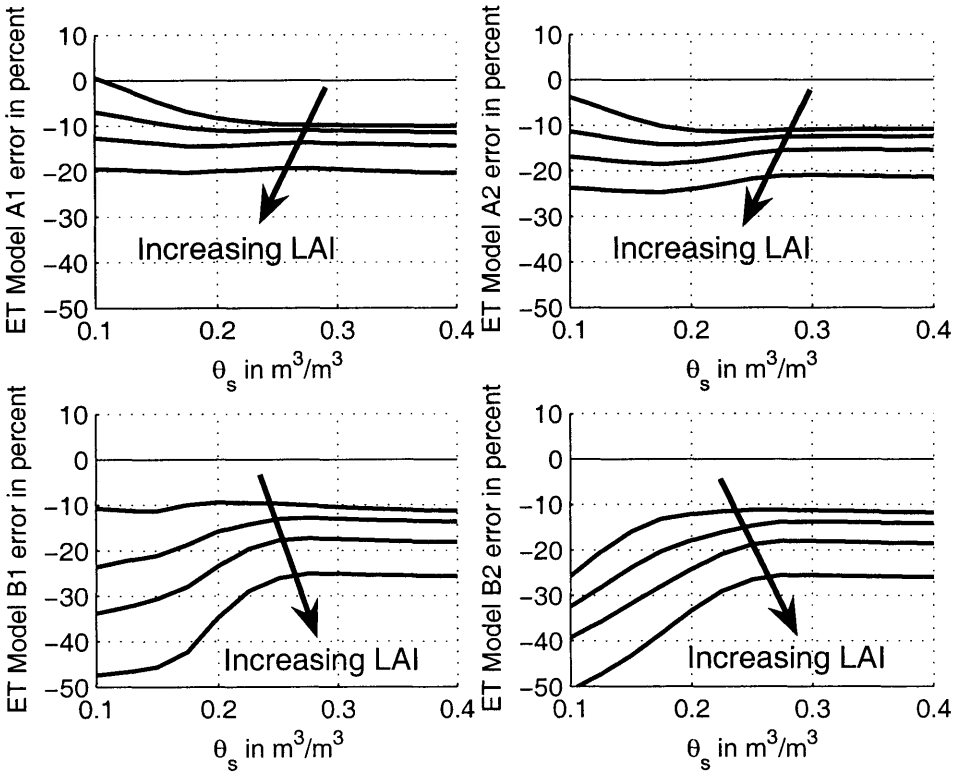

Figure B-31: Cumulated evapotranspiration estimation error for different models $\int_{t_0}^{t_{end}} ET_{model}(t) - ET_{SVAT}(t)\, dt$ in percents as a function of mean surface soil moisture for LAI=1, 2, 3 and 4.

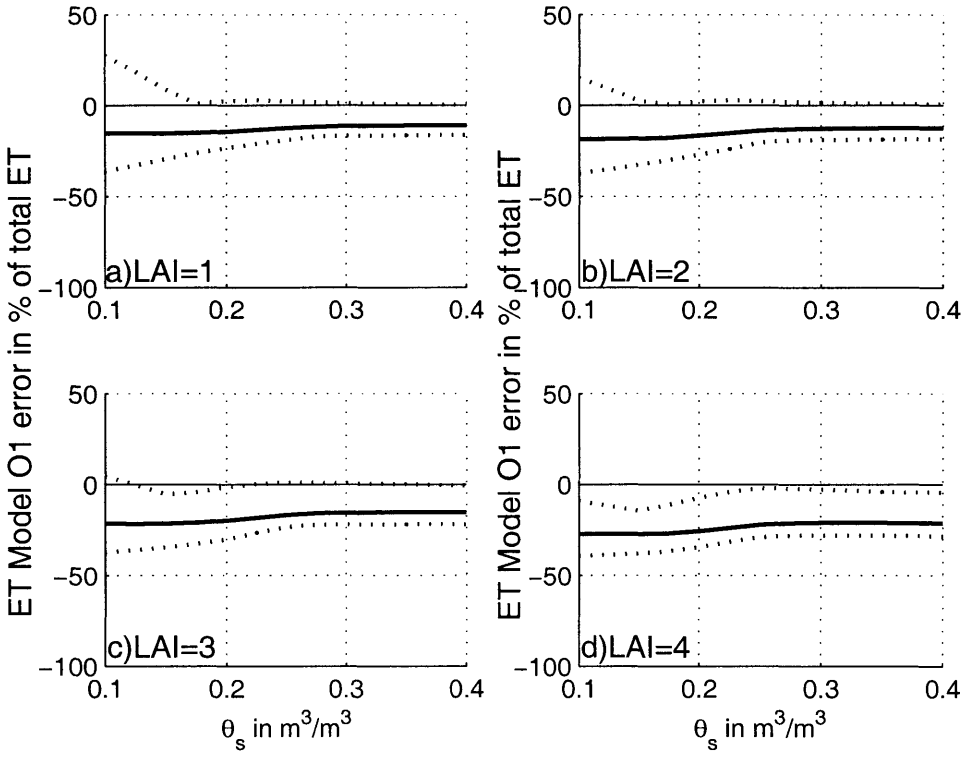

Figure B-32: Min/Max (dotted line) and mean (solid line) evapotranspiration error $\int_{t_0}^{t_{end}} ET_{O1}(t) - ET_{SVAT}(t)\, dt$ in percents, when using the constant EF assumption and measuring EF at different hour of the day between 10AM and 4PM, as a function of mean surface soil moisture for a) LAI=1, b) LAI=2, c) LAI=3, d) LAI=4.

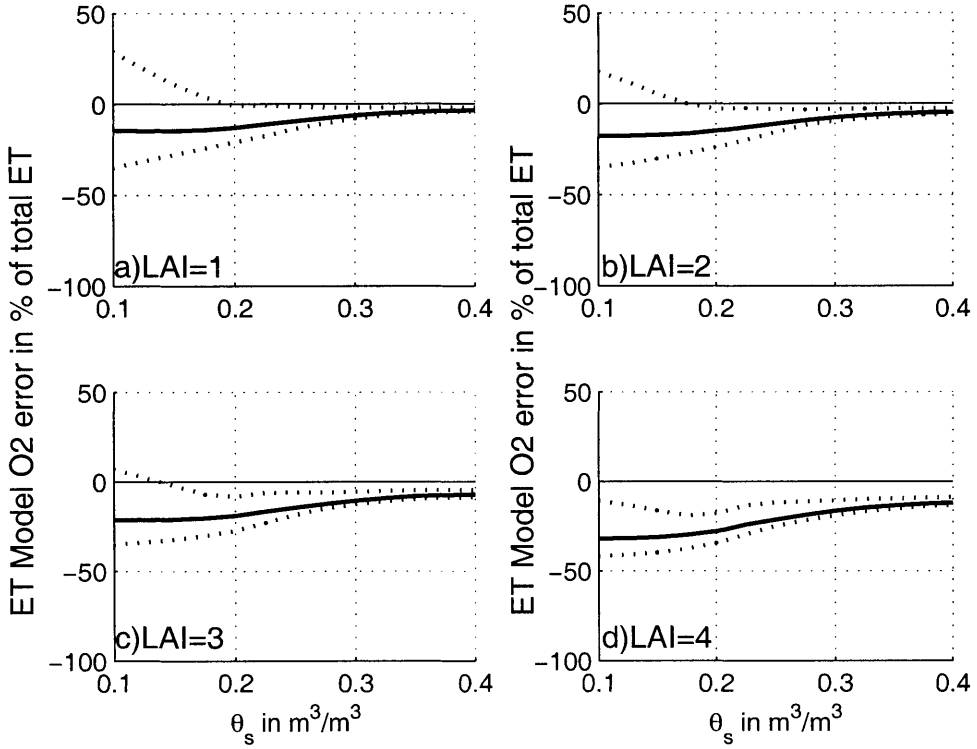

Figure B-33: Min/Max (dotted line) and mean (solid line) evapotranspiration error $\int_{t_0}^{t_{end}} ET_{O2}(t) - ET_{SVAT}(t)\,dt$ in percents, when using the constant EF' assumption and measuring EF' at different hour of the day between 10AM and 4PM, as a function of mean surface soil moisture for a) LAI=1, b) LAI=2, c) LAI=3, d) LAI=4.

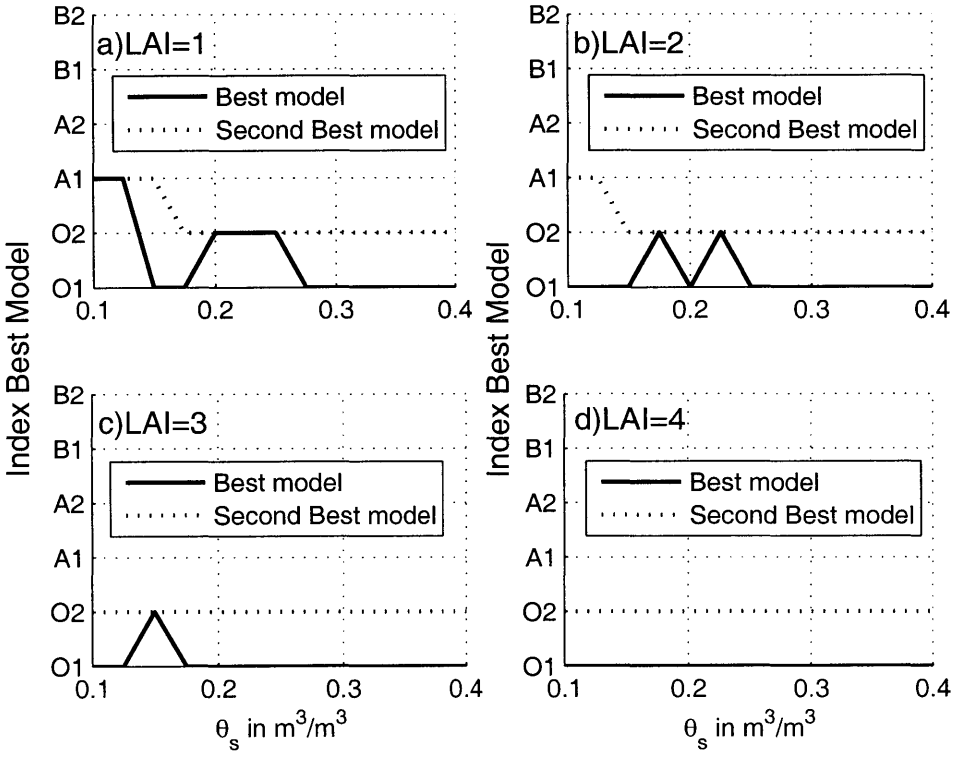

Figure B-34: First and second best evapotranspiration forecasting models as a function of surface soil moisture

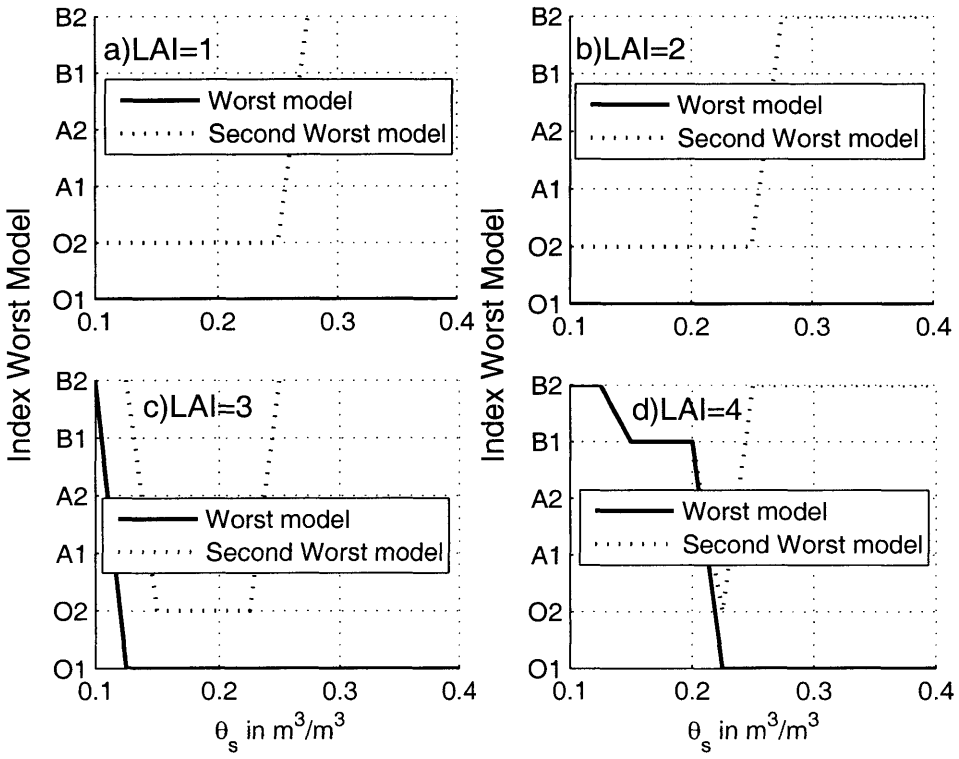

Figure B-35: First and second worst evapotranspiration forecasting models as a function of surface soil moisture

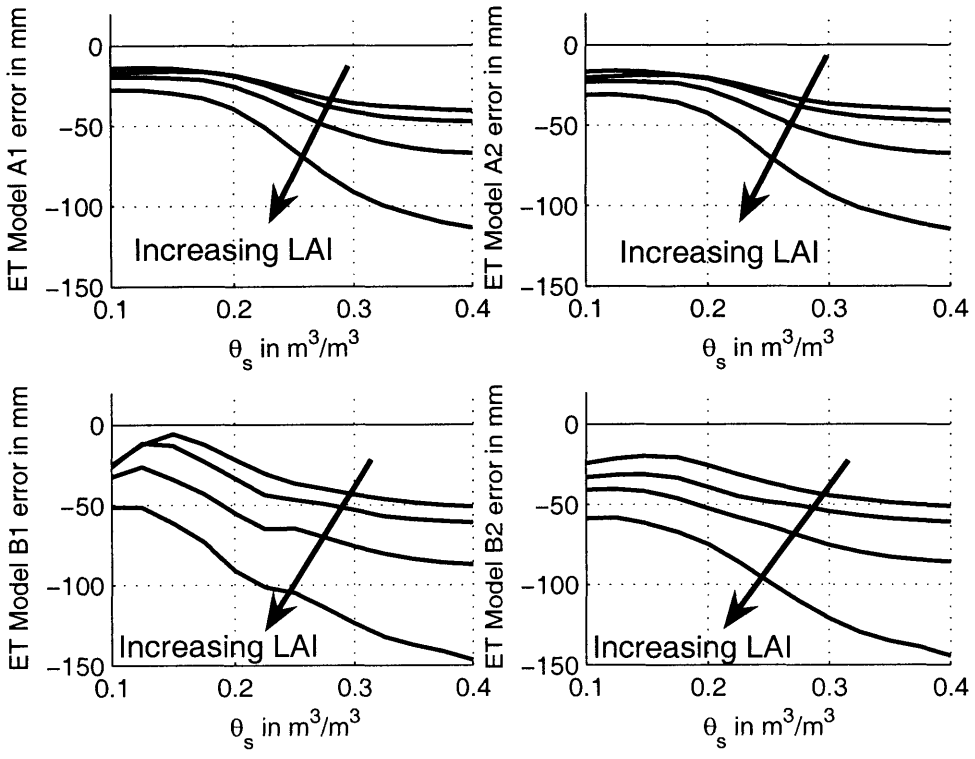

Figure B-36: Cumulated evapotranspiration estimation error for different models $\int_{t_0}^{t_{end}} ET_{model}(t) - ET_{SVAT}(t)\, dt$ in mm as a function of mean surface soil moisture for LAI=1, 2, 3 and 4.

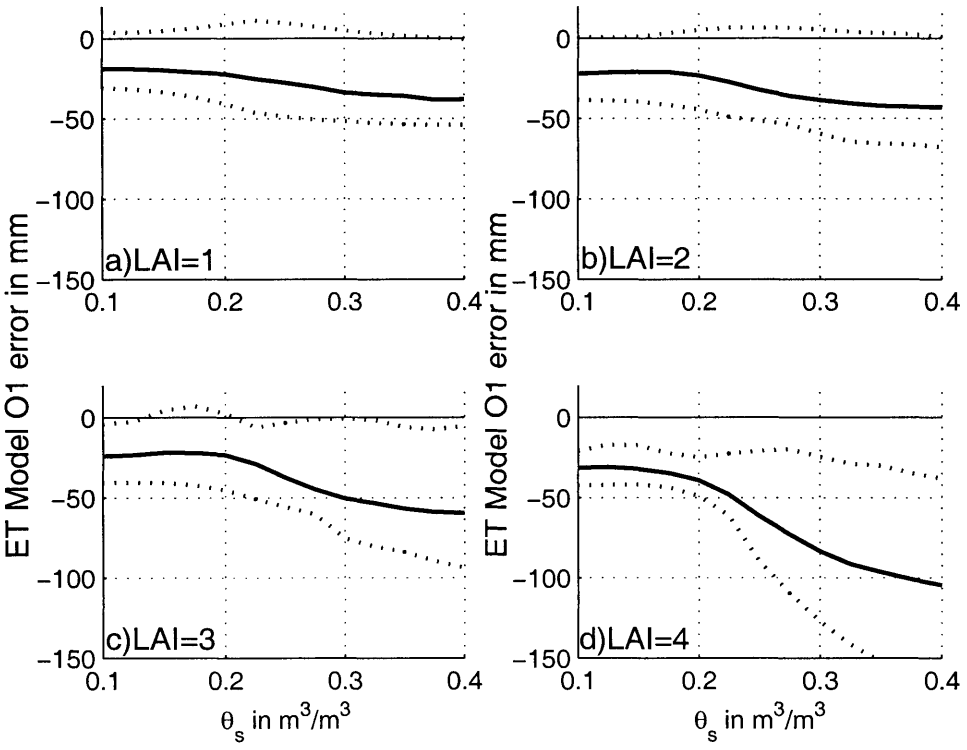

Figure B-37: Min/Max (dotted line) and mean (solid line) evapotranspiration error $\int_{t_0}^{t_{end}} ET_{O1}(t) - ET(t)\,dt$ in mm, when using the constant EF assumption and measuring EF at different hour of the day between 10AM and 4PM, as a function of mean surface soil moisture for a) LAI=1, b) LAI=2, c) LAI=3, d) LAI=4.

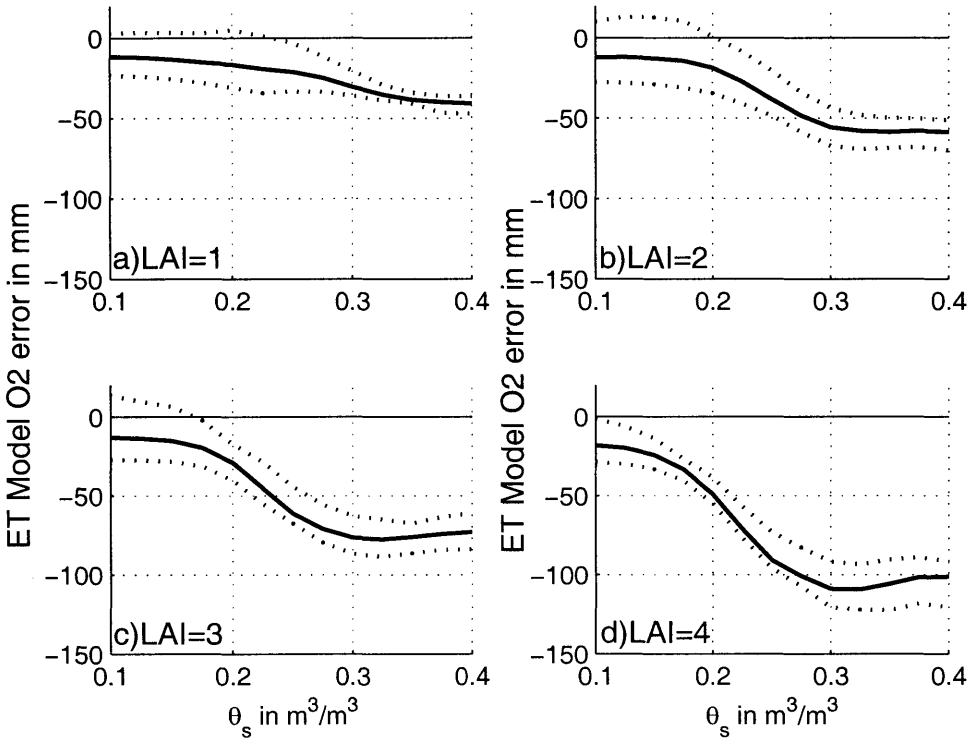

Figure B-38: Min/Max (dotted line) and mean (solid line) ET error $\int_{t_0}^{t_{end}} ET_{O2}(t) - ET(t)\,dt$ in mm, when using the constant EF' assumption and measuring EF' at different hour of the day between 10AM and 4PM, as a function of mean surface soil moisture for a) LAI=1, b) LAI=2, c) LAI=3, d) LAI=4.

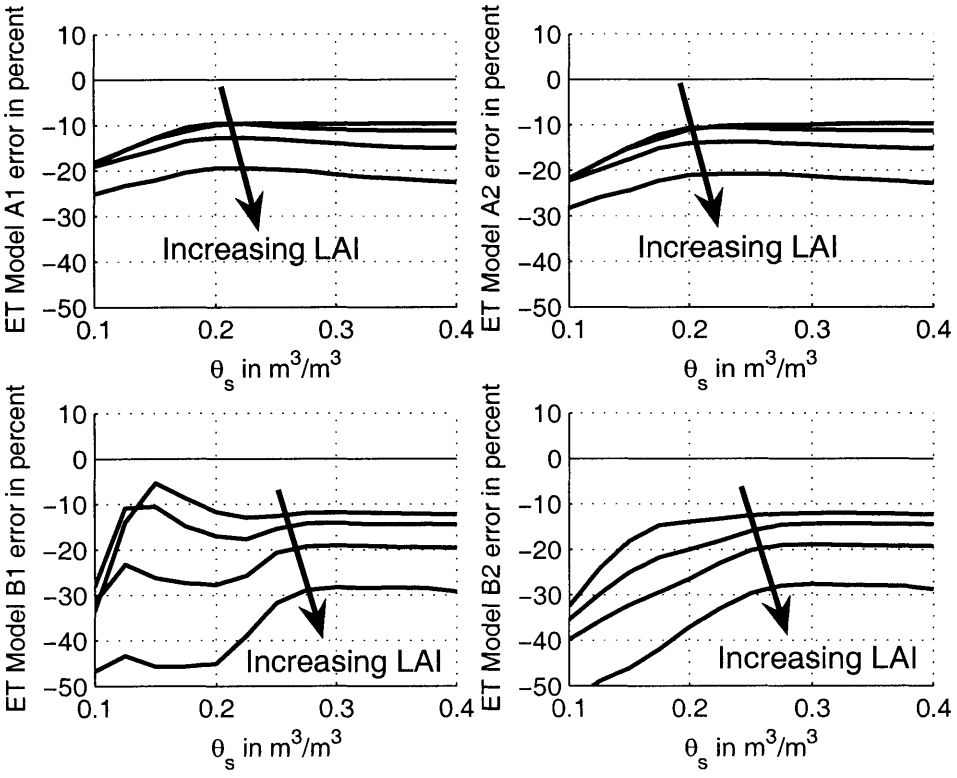

Figure B-39: Cumulated evapotranspiration estimation error for different models $\int_{t_0}^{t_{end}} ET_{model}(t) - ET_{SVAT}(t)\, dt$ in percents as a function of mean surface soil moisture for LAI=1, 2, 3 and 4.

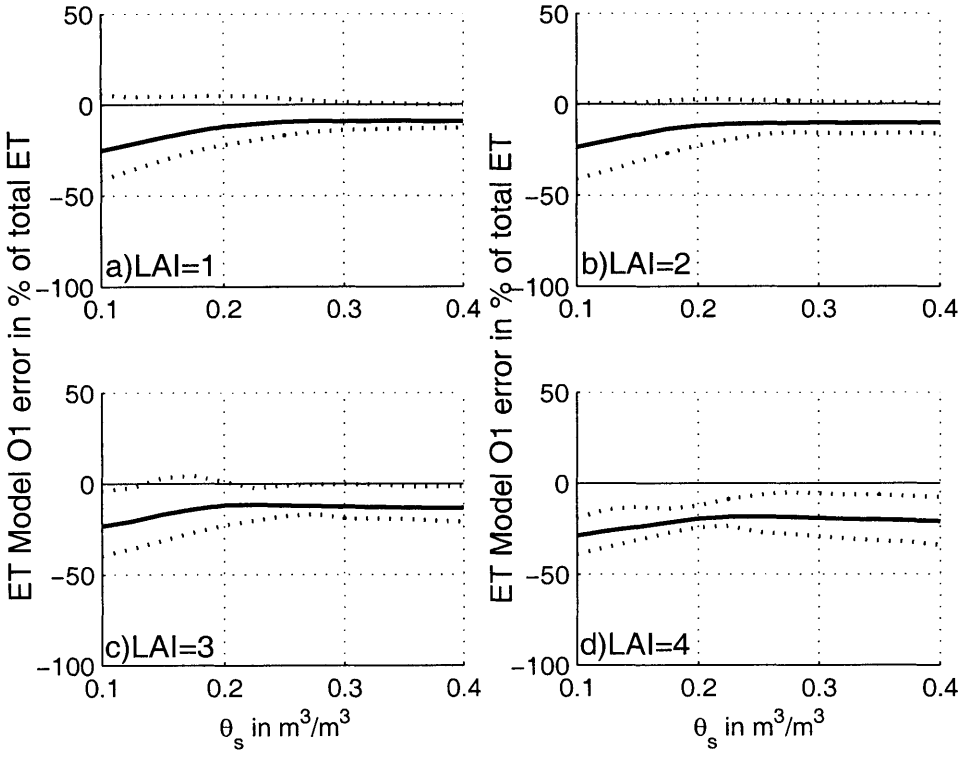

Figure B-40: Min/Max (dotted line) and mean (solid line) evapotranspiration error $\int_{t_0}^{t_{end}} ET_{O1}(t) - ET_{SVAT}(t)\, dt$ in percents, when using the constant EF assumption and measuring EF at different hour of the day between 10AM and 4PM, as a function of mean surface soil moisture for a) LAI=1, b) LAI=2, c) LAI=3, d) LAI=4.

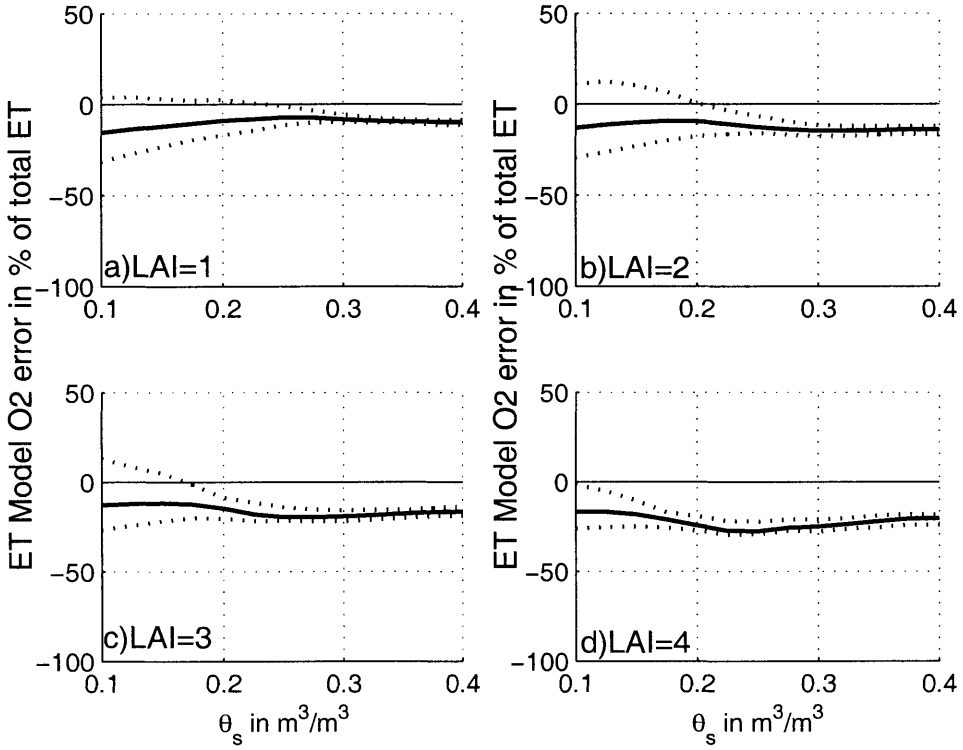

Figure B-41: Min/Max (dotted line) and mean (solid line) evapotranspiration error $\int_{t_0}^{t_{end}} ET_{O2}(t) - ET_{SVAT}(t)\,dt$ in percents, when using the constant EF' assumption and measuring EF' at different hour of the day between 10AM and 4PM, as a function of mean surface soil moisture for a) LAI=1, b) LAI=2, c) LAI=3, d) LAI=4.

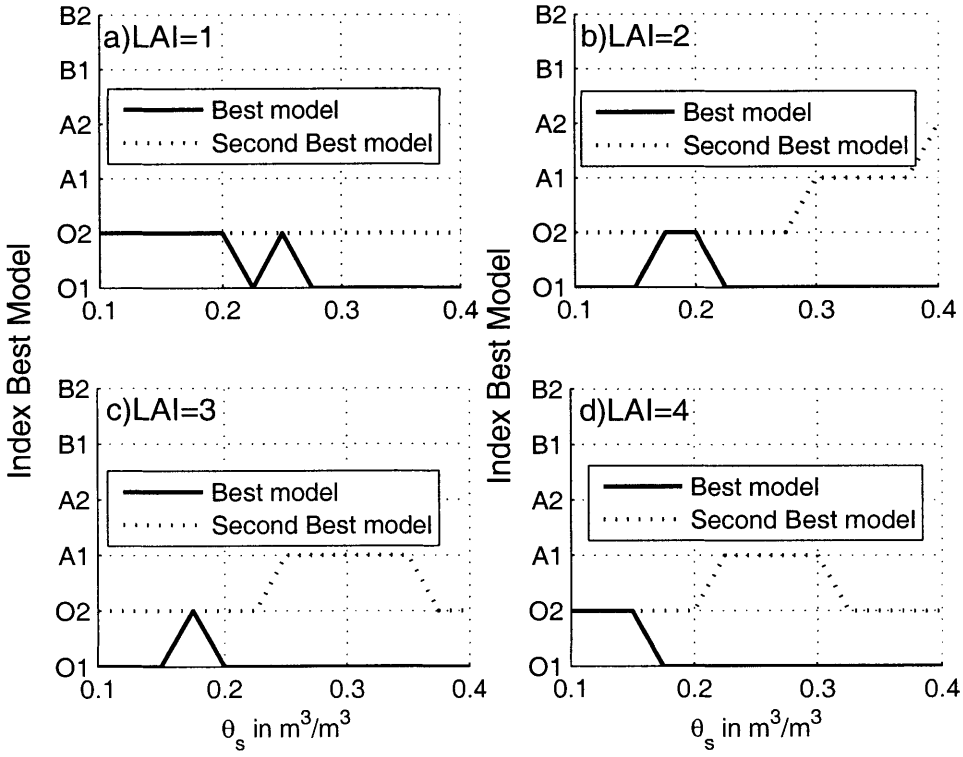

Figure B-42: First and second best evapotranspiration forecasting models as a function of surface soil moisture

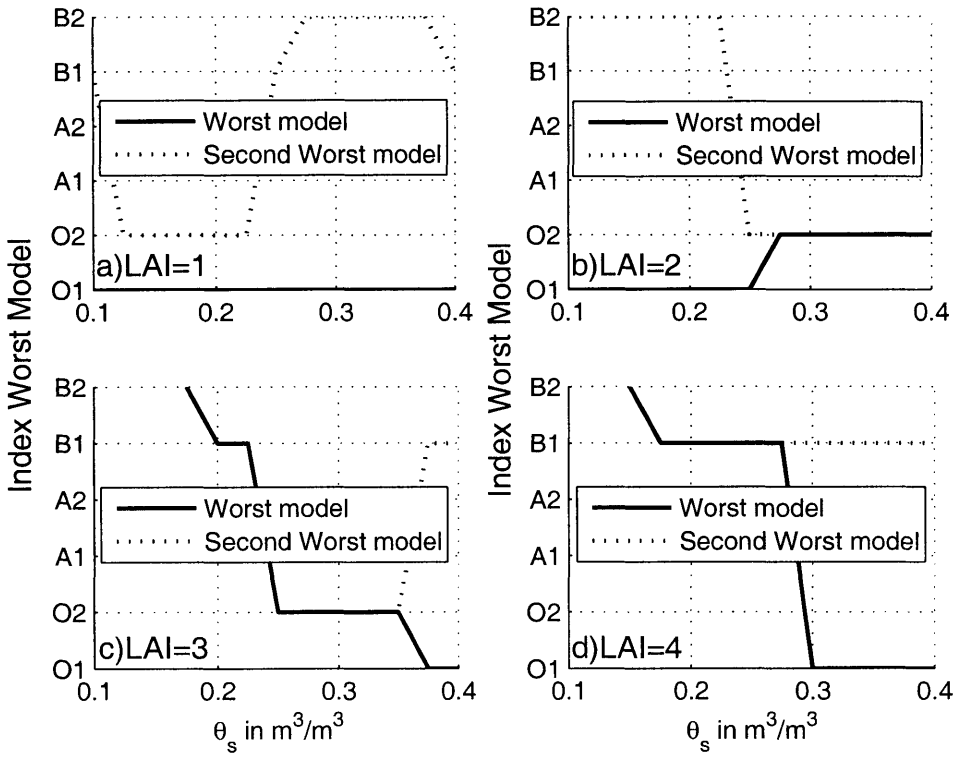

Figure B-43: First and second worst evapotranspiration forecasting models as a function of surface soil moisture

Appendix C

Fourier Analysis of the soil heat flux G

First, we are interested in the daily behavior of the soil heat flux $G(t)$. Hence, we can assume that the soil heat flux is a daily periodic function, so that the frequencies to be considered are the harmonics of the day frequency. The daily average value of the soil heat flux is also assumed to be zero.

$$\forall t : \qquad G(t) = \sum_{n=1}^{+\infty} G_n \exp(in\nu t) \tag{C.1}$$

Where ν represents the daily frequency:$\nu = 2\pi/86400\ in\ s^{-1}$ We assume that the soil temperature evolution follows a diffusive equation, and that the heat flux is given by Fourier's law:

$$\forall (\mathbf{x}, t) : \qquad \phi = -\lambda(\mathbf{x}, t)\nabla T \tag{C.2}$$

. In 3-D, the diffusive equation reads:

$$\forall(\mathbf{x},t): \qquad \rho C_m \frac{\partial T}{\partial t} = -\nabla \cdot \phi \tag{C.3}$$

But we assume that the flux is mostly along the vertical axis, so that the 3-D diffusion equation can be approximated by a 1-D diffusive equation:

$$\forall(z,t): \qquad \rho C_m \frac{\partial T}{\partial t} = -\frac{\partial}{\partial z}(-\lambda \frac{\partial T}{\partial z}) \tag{C.4}$$

One of the problem is that the conductivity k and the volumetric specific heat ρC_m are not homogeneous nor constant. Indeed, their values depends on both the soil composition, which clearly depends on the depth, and the soil water content at a given depth that clearly is inhomogeneous non-constant. However, to have some understanding on the propagation of the daily heat wave through the soil layer, one can assume that those parameters are constant and for instance equal to their value at the top horizon layer.

We also have the following boundary conditions:

$$\forall(z,t): \qquad \lambda \frac{\partial T}{\partial z}_{|z=0} = G(t) \qquad : \text{Flux continuity at the surface (z = 0)} \tag{C.5}$$

$$\lim_{z\to\infty} T(z,t) = T_{deep} \qquad : \text{Constant temperature at infinite horizon} \tag{C.6}$$

This PDE was solved by Carslaw and Jaeger 1959 and lead to:

$$T(z,t) = T_{deep} + \sum_{n=1}^{\infty} T_n(z) \exp(in\nu t) \tag{C.7}$$

The spatial component of the temperature is $T_n(z)$ expresses as:

$$T_n(z) = \frac{G_n}{\lambda(1+i)/d_n} \exp\left(\frac{-(1+i)z}{d_n}\right) \tag{C.8}$$

Where the penetration depths are defined as:

$$d_n = \left(\frac{2\lambda}{n\nu\rho C_m}\right)^{1/2} \tag{C.9}$$

Therefore the Fourier coefficients of T can be found using the Fourier transform of G. We can rewrite it as following:

$$T_n(z,t) = \frac{G_n d_n}{\sqrt{2}} \exp\Big(i(n\nu t - z/d_n - \pi/4)\Big) e^{-z/d_n} \tag{C.10}$$

Hence, there is a phase difference of $-\pi/4$ between the soil heat flux and the soil temperature, i.e there is a $1/8^{th}$ day delay between the soil heat flux and its repercussion on the soil temperature.

In particular, the surface temperature $T_s(t) = T(0,t)$ can be written:

$$T_s(t) = T_{deep} + \sum_{n=1}^{\infty} \frac{G_n}{\lambda(1+i)/d_n} \tag{C.11}$$

This can be rewritten as:

$$T_s(t) = T_{deep} + \sum_{n=1}^{\infty} \frac{G_n d_n}{\sqrt{2}} \exp\Big(i(n\nu t - \pi/4)\Big) \tag{C.12}$$

So the n^{th} harmonic of the temperature can directly be related to the n^{th} harmonic of the soil heat flux. So Ts and G Fourier coefficients can be related to each other using the following transfer function.

$$H_n = (1+i)(\lambda/d_n) \tag{C.13}$$

The soil surface heat flux cannot directly be observed, however we can have access to continuous in situ measurement of the soil temperatures. Finally, we can find the soil heat flux using:

$$G_n = H_n T_n(0) \tag{C.14}$$

And the soil surface heat flux $G(t)$ can simply be written:

$$G(t) = \sum_{n=1}^{\infty} H_n T_n(0) \exp(in\nu t) \tag{C.15}$$

Now if we consider only the effect of the principal daily frequency and no harmonic, the surface soil heat flux will be:

$$G(t) = G_1 e^{i(\nu t + \phi_1)} \tag{C.16}$$

where G_1 is the amplitude of the surface soil heat flux, ν is the daily angular frequency, and ϕ_1 is the daily phase of the soil surface heat flux. This should be between $\pi/3$ and $\pi/4$ as the soil heat flux is generally maximum just before noon. Using the flux boundary condition at the surface, the soil heat flux can be directly related to the surface temperature:

$$G(t) = H_1 T_1(0) \tag{C.17}$$

And using the fact that the temporal differentiation operator in our single frequency case is simply:

$$\frac{\partial}{\partial t} \equiv i\nu \tag{C.18}$$

This lead to the Force-restore approximation:

$$\frac{1}{\nu}\frac{\partial T_s(t)}{\partial t} + T_s(t) - T_{deep} = \frac{d_1}{\lambda} G(t) \tag{C.19}$$

Therefore, it is important to keep in mind which assumptions led to the Force-Restore approximation. To obtain this equation, only the diurnal principal frequency was considered. Hence, by construction the Force-restore equation won't be able to simulate the higher frequency behavior of the soil temperature, contrary to a diffusive model. So in a case of sparse vegetation, where the soil heat flux component is really an important part of the land surface budget, it will be necessary to use a diffusive model for radiative temperature assimilation. The force-restore equation will only be able to catch the daily behavior of the temperature. That is also why we decided to use a diffusive soil layer for the SVAT model, instead of a Force-restore model, because it allows a finer temporal description of the soil temperature and heat flux.

In fact, the Force-restore relationship can easily be generalized for a non-monochromatic signal, because the Force-restore relationship is true for any multi-frequency signal frequency wise:

$$n = 1, 2, 3, ... \frac{1}{n\nu} \frac{\partial T_n(0,t)}{\partial t} + T_n(0,t) - T_{deep} = \frac{d_n}{\lambda} G_n(t) \tag{C.20}$$

But using the expression of the penetration depth from Eq. (C.9), this can be rewritten as:

$$n = 1, 2, 3, ...\mathbb{N} \qquad G_n(t) = \left(\frac{\rho C_m \lambda}{2}\right)^{1/2} \left(\frac{1}{\sqrt{n\nu}} \frac{\partial T_n(0,t)}{\partial t} + \sqrt{n\nu}(T_n(0,t) - T_{deep})\right) \tag{C.21}$$

Finally, we can estimate the soil surface heat flux if we know the surface temperature using the above equation. However, to have a good reconstruction of the soil heat flux De Silan in his 1997's paper [21] explained that we need at least 18 harmonics of surface temperature. This can be achieved if continuous measurements of surface temperature are recorded. However, there will be two unsolvable issues if one wants to use this method with remote sensing temperature images. First, the temperature measured by satellite is a mix of canopy temperature and soil temperature, so that we cannot have directly access to the surface temperature. Second, remote sensing only allow sparse time measurements of temperature, hence we cannot obtain many temperature frequency harmonics. Thereby the soil heat flux cannot be reconstructed using remote sensing temperature measurements.

Bibliography

[1] Bastiaanssen WGM, Pelgrum H, Droogers P, et al. (1997), Area-average estimates of evaporation, wetness indicators and top soil moisture during two golden days in EFEDA, *Agricultural and Forest Meteorology*, 87 (2-3), 119-137.

[2] Betts AK, Viterbo P, Wood E (1998), Surface energy and water balance for the Arkansas Red River basin from the ECMWF reanalysis, *Journal of Climate*, 11 (11), 2881-2897.

[3] Boone A, (2002), Description du Schma explicite du sol : ISBA-DIF (ISBA-DIFfusion), CNRM-Mto-France, *Internal note.*

[4] Boulet G, Chehbouni A, Braud I, et al., (1999), Mosaic versus dual source approaches for modelling the surface energy balance of a semi-arid land, *Hydrology and Earth System Sciences*, 3 (2), 247-258.

[5] Brooks, R.H. and Corey A.T., (1966), Properties of porous media affecting fluid flow, *Journal Irrig. Drain. Div. Am. Soc. Civil Eng.*, 92 (IR2), 61-88.

[6] Brutsaert W, (1975), On a derivable formula for long-wave radiation from clear skies. *Water Resources Research*, 11 (5), 742-744.

[7] Brutsaert W, (1982), Evaporation Into the Atmosphere, *D. Reidel, Hingham, Mass*, 299 pp.

[8] Campbell GS, (1974), A simple method for determining unsaturated conductivity from moisture retention data, *Soil Sci.*, 117, 311-314.

[9] Castelli F, Entekhabi D, Caporali E, (1999), Estimation of surface heat flux and an index of soil moisture using adjoint-state surface energy balance, *Water Resources Research*, 35 (10),3115-3125.

[10] Caparrini F, Castelli F, Entekhabi D, (2003), Mapping of land-atmosphere heat fluxes and surface parameters with remote sensing data, *Boundary-Layer Meteorology*, 107 (3), 605-633.

[11] Caparrini F, Castelli F, Entekhabi D, (2004), Estimation of surface turbulent fluxes through assimilation of radiometric surface temperature sequences, *Journal of Hydrometeorology*, 5 (1), 145-159.

[12] Caparrini F, Castelli F, Entekhabi D, (2004), Variational estimation of soil and vegetation turbulent transfer and heat flux parameters from sequences of multisensor imagery, *Water Resources Research*, 40 (12).

[13] Cayrol P, Kergoat L, Moulin S, Dedieu G, Chehbouni A, (2000), Calibrating a Coupled SVAT-Vegetation Growth model with Remotely Sensed Reflectance and Surface Temperature - A Case Study for the HAPEX-Sahel Grassland Sites, *Journal of App. Meteo.*, 39, 2452-2472.

[14] Chehbouni A, Lo Seen D, Njoku EG, Monteny BA, (1996), A Coupled Hydrological and Ecological modeling Approach to examine the Relationship between Radiative and Aerodynamic Surface Temperature over Sparsely Vegetated Surfaces, *Remote Sensing Environment*, 58 ,177-186.

[15] Chehbouni A, Nouvellon Y, Lhomme JP et al., (2001), Estimation of surface sensible heat flux using dual angle observations of radiative surface temperature, *Agricultural and Forest Meteorology*, 108 (1), 55-65.

[16] Choudhury BJ and Idso SB, (1985), An empirical model for stomatal resistance of field-grown wheat, *Agric. For. Meteorol.*, 36, 65-82.

[17] Clothier BE, KL Clawson, PJ Pinter Jr., MS Moran, RJ Reginato, and RD Jackson, (1986), Estimation of soil heat flux from net radiation during the growth of alfalfa, *Agric. For. Meteor.*, 37, 319-329.

[18] Crago R, Brutsaert W, (1996), Daytime evaporation and the self-preservation of the evaporative fraction and the Bowen ratio, *Journal of Hydrology*, 178 (1-4), 241-255.

[19] Crago RD, (1996), Conservation and variability of the evaporative fraction during the daytime, *Journal of Hydrology*, 180 (1-4), 173-194.

[20] Crago RD, (1996), Comparison of the evaporative fraction and the Priestley-Taylor alpha for parameterizing daytime evaporation, *Water Resources Research*, 32 (5), 1403-1409.

[21] De Silan AP, Monteny BA, Lhomme JP, (1997), The correction of soil heat flux measurements to derive an accurate surface energy balance by the Bowen ratio method, *Journal of Hydrology*, 188-189, 453-465.

[22] De Vries DA, (1958), Simultaneous transfer of heat and moisture in porous media, *Eos, Trans. Amer. Geophys. Union*, 39 (5), 909-916.

[23] De Waele S, (2003), Automatic inference from finite time observations of stationary stochastic signals, *Delft University of Technology, Van den Hof PMJ, Ponsen and Looijen BV, Wageningen, 2003, p.205, ISBN:90-6464-923-5.*

[24] Deardorff JW, (1978), Efficient prediction of ground surface temperature and moisture with inclusion of a layer of vegetation, *Journal of Geophysical Research*, 83 (C4),1887-1903.

[25] Habets F, Boone A, and Noilhan J, (2002), Simulation of a Scandinavian basin using the diffusion transfer version of ISBA, *Global and Plan. Change.*

[26] Jarvis PG, (1975), Water transfer in plants, *In: de Vries, D.A., Afgan, N.G. (Eds.), Heat and Mass Transfer in the Plant Environment. Scripta, Washington, DC*, 369-394.

[27] Jarvis PG, (1976), The interpretation of leaf water potential and stomatal conductance found in canopies in the field, *Phil. Trans. R. Soc. London, Ser. B*, 273, 593-610.

[28] Jones HG, (1978), Modelling diurnal trends of leaf water potential in transpiring wheat, *J. Appl. Ecol.* 15, 613-626.

[29] Jones HG, (1992), *Plants and Microclimate, 2nd Edition. Cambridge University Press, Cambridge*, 1992.

[30] Kondo J, Saigusa N, and Takeshi S, (1990), A parameterization of evaporation from bare soil surfaces, *J. Appl. Meteor.*, 29, 385-389.

[31] Kustas WP, CST Daughtry, (1990), Estimation of the soil heat flux/net radiation ratio from spectral data., *Agric. For. Meteor.*, 49, 205-233.

[32] Lhomme JP, Elguero E, (1999), Examination of evaporative fraction diurnal behaviour using a soil-vegetation model coupled with a mixed-layer model, *Hydrology and Earth System Sciences*, 3 (2), 259-270.

[33] Lhomme JP, Chehbouni A, (1999), Comments on dual-source vegetation-atmosphere transfer models, *Agricultural And Forest Meteorology*, 94 (3-4), 111-115.

[34] Lhomme JP, (2001), Stomatal control of transpiration: examination of the Jarvis-type representation of canopy resistance in relation to humidity, *Water Resour. Res.* , 2001.

[35] LoSeen D, Chehbouni A, Njoku E, et al., (1997), An approach to couple vegetation functioning and soil-vegetation-atmosphere-transfer models for semiarid grasslands during the HAPEX-Sahel experiment, *Agricultural and Forest Meteorology*, 83 (1-2), 49-74.

[36] Mahfouf J-F, Noilhan J, (1991), Comparative study of various formulations of evaporation from bare soil using in-situ data, *J. Appl. Meteorol.*, 30, 1354-1365.

[37] Monteith JL, (1981), Evaporation and surface temperature, *Quart. J. R. Meteorol. Soc.*, 107, 1-27.

[38] Nichols WD, (1992), Energy budgets and resistances to energy transport in sparsely vegetated rangeland, *Agricultural and Forest Meteorology*, 60, 221-247.

[39] Nichols WE, Cuenca RH, (1993), Evaluation of the evaporative fraction for parameterization of the surface, energy-balance, *Water Resources Research*, 29 (11), 3681-3690.

[40] Noilhan J and Planton S, (1989), A simple parameterization of land surface processes for meteorological models, *Mon. Weather Rev.*, 117, 536-549.

[41] Shen YJ, Zhang YQ, Kondoh A, et al., (2004), Seasonal variation of energy partitioning in irrigated lands, *Hydrological Processes*, 18 (12), 2223-2234.

[42] Shuttleworth WJ, Wallace JS, (1985), Evaporation from sparse crops - an energy combination theory, *Quart. J. Royal Meteorol. Soc.*, 111, 839-855.

[43] Shuttleworth WJ, Gurney RJ, Hsu AY, Ormsby JP, (1989), Fife: The variation in energy partition at surface flux sites, *IAHS Publ. 1989*, 186, 67-74.

[44] Shuttleworth WJ, Gurney RJ, (1990), The theoretical relationship between foliage temperature and canopy resistance in sparse crops, *Quart. J. Royal Meteorol. Soc.*, 116, 497-519.

[45] Shuttleworth WJ, (1991), Evaporation models in hydrology, *In T.J. Schmugge and J. Andr, eds, Land surface evaporation, Springer, New York*, 93-120.

[46] Stewart JB, (1988), Modelling surface conductance of pine forest, *Agric. For. Meteorol.*, 43, 19-37.

[47] Stewart JB and Gay LW, (1989), Preliminary modelling of transpiration from the FIFE site in Kansas, *Agric. For. Meteorol.*, 48, 305-315.

[48] Taconet O, Bernard R, Vidalmadjar D, Evapotranspiration over an agricultural region using a surface flux temperature model based on NOAA AVHRR data, *Jounal of Climate and Applied Meteorology*, 25 (3), 284-307.

[49] Taconet O, Carlson T, Bernard R, et al., (1986), Evaluation of a surface vegetation parameterization using satellite measurements of surface temperature, *Jounal of Climate and Applied Meteorology*, 25 (11), 1752-1767.

FREQUENCY ANALYSIS PAPERS:

[50] Castiglioni P, Di Rienzo M, (1996), On the evaluation of heart rate spectra: the Lomb Periodogram Computersin Cardiology 1996, IEEE Computer Society Press, 505-508.

[51] Chang KL et al , (2001), Comparison and clinical application of frequency domain methods in analysis of neonatal heart rate time series. Ann Biomed Eng.

[52] Laguna P, et al (1998)Power spectral density of unevenly sampled data by least-square analysis: performance and application to heart rate signals. IEEE BME.

[53] Lomb NR., (1976), Least-squares frequency analysis of unequally spaced data. Astrophys Space Sci, (39), 447-462.

[54] Schimmel M. , (2001), Emphasizing difficulties in the detection of rhythms with Lomb-Scargle Periodograms. Biol Rhythm Res.

[55] Van Dongen HPA et al (1999) A procedure of multiple period searching in unequally spaced time-series with the Lomb-Scargle method. Biol Rhythm Res.

SOIL HEAT FLUX PAPERS:

[56] Camillo P , (1989), Estimating Soil Surface Temperatures From Profile Temperature And Flux Measurements, *Soil Science*, 148 (4), 233-243.

[57] Carslaw HS, (1959), *Conduction of Heat in Solids*, Clarendon Press, 150pp.

[58] Carson JE, (1963), Analysis of Soil and Air Temperatures by Fourier Techniques, *Journal of Geophysical Research*, 68, 2217-2234.

[59] De Silans AP, Monteny BA, Lhomme JP, (1997), The correction of soil heat flux measurements to derive an accurate surface energy balance by the Bowen ratio method, *Journal of hydrology*, 189 (1-4), 453-465.

[60] Deardorff JW, (1978), Efficient prediction of ground surface temperature and moisture with inclusion of a layer of vegetation, *Journal of Geophysical Research*, 83, 1889-1903.

[61] Dickinson RE, (1988), The Force-Restore Model for Surface Temperatures and Its Generalizations, *Jounal of Climate*, 1, 1086-1097.

[62] Gao ZQ, Fan XG, Bian LG, (2003), An analytical solution to one-dimensional thermal conduction-convection in soil, *Soil Science*, 168 (4), 309-309.

[63] Guaraglia DO, Pousa JL, Pilan L, (2001), Predicting temperature and heat flow in a sandy soil by electrical modeling, *Soil Science Society of America Journal*, 65 (4), 1074-1080.

[64] Horton R, Wierenga PJ, (1983), Estimating the soil heat-flux from observations of soil-temperature near the surface, *Soil Science Society of America Journal*, 47 (1), 14-20.

[65] Hu Z, Islam S, (1995), Prediction of ground surface temperature and soil moisture content by the force-restore method, *Water Resour. Res.*, 31 (10) , 2531-2540.

[66] Karam MA, (2000), A thermal wave approach for heat transfer in a nonuniform soil, *Soil Science Society of America Journal*, 64 (4), 1219-1225.

[67] Lin JD, (1980), On the force-restore method for prediction of ground surface temperature, *Journal of Geophysical Research*, 85,3251-3254.

[68] Massman WJ, (1993), Periodic temperature-variations in an inhomogeneous soil - a comparison of approximate and exact analytical expressions, *Soil Science*, 155 (5), 331-338.

[69] Mihailovic DT, Kallos G, Arsenic ID, et al, (1999), Sensitivity of soil surface temperature in a force-restore equation to heat fluxes and deep soil temperature, *International Journal Of Climatology*, 19 (14), 1617-1632.

[70] Milly PCD, (1986), An event-based simulation model of moisture and energy fluxes a a bare soil surface, *Water Resources Research*, 22, 1680-1692.

[71] Ren DD, Xue M, (2004), A revised force-restore model for land surface modeling, *Journal Of Applied Meteorology*, 43 (11), 1768-1782.

SENSITIVITY

[72] Collins DC, Avissar R, (1994), An evaluation with the fourier amplitude sensitivity test (FAST) of which land-surface parameters are of greatest importance in atmospheric modeling, *Journal Of Climate*, 7 (5), 681-703.

[73] Rodriguez-Camino E, Avissar R, (1998), Comparison of three land-surface schemes with the Fourier amplitude sensitivity test (FAST), *Tellus Series A-Dynamic Meteorology And Oceanography*, 50 (3), 313-332.